Precambrian Geology of the Elk Mountain - Spring Mountain Area, San Miguel County, New Mexico

by

Ingrid Klich

Submitted in Partial Fulfillment

of the Requirements for the Degree of

Master of Science in Geology

New Mexico Institute of Mining and Technology

Socorro, New Mexico

February, 1983

ABSTRACT

Precambrian rocks of the Elk Mountain - Spring Mountain area, San Miguel County, New Mexico consist primarily of a bimodal (mafic-felsic) metavolcanic assemblage, plus locally abundant metasedimentary rocks (predominantly of volcanic provenance, plus ironstone, shales, and limestone), and a complex of intrusives including meta- diabase and gabbro, tonalite, granite, syenite and pegmatites. The metavolcanic suite is largely comprised of subaqueous basalts (with well-preserved pillow-structures), plus lesser amounts of felsic volcanic and volcaniclastic rocks ranging from rhyolites to dacites.

The supracrustal succession has been subjected to at least two periods of tight to isoclinal folding, accompanied by intense tectonic transposition such that present orientations of lithologic units no longer represent their original stratigraphy. Thus, delineation of a stratigraphic section for the supracrustal rocks within the study area is not yet possible. Rocks of the supracrustal succession have been variably metamorphosed to lower amphibolite facies with slight retrograde metamorphism to greenschist facies.

Chemical analyses verify the compositional bimodality of the supracrustal assemblage. The mafic rocks are characterized mainly as subalkaline, low-K tholeiites,

whereas the felsic rocks appear to be both tholeiitic and calc-alkaline. Tectonic discrimination diagrams suggest formation of these rocks at an island arc - destructive plate boundary. The submarine environment, bimodal volcanic suite, and relationship to associated sedimentary rocks are all compatible with deposition in a marginal back-arc basin adjacent to an immature arc-system.

The potential for volcanogenic base-metal sulfide deposits within the study area appears to be very low. In addition, occurrences of ironstone and hydrothermal quartz veins are only localized, and cannot be considered economical. Mineralization associated with pegmatite intrusives (similar to that which was mined at the Elk Mountain deposit in the early 1940's) occurs throughout the southern and western portions of the study area, but under present economic conditions is not considered an important resource.

ACKNOWLEDGMENTS

Financial support for this study was provided in part by a U.S. Department of the Interior Research Fellowship (Award No G-5194015) and in part by the New Mexico Bureau of Mines and Mineral Resources.

I would like to acknowledge and greatfully thank Dr. James M. Robertson, not only for serving as my thesis adviser, but for suggesting this project and sharing his knowledge of Precambrian geology, for providing continued support and enthusiasm, and finally for critically reviewing this manuscript. A special thanks also to Drs. J.A. Grambling, K.C. Condie and J.F. Callender for their invaluable contributions, suggestions and enthusiasm in the field, and in addition to Dr. D.I. Norman for their helpful editorial comments. In addition, I thank Jeanette and Peter Abundis for their assistance in the field; Babette Faris, Phillip Allen, Gary Anderson, and Bob North for assistance with the geochemical analyses; and my colleagues to numerous to list, whose endless sense of humor make life enjoyable. Finally, I would like to thank my parents, who's unfailing love and encouragement, not only for myself but for each other, made my education possible.

TABLE OF CONTENTS

APPENDIXES

PLATES

FIGURES

TABLES

INTRODUCTION

LOCATION

The study area comprises approximately sixteen square kilometers of the southern Sangre de Cristo Mountains in north-central New Mexico, and lies within portions of the Elk Mountain and Rociada (7.5-min.) quadrangles (see Fig. 1). A large portion of the study area also lies within the Pecos Wilderness.

U.S. Forest Service Primitive Roads 645 and 156 provide limited vehicle access into the southeastern region of the study area. Primitive road 645 heads due east from the Terrero (Pecos) Mine, located approximately 14.5 miles north of Pecos, New Mexico, along New Mexico highway 63. Along the ridge west of Cow Creek, Primitive Road 156 forks to the left. Near the headwaters of Cow Creek this road forks again; to the right towards Elk Mountain, and to the left towards the Elk Mountain (Kept Man) Pegmatite Mine. Foot access to other portions of the study area is provided by several pack trails

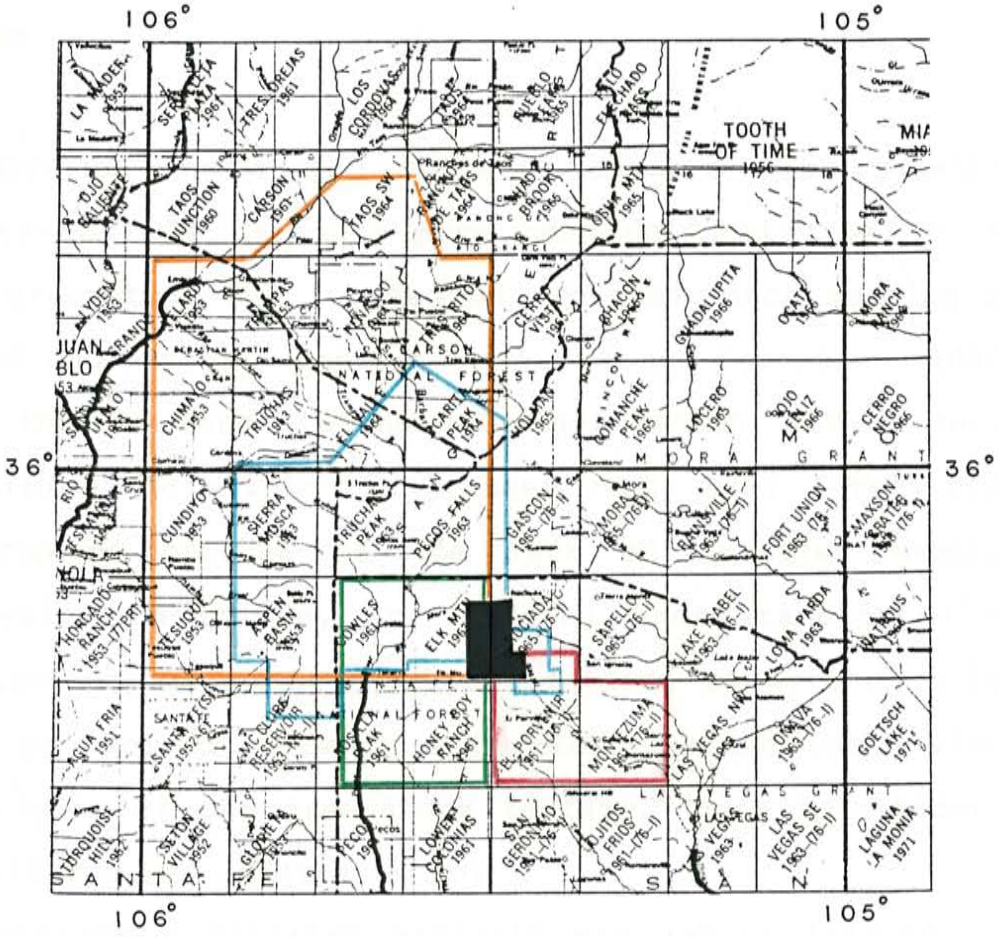

Figure 1. Location map showing previous investigations which include part or all of this study.

PURPOSE

Several Precambrian volcanic centers with potential massive-sulfide deposits have been delineated within the Pecos greenstone belt, based on reconnaissance mapping and limited geochemical sampling by Moench and Robertson (1980). Two of these centers - along Hollinger Canyon, and on Spring Mountain - lie within the present study area This study was proposed because of the lack of detailed mapping, geochemical analyses, and general understanding of the distribution and stratigraphic relations among the various mafic and felsic volcanic and volcaniclastic rocks within this region of the greenstone terrane. More specifically, this project was undertaken to:

1) construct a detailed geologic map (scale 1:12,000) of the Precambrian rocks within the Elk Mountain-Spring Mountain Area;
2) subdivide the volcanic and volcaniclastic rocks into lithologically distinct units on the basis of field relations, petrography, and geochemistry;
3) define mechanisms of emplacement and possible depositional environments for the rocks within the study area;
4) define and evaluate the stratigraphic and/or structural relationships between the Elk Mountain-Spring Mountain volcanic section and a mainly sedimentary section that

extends into the northeast corner of the study area;

5) evaluate the massive-sulfide potential of the volcanic terrane;

6) describe the geology and petrology of the syenite body that intrudes the volcanic section between Beaver and Daily Creeks;

7) reconstruct a Precambrian structural and metamorphic history of the area;

8) speculate on the similarities with other Southwestern Proterozoic greenstone terranes, and on possible tectonic settings.

PREVIOUS WORK

Until recently much of the geologic mapping of Precambrian rocks in the southern Sangre de Cristo Mountains, New Mexico, has been reconnaissance in nature (Miller et.al., 1963, and Mathewson, unpub. map). Additional reconnaissance mapping of the Pecos Wilderness and adjacent areas by R.H. Moench and J.M. Robertson during the summers of 1976 and 1977 led to the delineation of a Proterozoic volcano-sedimentary terrane known as the Pecos greenstone belt (see Robertson and Moench, 1979; Moench and Robertson, 1980).

A detailed study by Riesmeyer (1978) describes the volcanogenic massive-sulfide deposits in the Pecos Mining District and notes their restriction to distinct felsic volcanic centers where they tend to occur at the contact between subaqueous felsic volcanics and overlying sedimentary rocks. Wyman (1980) describes the geology, geochemistry, and economic potential of a number of ultramafic bodies exposed southwest of Elk Mountain. These rocks exhibit both extrusive and intrusive textures and are suggested to be, in large part, komatiitic. They are believed to represent a portion of the basal stratigraphy of the Pecos greenstone volcano-sedimentary terrane. Moench and Erickson (1980) remapped rock units within the southern portion of the formerly interpreted granitic terrane of the Santa Fe Range (Miller et. al., 1963; Budding, 1972) west of the Pecos-Picuris fault. Their study revealed a succession of metasediments and metavolcanics very similar to those exposed within the greenstone terrane. Large tungsten and base-metal anomalies suggest to Moench and Erickson, that stratabound scheelite deposits may be present peripherally to volcanogenic massive-sulfide deposits in this region. Wakefield (M.S. thesis in progress, N.M.I.M.T) is currently studying the rocks in an area delineated by Moench and Erickson (1980) as the Ruiz Canyon volcanic center. Fulp (1982) describes the geology and mineralization of the Dalton Canyon volcanic center and suggests that sulfide

deposits are strataform volcanogenic deposits.

Detailed mapping and structural analyses in the Truchas Peaks region (Grambling, 1979) and in the Rio Mora area (Grambling and Codding, 1982) suggest that Precambrian rocks in the quartzite terrane, just north of the Pecos greenstone belt, have undergone at least two periods of tight to isoclinal folding and metamorphism to the middle amphibolite facies. These rock units are believed to be correlative with Ortega Group rocks in the Picuris Range to the northeast. Their studies along the contact between the quartzite terrane and the greenstone terrane led to the interpretation that the quartzite terrane is younger than the greenstone terrane. Codding (in press) describes the rocks in an area adjacent to the northern boundary of this study area as part of a Master's thesis at the University of New Mexico.

METHOD OF INVESTIGATION

Field work for this study was primarily done during the summer months of 1981, and later completed in June of 1982. The study area was mapped at a scale of 1;12,000 on enlargements made from U.S.G.S. quadrangle maps.

Eighty thin sections were studied petrographically to supplement field correlations and to characterize petrographic textures representative of the units described.

Plagioclase compositions were determined by the Michel-Levy method as described in Kerr (1977), and staining for potassium aided in the identification of alkali feldspars.

Twenty-one samples were analyzed by the author for major, minor, and selected trace and rare-earth elements using both X-ray fluorescence (XRF) and instrumental neutron activation analysis (INAA) techniques as described by Jenkins and De Vries (1975), and Gordon et. al. (1968), respectively. Sample preparation, standard concentrations, instrumental parameters, and analytical errors are discussed in Appendixes C, D, and E. Loss on ignition values were also determined by the author, and CIPW norms were calculated using the New Mexico Tech DEC20 computer system.

GEOLOGIC SETTING

Regional Geology

Igneous and metamorphic rocks of Proterozoic age are exposed in a number of the major uplifted structural blocks in north-central New Mexico (Fig. 2). The study area lies along the southeastern crest of the Sangre de Cristo uplift. This north-trending mountain range extending into southern Colorado is bounded by the Great Plains on the east and by the Rio Grande Rift on the west. Locally, the southern portion of this range is bounded on the east by the Las Vegas basin, on the west by the Española basin, and on the south by Glorieta Mesa (Baltz, 1978). The eastern boundary is dominated by several thrust and high-angle reverse faults activated largely during the Laramide orogeny, perhaps as early as the Pennsylvanian, and again in late Tertiary times (Baltz and Bachman, 1956; Baltz, 1972, 1978; Baltz and O'Neill, 1980).

Geologic mapping in this region has led to the delineation of four general Precambrian terranes (Fig. 3): (1) a greenstone terrane, known as the Pecos greenstone belt; (2) a quartzite terrane; (3) a plutonic terrane; and (4) a mixed terrane (Robertson and Moench, 1979). The Pecos greenstone belt is bounded on the south and west by the plutonic terrane composed of granitic intrusives

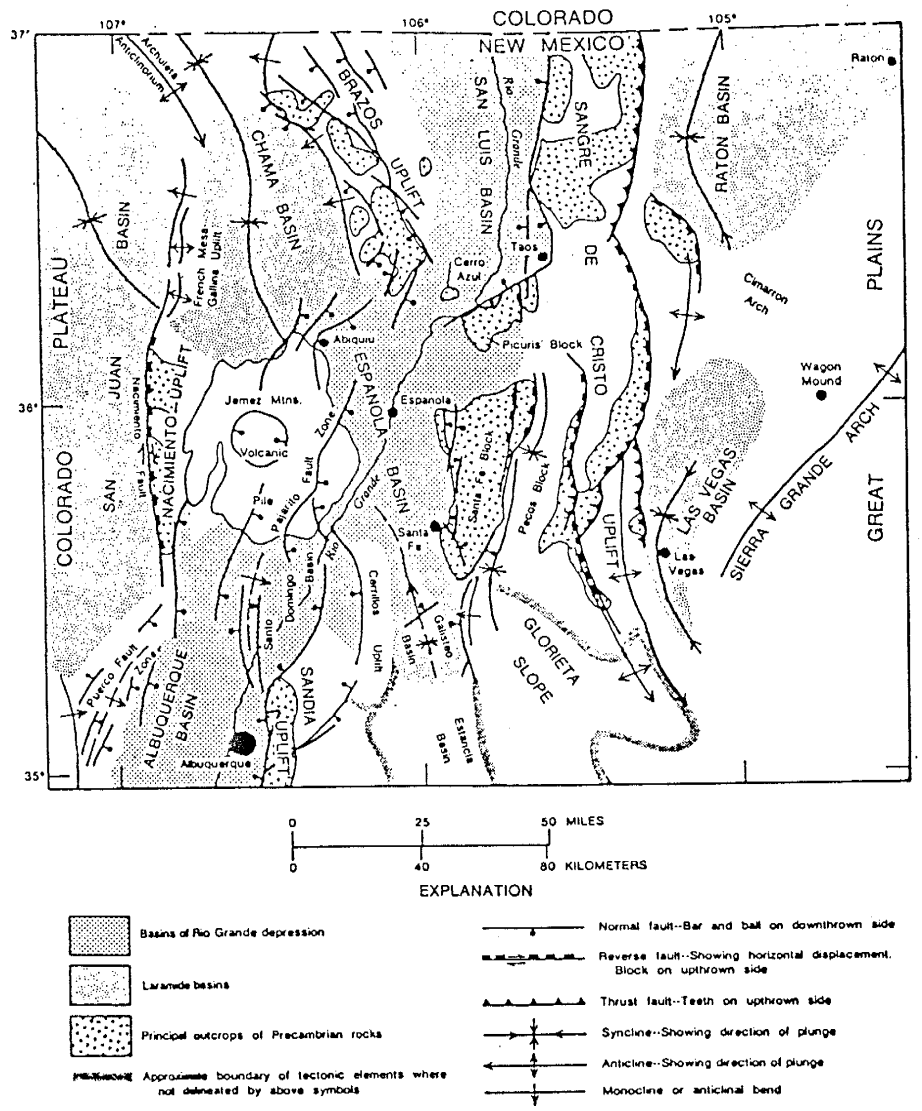

Figure 2. Geologic provinces of north-central New Mexico (from Baltz, 1978).

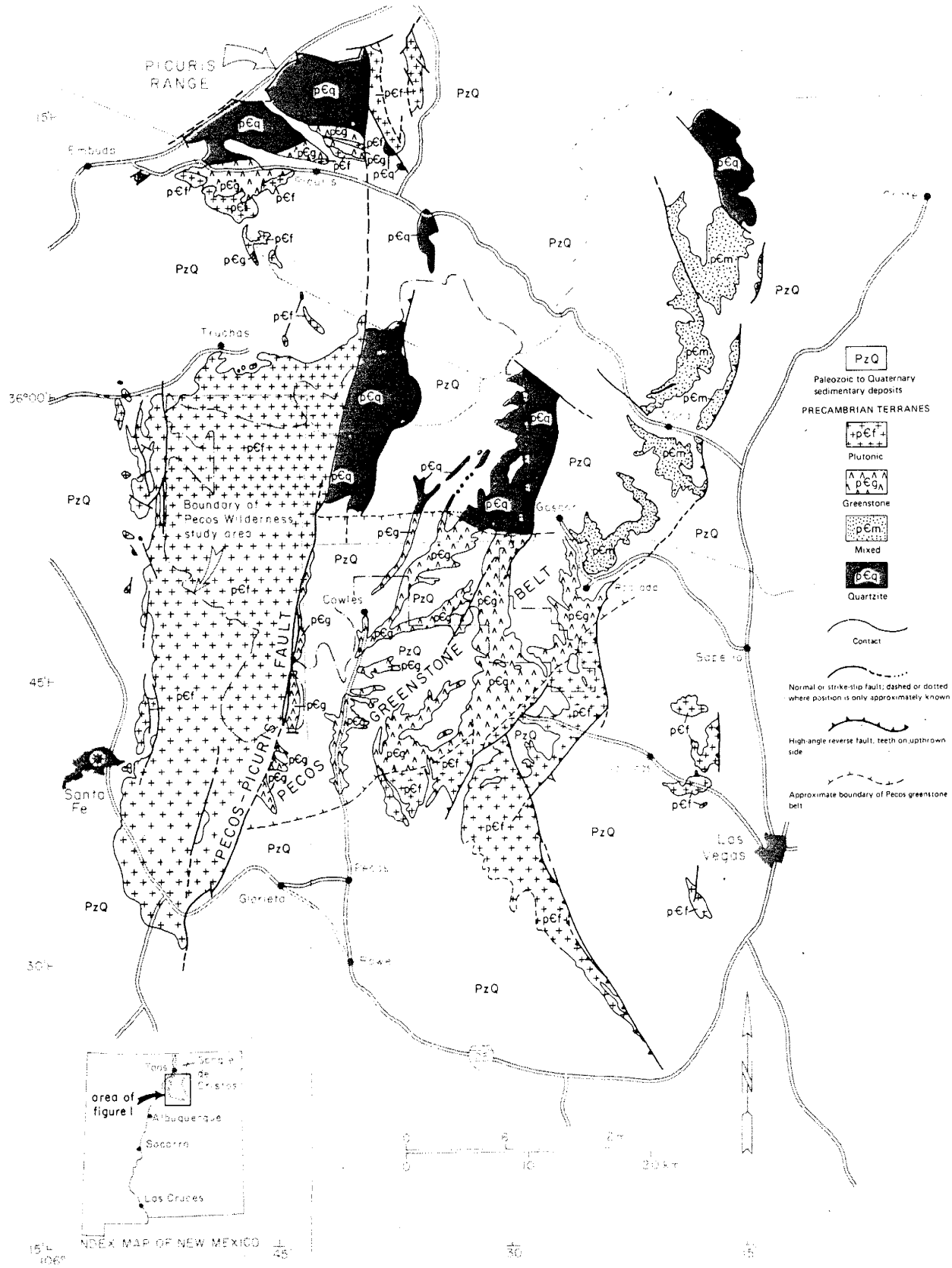

Figure 3. Regional geologic map of the southern Sangre de Cristo Mountains, New Mexico (from Robertson and Moench, 1979).

collectively called the Embudo Granite (Miller et. al., 1963; Budding, 1972; Fullagar and Shriver, 1973). Recent detailed mapping by Moench and Erickson (1980) suggests that the southwestern boundary of the Pecos greenstone belt be extended across the Pecos-Picuris fault into this plutonic terrane, at least as far as the Garcia Ranch fault. Additional mapping of undivided felsic gneisses and stratified rocks may extend this boundary even further to the west of this fault. To the north, the greenstone terrane is bounded by a thick succession of quartzites, pelitic-schists, and graphitic phyllites of the quartzite terrane (Grambling, 1979; Grambling and Codding, 1982). The mixed terrane, to the northeast of the greenstone terrane, is composed of quartz-feldspar paragneiss, aluminous quartz-mica schist, quartzite, thin layers of calc-silicate rock, and amphibolite (Robertson and Moench, 1979). Detailed lithologies of the greenstone terrane are discussed later in the text. The entire Precambrian terrane is unconformably overlain by Paleozoic limestones, shales, sandstones, arkoses, and conglomerates (see Miller et. al., 1963), although locally along the eastern boundary, Precambrian rocks are thrust over Paleozoic strata (Baltz and Bachman, 1956; Baltz, 1972, 1978).

Phanerozoic Geology of the Elk Mountain-Spring Mountain Area

Quaternary Deposits

Quaternary regolith and colluvium is ubiquitous throughout the mapped region, covering much of the area's Precambrian outcrops. Streams within the study area are immature and commonly flow on bedrock. Along the eastern region, where stream-gradients are less abrupt, Quaternary alluvial gravel and boulder deposits are found in the streambeds of major drainages. The Quaternary deposits consist primarily of Precambrian rocks with a relatively minor Paleozoic component. Since this study focuses on Precambrian igneous and metamorphic rocks in this region, the accompanying map shows only basement rocks; no Quaternary deposits were mapped.

Tertiary (?) Dikes (?)

Porphyritic rhyolite is found in the northwest region of the study area. It occurs only in float within the Precambrian terrane and defines narrow, linear horizons, generally trending north-northeast. Such horizons are tentatively interpreted as dikes, and may reflect the trends of a larger intrusive body at depth.

Fresh surfaces are light gray in color, commonly weathering various shades of brown. Euhedral to subhedral phenocrysts of orthoclase, plagioclase, and biotite (≤2mm) may comprise up to 20% of the rock. The aphanitic matrix (≤0.05mm) consists primarily of orthoclase, plagioclase, quartz and biotite. Secondary muscovite is interstitial in the groundmass together with minor magnetite. Orthoclase is the predominant feldspar, generally exhibiting carlsbad twinning. Subordinant plagioclase (An15-25) is twinned according to the albite law. Weak alteration to sericite occurs along cleavages. Subhedral to euhedral biotite is pale brown in color. Quartz phenocrysts are commonly subhedral to rounded and optically continuous. Such rocks have not previously been documented within the Pecos area, although other occurrences are believed to exist in outcrop along Indian Creek to the southwest of this study area (Osburn, per. commun., 1982). Clark and Read (1972) describe a similar rhyolite porphyry in the Taos-Red River area.

Major-element concentrations are generally consistent with average values reported for rhyolitic rocks (see Table 1). TiO_2 and FeO values are slightly low, but are still within reasonable limits for rhyolites. Ewart (1979) has compiled abundant geochemical data from a variety of Tertiary salic volcanic rocks, and has classified them on the basis of silica content, and geographic and/or tectonic regions. Data from orogenic volcanic sequences are further

TABLE 1

Chemical Analysis of Cenozoic Rhyolites

	1	2	3	4	5	6	7	8	9
SiO2	73.55	74.00	70.35	75.01	70.88	75.57	73.04	74.75	76.60
TiO2	0.01	0.27	0.54	0.34	0.39	0.21	0.31	0.20	0.11
Al2O3	15.55	13.53	14.90	12.99	15.03	13.61	14.24	13.67	12.57
Fe2O3	0.75	1.47	2.10	1.39	1.17	0.62	1.44	0.95	0.74
FeO	0.01	1.16	1.95	1.47	1.59	1.03	0.54	0.61	0.56
MnO	0.03	0.01	0.11	0.09	0.06	0.06	0.07	0.05	0.04
MgO	0.17	0.41	0.92	0.58	0.82	0.36	0.47	0.29	0.11
CaO	1.51	1.16	3.92	2.57	2.52	1.49	1.36	1.14	0.56
Na2O	4.60	3.62	3.99	4.17	4.76	4.21	3.76	3.63	3.76
K2O	3.82	4.38	1.07	1.18	2.65	2.79	4.70	4.67	4.93
P2O5	0.02	0.01	0.15	0.22	0.12	0.06	0.08	0.05	0.03
(n)	(1)	n/a	(19)	(14)	(27)	(10)	(143)	(200)	(45)
Rb	114	n/a	n.d.	n.d.	61	44	180	182	185
Ba	1864	n/a	445	403	699	613	957	631	537
Sr	625	n/a	285	117	467	500	249	184	18
Zr	42	n/a	n.d.	n.d.	115	200	217	142	157
Y	4	n/a	11	11	12	80	29	32	40
Nb	11	n/a	n.d.	n.d.	5	n.d.	27	19	29
Hf	2	n/a	n.d.	4	n.d.	6	n.d.	n.d.	n.d.

1. rhyolite, this study
2. ave. rhyolite (Le Maitre, 1976)
3. ave. low-K orogenic rhyolite (SiO2=69-73%), Japan (Ewart, 1979)
4. ave. low-K orogenic rhyolite (SiO2>73%), Japan (Ewart, 1979)
5. ave. calc-alkaline orogenic rhyolite, (SiO2=69-73%) high-Cascades (Ewart, 1979)
6. ave. calc-alkaline orogenic rhyolite, (SiO2>73%) high-Cascades (Ewart, 1979)
7. ave. high-K orogenic rhyolite, (SiO2>69%) western U.S.A.-eastern belt (Ewart, 1979)
8. ave. high-K orogenic rhyolite, (SiO2>69%) western U.S.A.-western belt (Ewart, 1979)
9. ave. rhyolite from bimodal volcanic association, western U.S.A (Ewart, 1979)

n/a=not analyzed
n.d.=not determined
(n)=number of samples analyzed

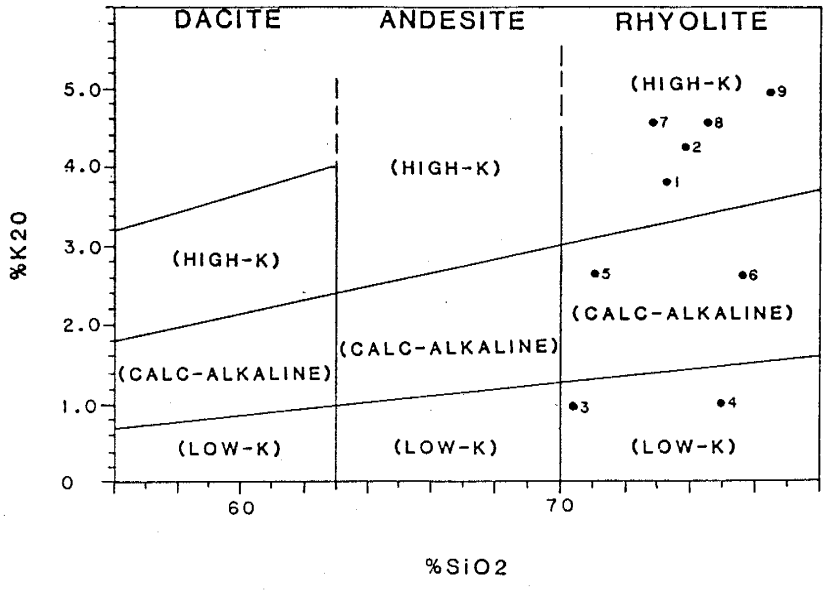

1. rhyolite, this study
2. ave. rhyolite (Le Maitre, 1976)
3. ave. low-K orogenic rhyolite (SiO2=69-73%), Japan (Ewart, 1979)
4. ave. low-K orogenic rhyolite (SiO2>73%), Japan (Ewart, 1979)
5. ave. calc-alkaline orogenic rhyolite, (SiO2=69-73%) high-Cascades (Ewart, 1979)
6. ave. calc-alkaline orogenic rhyolite, (SiO2>73%) high-Cascades (Ewart, 1979)
7. ave. high-K orogenic rhyolite, (SiO2>69%) western U.S.A.-eastern belt (Ewart, 1979)
8. ave. high-K orogenic rhyolite, (SiO2>69%) western U.S.A.-western belt (Ewart, 1979)
9. ave. rhyolite from bimodal volcanic association, western U.S.A (Ewart, 1979)

Figure 4. SiO_2 vs K_2O diagram for Cenozoic volcanic rocks (after Ewart, 1979).

divided into "low-K", "calc-alkaline" and "high-K" rhyolites based on the subdivision proposed by Peccerillo and Taylor (1976). Selected examples are included in Table 1, and are plotted on a SiO_2 versus K_2O variation diagram (Fig. 4). This diagram shows the potassium-enriched nature of the rhyolite from this study. This rhyolite appears similar to other Tertiary, high-K, orogenic rhyolites, both in relation to geochemical analyses and to reported mineral assemblages, assuming that orthoclase represents original sanidine.

The lack of metamorphic textures and its similarity to other known Tertiary rhyolites within the Sangre de Cristo Mountains suggests a Tertiary age for this unit.

Paleozoic Rocks

Sedimentary rocks of Pennsylvanian and Mississippian age lie unconformably over Precambrian rocks within the mapped area. Locally, Precambrian rocks are in fault contact with the younger Paleozoic strata. Detailed stratigraphic descriptions of the formations present in this area and surrounding regions of the southern Sangre de Cristo Mountains have been documented by Miller et. al. (1963); Baltz (1972); Baltz and O'Neill (1980), and are adequate for this study. Subdividing Paleozoic deposits was not attempted, as the major emphasis of this thesis is confined to the Precambrian rocks.

PRECAMBRIAN GEOLOGY

Geology of the Pecos Greenstone Belt

The Pecos greenstone belt is characterized by Robertson and Moench (1979) and Moench and Robertson (1980) as a complex assemblage of interrelated meta- volcanic, volcaniclastic, and sedimentary rocks. This succession has been intruded by an inferred subvolcanic complex of the same general age as the volcano-sedimentary assemblage, and by a slightly younger plutonic complex (Fig. 5).

Metamorphosed volcanic rocks are compositionally bimodal, comprised primarily of subaqueous metabasalts and locally important porphyritic felsic volcanics. Volcaniclastic rocks predominantly felsic in composition, along with cherty iron-formation are interbedded with these volcanic rocks. This bimodal volcanic succession is included in the 1.72 to 1.80 b.y.-old supracrustal age province recognized by Condie (1982). Stacey et. al. (1976) report model lead ages of 1.71 b.y. and 1.72 b.y. on galena from massive-sulfide deposits associated with the felsic volcanic and volcaniclastic rocks at the Pecos and Jones mines, respectively. Interstratified metasedimentary rocks consist of metamorphosed feldspathic sandstone, aluminous shale, conglomerate, small amounts of volcaniclastic graywacke, thin layers of carbonate rock, and minor clastic

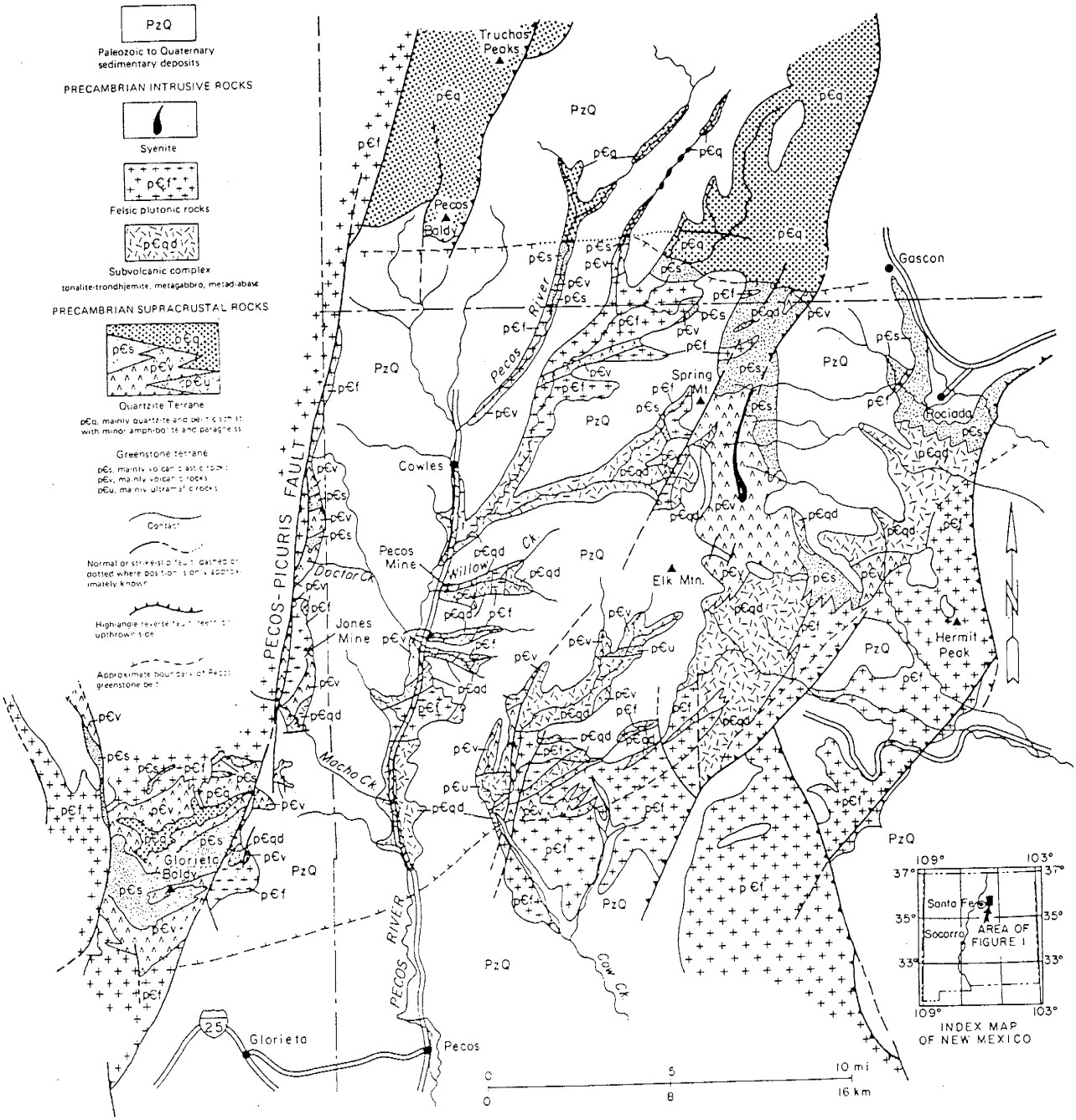

Figure 5. Generalized geologic map of the Pecos greenstone belt (Robertson, in press).

iron-formation. This sedimentary assemblage predominates in the northeast region of the greenstone terrane, and is complexly interstratified with volcanic rocks further south.

The subvolcanic complex consists of hypabyssal intrusions of metadiabase, quartz diorite, trondhjemite, and minor ultramafic rocks, that crosscut the metavolcanics and metasediments of the greenstone terrane. A well-foliated quartz diorite body exposed west of the Pecos-Picuris fault, has been dated at approximately 1.65 b.y. by Silver (in Stacey et. al., 1976) using U-Pb zircon methods. Robertson and Moench (1979) suggest that trondhjemites in the Pecos greenstone belt may be related, and have similar ages to other trondhjemites of northern New Mexico and southern Colorado, dated at 1.7 to 1.8 b.y. by Barker et. al. (1974 and 1976). A U-Pb (zircon) age of 1.72 b.y. has been determined for a well-foliated tonalite-trondhjemite body exposed along the Pecos River (Bowring, 1982).

Rocks of the plutonic complex intrude the subvolcanic complex, as well as the stratified rocks of the greenstone terrane. Moench and Robertson (1980) believe these rocks are related to the 1.7 b.y. and possibly the 1.4 b.y. age group of intrusives in Colorado (see Tweto, 1977). This batholithic complex of tonalite, granodiorite, granite, syenite, and pegmatite, exhibits a wide variety of igneous and metamorphic textures (see Moench and Robertson, 1980).

Register and Brookins (1979) report a Rb-Sr isochron age of 1,465 ± 50 m.y. for a phase of the Embudo Granite exposed within the plutonic terrane, west of the Pecos-Picuris fault.

Within this region, metamorphism to greenschist and amphibolite facies has been accompanied by at least two periods of deformation. Metamorphic and/or tectonic events at 1,673 m.y., 1,425 m.y., 1,350 m.y., and 1,250 m.y. for rocks of north-central New Mexico are summarized by Long (1972); Long (1974); Gresens (1975); and Callender et. al. (1976).

General Stratigraphy of the Elk Mountain-Spring Mountain Area

Structural and stratigraphic studies of Precambrian rocks in the Rio Mora area and Picuris Range by Grambling and Codding (1982) and Holcombe and Callender (1982), respectively, indicate that rocks in these regions have undergone at least two generations of tight to isoclinal folding, along with variable amounts of transposition The present compositional banding may therefore bear no resemblance to the original stratigraphy, at least in terms of present orientations, and stratigraphic younging directions may be random, thus providing erroneous information about both local and regional stratigraphic relations (see Turner and Weiss, 1963; Hobbs et. al., 1976).

Field relations in the study area suggest that the complex sequence of interlayered supracrustal rocks, comprised of amphibolite, felsic volcanic and volcaniclastics, and metasediments, predate all other rocks in this region. Age relations among these supracrustal units are uncertain in this area due to limited stratigraphic facing relationships and evidence of intense tectonic transposition among these units. Crosscutting relations indicate that this assemblage has been extensively intruded by amphibolite, tonalite, granite, syenite, and a network of granitic pegmatite dikes. Table 2 shows relative

abundances of the major lithologies based on areal distribution, and a generalized sketch illustrating their relationships is presented in Figure 6.

Metamorphic rock names or prefixes are used throughout this study, except for igneous rocks where enough textural and geochemical evidence exists to support the use of original rock names. Thus, the intrusive rocks are classified using igneous terminology, and felsic supracrustal rocks with relict igneous textures are referred to as felsic volcanic and volcaniclastic rocks, rather than feldspathic schists. Metasedimentary rock names are based on metamorphic textures and mineral assemblages, which will be listed in decreasing order of abundance.

TABLE 2

Relative Abundances of Major Lithologic Units Based on Areal Distribution

TONALITE(t)	AMPHIBOLITE(a)	FELSIC VOLCANIC AND VOLCANICLASTIC ROCKS (fvc)
6%	50%	10%
GRANITES(gr)		
4%		METASEDIMENTARY ROCKS(ms)
SYENITE(sy)		15%
15%		

Intrusive Rocks

Supracrustal Rocks

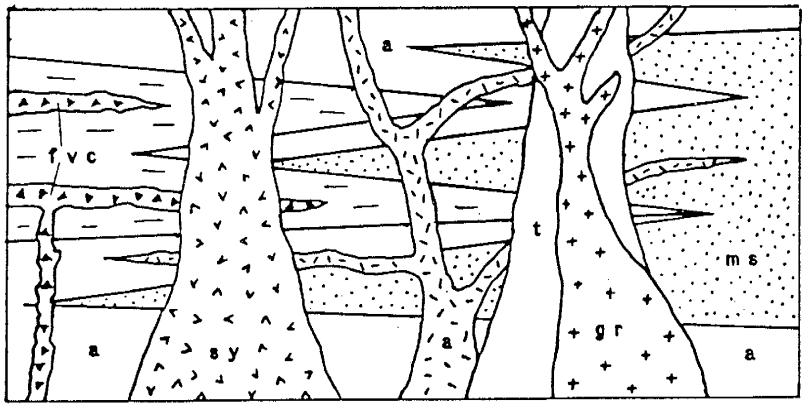

Figure 6. Schematic cross-section showing relations among major lithologic units.

AMPHIBOLITES

Amphibolites are the most abundant rock type within the mapped area and comprise approximately 50% of the total area of the Precambrian rocks. To the north of Spring Mountain they decrease in relative abundance giving way to a series of mafic and felsic metasedimentary rocks (Codding, in press). Due to their resistance to weathering, amphibolites commonly form massive, prominent cliffs. Outcrops typically contain contorted quartzo-feldspathic veins, as small as a few millimeters wide. These veins may be concordant or discordant to the amphibolite foliation and may show ptygmatic folding patterns. Locally both the veins and the amphibolites are intensely epidotized. Amphibolites are massive to well-foliated and range from aphanitic to coarse-grained. In the field and on the map, using an arbitrary distinction based on grain size, the amphibolites were divided into two groups: (1) aphanitic to fine-grained (<1mm), and (2) medium- to coarse-grained (≥1mm). Field and petrographic relationships, plus relict textures and structures, indicate multiple origins for both groups, including intrusive, extrusive, and volcaniclastic protoliths. Thus the amphibolites are, at least collectively, both supracrustal and intrusive in origin, and are therefore described separately in a section of their own.

Aphanitic- to Fine-Grained Amphibolites

The best exposures of this map unit occur in Hollinger Canyon and east of the ridge between Elk Mountain and Spring Mountain, along the headwaters of Johns Canyon and Beaver Creek. Outcrops are massive, generally very dense to only moderately foliated. In the northern portion of the study area these rocks are biotite rich, and may exhibit two well-developed intersecting foliations. Contacts with other rock units are commonly sharp, except with the pelitic-schists, gneisses and phyllites, in which relationships appear to be gradational. These amphibolites are dark greenish-gray to black and display a variety of relict igneous structures and textures, and to a lesser extent, sedimentary features suggesting the occurrence of both ortho- and para-amphibolites.

Ortho-amphibolites are characterized by well-preserved pillow structures, inter-pillow breccias, amygdules, and intrusive contact relationships. Narrow, arcuate selvages several centimeters in thickness define individual pillows and/or lava tubes up to 1.5 meters in diameter (Fig. 7). Selvages are typically darker green in color than the rest of the structure. Pillow-breccias consist of smaller (typically $\leq$ 30 cm), irregularly-shaped fragments and pods, with or without well-developed selvages, set in a mafic matrix (Fig. 8).

Figure 7. Cross-sectional exposure of isolated pillow (or lava tube) in aphanitic- to fine-grained amphibolite.

Figure 8. Irregular shaped fragments and pods of pillow-breccia in aphanitic- to fine-grained amphibolite.

These pillows provide the best stratigraphic facing relationships in this area (see Plate 1). Junctions among pillows may be voids but are commonly filled with inter-pillow breccia consisting of small (1-3cm) subangular to subrounded selvage and pillow fragments in a fine-grained mafic matrix. Such breccias may form by explosive fragmentation of the glass rind of rapidly cooling lava tubes and pillows (Rittman, 1962), but erosion, gravity-induced breakup, and deposition of pillow fragments during their formation is also common. Spherical to slightly elongate amygdules less than 3mm in diameter are quite common, and represent relict vesicles. Irregular contact relationships in addition to xenoliths of felsic volcanic, volcaniclastic and metasedimentary rocks within very-fine grained amphibolite along such contacts, indicate that amphibolites from this unit also occur as intrusives. Mafic dikes and/or sills of varying thickness are abundant in the southern half of the study area, intruding both metasedimentary and felsic volcanic and volcaniclastic rocks. In general, these ortho-amphibolites appear to be very-fine grained and dense, only rarely exhibiting well-developed foliations.

In thin section, aphanitic- to fine-grained amphibolites consist predominantly of light olive- to bluish-green hornblende laths (25-40%) actinolite-tremolite (0-25%) and plagioclase (30-35%), with minor amounts of

chlorite (0-15%) quartz (<10%) magnetite (<8%) sericite (<5%), and trace amounts of biotite, epidote, sphene, and apatite. Plagioclase grains are generally untwinned, although values of An 38-42 were obtainable from one sample containing abundant plagioclase laths with combined carlsbad-albite twins. Amphibole and biotite are partially replaced by chlorite. Amygdules may exhibit concentric layering, typically with quartz and magnetite along the edges and sericite, plagioclase, amphibole, epidote,and hematite concentrated in the centers (Fig. 9). Others show small hornblende laths radiating from the rims with centers of quartz, plagioclase and epidote. Pillow-selvages may show a coarsening of grain size along the rims, although the darker color of the pillow margins appears to be primarily a compositional change. The darker edges are predominantly actinolite or hornblende plus epidote. Towards the center plagioclase becomes increasingly abundant, commonly as minute laths exhibiting carlsbad twinning (Fig. 10). This figure also shows two horizons of relict micro-vesicles (<0.2mm) concentrated along the outer and inner edges of the selvage.

Such layering suggests two or more periods of lava flowage; the first episode producing a lava tube with volatiles rising towards the surface, and a later, slightly more alkali-rich, lava which cools within the pre-existing lava tube.

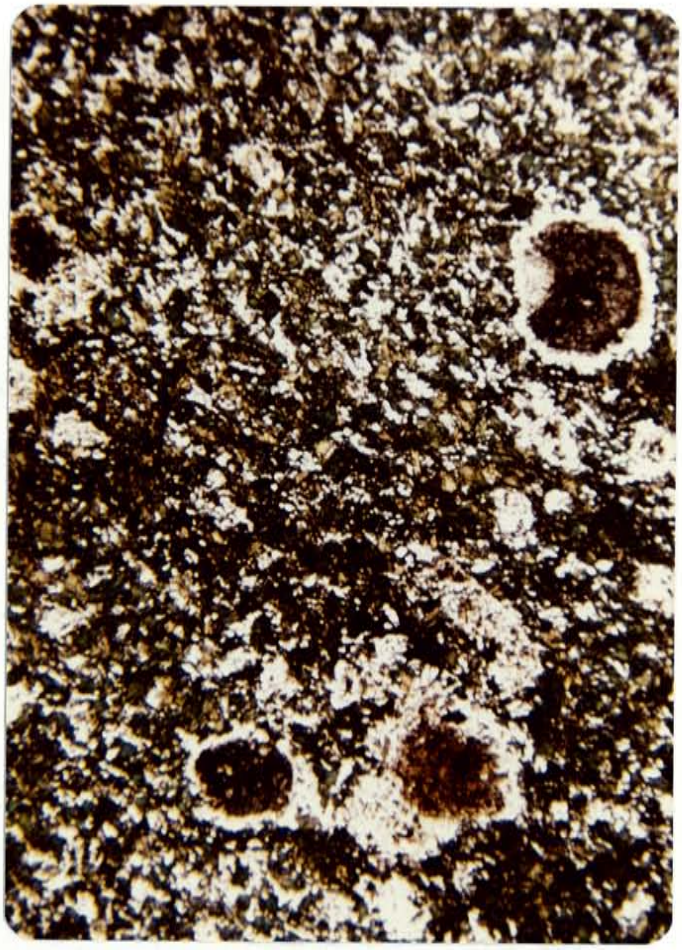

1 mm

Figure 9. Photomicrograph of amygdules in metabasalt, 1X, plane-light.

Figure 10. Photomicrograph of pillow-selvage in metabasalt, with core of pillow downward, 1X, plane-light.

The volatiles of this later lava are thus trapped along the inner margin of the initial tube. This may account for the compositional variations observed between the selvages and the inner pillow, although spilitization and/or metamorphic diffusion may also produce such variability in the composition of lavas.

Para-amphibolites are more difficult to distinguish in the field. They are recognized by their greater quartz and biotite content, and may be slightly coarser-grained. Foliations are more pronounced, and thin ($\leq$ 1cm) compositional banding with felsic horizons commonly imparts a gneissic texture on these rocks. In addition to hornblende and plagioclase, these rocks may contain up to 40% quartz plus biotite. Mineralogical banding consists of foliated hornblende and biotite laths interlayered with granoblastic quartz, plagioclase and epidote. Relict detrital quartz grains are characterized by faint overgrowths.

Medium- to Coarse-Grained Amphibolites

Medium- to coarse-grained ($\geq$1mm) amphibolites are generally massive to well-foliated, commonly with relict igneous textures. Grainsize is generally skewed towards the 1-5mm range, but locally hornblende laths may exceed 5mm in length. This map unit is typically dark greenish-gray to

green in color both on fresh and weathered surfaces. Contacts with the other supracrustal rocks appear sharp. Small (1-3mm) white, subhedral plagioclase laths are typically randomly oriented and generally well-pronounced against the dark-green mafic matrix (Fig. 11). Such relict subophitic texture is commonly observed on weathered surfaces of less-deformed rocks and suggests that these amphibolites are also ortho-amphibolites.

In thin section, these amphibolites predominantly consist of green hornblende (40-60%) actinolite-tremolite (10-35%) and plagioclase (20-35%), with minor amounts of chlorite (<10%) quartz (<5%) magnetite (<5%) sericite (<5%), and trace amounts of biotite, sphene, and epidote. Plagioclase is andesine (An 30-38) in composition, and is both untwinned and twinned according to the albite and combined carlsbad-albite laws. Sericitic alteration of plagioclase is common. The overall texture ranges from granoblastic or decussate to well-foliated depending on the habit and orientation of the amphibole laths.

This unit also includes a distinctive, non-foliated porphyritic-amphibolite containing large (up to 3 cm) equidimensional, euhedral to subhedral, plagioclase phenocrysts and glomeroporphyritic aggregates in a fine-grained (<1mm) mafic matrix (Fig. 12). It is intrusive into the supracrustal succession, but does not appear to

crosscut the younger granitic intrusives. Plagioclase crystals are labradorite (An 55-62) in composition, and may comprise up to 50% of the rock. On the weathered surfaces, the phenocrysts are milky white to light greenish-gray, commonly exhibiting synneusis texture. In thin section, they may appear completely opaque due to intense sericitization. The dark green matrix consists primarily of actinolite, hornblende, chlorite and sericite, with minor or trace amounts of biotite, quartz, magnetite and epidote.

Thus, amphibolites within this study area are complex and appear to have originated in various ways. The finer-grained amphibolites are thought to represent subaqueous meta-basalt flows, mafic volcaniclastic sediments, and shallow dikes and sills. The coarser-grained amphibolites are believed to be diabasic and gabbroic hypabyssal dikes and sills, and probably represent feeders to higher parts of the volcanic pile.

Figure 11. Relict subophitic texture in medium-grained amphibolite (metadiabase).

Figure 12. Cumulate plagioclase in porphyritic-amphibolite.

SUPRACRUSTAL ROCKS

Field relations indicate that the supracrustal succession of felsic volcanic and volcaniclastic rocks metasedimentary rocks, and amphibolite are the oldest rocks within the map area. Although the amphibolites comprise a major portion of this succession, they have been described separately (see page 24). Stratigraphic facing relationships have not been recognized within the metasedimentary rocks or the felsic volcanic and volcaniclastic rocks. Internal and map-scale transposition is well-developed among each of these units and has produced discontinuous, lenticular horizons which appear to be interlayered with one another. Throughout this region, the supracrustal rocks are intruded by younger syn- to post-tectonic igneous plutons.

Felsic Volcanic and Volcaniclastic Rocks

Felsic volcanic and volcaniclastic rocks make up approximately 10% of the Precambrian rocks in this region and predominate along the eastern and southern margins of the field area, with minor occurrences in the northwestern, central, and southwestern regions of the map area (see plate 1). They are commonly intimately interlayered with the other rock units of this area. Such layering is both tabular and lenticular, and is best developed where felsic

volcanic or volcaniclastic rocks are intimately interlayered with the metasedimentary rocks. Along the eastern boundary north of Beaver Creek, several outcrops show intrusive relations into the surrounding amphibolites. In the southern region, felsic volcanic rocks are themselves intruded by numerous mafic dikes and sills of variable thickness, most of which are too small to be mapped at the present scale.

This map unit is generally massive, less commonly thinly laminated, with foliations defined by the alignment of mica grains, stretched phenocrysts and compositional layering. Banding is best observed on weathered surfaces and is produced by changes in the abundance of phenocrysts and by the presence or absence of mica-rich horizons.

Petrographically and chemically (see geochemistry section) this unit ranges from rhyolite to dacite. Fresh surfaces are typically pink to dark gray depending on the composition, but weathering produces a wide variety of colors ranging from light pinkish-tan to dark brown and gray. These rocks are porphyritic in texture with relict anhedral to euhedral feldspar and quartz phenocrysts comprising approximately 10 to 35% of the rock. Phenocrysts are generally 1 to 3 mm in length, with plagioclase crystals commonly ranging up to 10 mm in size (Fig. 13). In less deformed rocks, feldspar phenocrysts are randomly oriented

and less commonly broken crystal fragments are observed. Fine-grained biotite- and/or muscovite-rich lenses, ranging from 0.5cm to greater than 10 cm in length, commonly occur within these phenocryst-rich rocks and may represent relict pumice and/or lithic fragments (Fig. 14). The remainder of such rocks consist of a microcrystalline (<0.1mm) granoblastic matrix of predominantly quartz, feldspar and mica.

The rhyolites are predominantly pink in color with abundant quartz and less common alkali-feldspar phenocrysts in a matrix of predominantly quartz (25-40%) alkali feldspar (30-35%) muscovite (15-20%), with minor plagioclase (<10%) and biotite (<7%), and trace amounts of magnetite, epidote, sericite and sphene. Plagioclase and muscovite are typically poikiloblastic with abundant quartz feldspar, epidote and magnetite inclusions. Quartz phenocrysts are commonly fractured or consist of recrystallized multi-granular aggregates.

Rhyodacites consist of 30 to 35% plagioclase, 25 to 30% quartz, 10 to 15% alkali feldspar, 10 to 20% muscovite, and 8 to 10% biotite, with minor and trace amounts of sericite, epidote, chlorite, magnetite, and calcite. Relict quartz and plagioclase (An30-34) phenocrysts are common, with plagioclase exhibiting imperfect twinning according to the albite and carlsbad laws.

Figure 13. Relict plagioclase phenocrysts in metadacite.

Figure 14. Mafic fragment in metadacite.

Bent twin lamallae are rarely observed. Subhedral to euhedral quartz phenocrysts are commonly optically continuous. Muscovite occurs as poikiloblastic porphyroblasts or as small foliated laths.

The dacites are composed primarily of plagioclase (35-50%) quartz (30-35%) and biotite (10-20%), with minor amounts of hornblende (<10%) muscovite (5-10%) magnetite (<7%), and trace amounts of apatite, epidote, chlorite, sericite, and calcite. Plagioclase phenocrysts are generally observed alone or with rare rounded quartz metacrysts in a matrix of plagioclase, quartz, and abundant biotite plus hornblende, giving the rocks a dark gray hue. Plagioclase ranges in composition from oligoclase to andesine (An16-32) and exhibits albite and carlsbad twinning. Rarely, compositional zoning is observed.

It is difficult to determine the exact nature of these lithologically and structurally complex volcanic rocks. In the field, rhyodacites and dacites appear to be more abundant than rhyolites. Intrusive contacts suggest that some of the rhyolites represent hypabyssal intrusives. The presence of broken phenocrysts, possible pumice and/or lithic fragments, and the microcrystalline granoblastic nature of the matrix, suggests an extrusive origin. The microcrystalline groundmass is thought to represent recrystallized glassy material; relict glass shards or

eutaxitic textures are not observed. Thus a pyroclastic origin is quite probable. Although sedimentary structures are not well preserved in this unit, it is believed that many of the rocks within this map unit are also reworked volcanics, and thus represent a volcaniclastic or epiclastic origin. The abundance of muscovite and biotite grains, possible lithic fragments, and the broad gradational nature into compositionally similar rocks lacking phenocrysts (felsic granofels) also supports an epiclastic interpretation.

Metasedimentary Rocks

Metasediments make up approximately 15% of the Precambrian rocks and are common throughout most of the study area. They are typically interlayered with both amphibolites and felsic volcanic and volcaniclastic rocks. Four separate lithologies or groups of lithologies are distinguished in the field: (1) felsic granofels and gneisses; (2) pelitic-schists, mafic gneisses and phyllites; (3) ferruginous quartzites; and (4) calc-silicate rocks. The latter two units are potentially useful as marker horizons, but represent less than 10% of the total metasedimentary sequence and are not continuous enough to map separately at the present map scale. They are therefore only idealized on the map to show occurrences and general relationships to the other units.

The felsic granofels and gneisses comprise approximately 40% of the area mapped as metasedimentary rocks. These rocks are characterized by their very-fine grain size (≤0.5mm) and general lack of mafic minerals; the granofels typically being quite massive and structureless, whereas the felsic gneisses are thinly laminated and commonly occur intimately interlayered with pelitic-schists and gneisses. Compositional layering is both tabular and lenticular and is more common in the northern half of the field area (Fig. 15). Other sedimentary structures such as crossbedding or graded-bedding were not observed in these rocks. However, small-scale, tight to isoclinal fold-noses are common. This map unit closely resembles the felsic volcanic and volcaniclastic rocks described earlier, and is differentiated in the field by the lack of obvious relict-phenocrysts. Although contacts between these units are obscured in most locations, the felsic granofels and gneisses appear to be gradational with the felsic volcanic and volcaniclastic rocks. Felsic granofels and gneisses are buff to light gray on fresh surfaces but weather to various shades of pink, gray and brown. Mineralogically, they consist primarily of quartz (30-60%) alkali feldspar (0-25%) and plagioclase (15-30%), with minor amounts of muscovite and biotite. Magnetite, epidote and garnet are common accessory minerals. Thin sections typically display a decussate texture with a slight foliation imparted by the

mica grains when present. The feldspars are generally granoblastic and untwinned, only rarely exhibiting microcline, carlsbad or albite twinning. Plagioclase grains are oligoclase to andesine in composition where determinable by the Michel-Levy method. Quartz grains display undulatory extinction and less commonly show overgrowths around relict detrital grains.

This unit is interpreted as metamorphosed arkosic sandstones. Except for fine laminations, these rocks rarely exhibit well-developed sedimentary structures. Moench and Robertson (1980) report local occurrences of cross-laminations within these rocks, but none were observed in the present study area. The fine compositional banding common to this unit is believed to be predominantly tectonic in origin. Tight to isoclinal fold-noses and lenticular fragmentation within these units, suggest that these rocks have undergone intense transposition, and therefore the banding may no longer represent original bedding structures. Since this unit appears gradational into the felsic volcanic and volcaniclastic rocks, it may represent a distal reworked facies thereof. It is also possible that these sediments were eroded from a granitic source elsewhere outside of the study area. The abundance of feldspars suggests that such a source, whether extrusive or intrusive, would have been nearby since increased transport distances would tend to produce cleaner, more quartz-rich sediments.

Pelitic-schists, gneisses and phyllites make up as much as 50% of the metasedimentary sequence. The best outcrop exposures are along the south side of Hollinger Canyon and along the northern boundary of the map area. This map unit contains several rock types, none of which are distinctive or abundant enough to map separately at the present scale. Included in this unit are quartz - plagioclase - biotite ± hornblende ± muscovite schists and gneisses, plus chlorite-rich phyllites. Due to their greater mica content, rocks within this map unit exhibit the best preservation of multiple deformations. Although not commonly well-pronounced, two foliations may be recognized.

The schists and gneisses are typically fine- to medium-grained (0.1-2mm), poorly to well-foliated, and may exhibit compositional layering due to varying proportions of biotite. Such layering is believed to be the result of metamorphic segregation. Although contact relationships are unclear, these rocks appear to grade into the fine-grained amphibolites. Contact relationships with interlayered felsic granofels and gneisses are generally sharp and concordant to compositional banding. Figure 16 shows tectonically fragmented felsic granofels interlayered with pelitic-schist. Weathered surfaces range from pink to dark gray, and commonly resemble weathered varieties of both the felsic granofels and gneisses, and the fine- to medium-grained amphibolites.

Figure 15. Compositional layering in felsic gneiss.

Figure 16. Lenticular fragments of felsic granofels in pelitic-schist.

The abundance of biotite and the light- to medium-gray color on freshly broken surfaces distinguishes these rocks in the field. Magnetite, garnet, staurolite and tourmaline are common accessory minerals, the latter three typically occurring as porphyroblasts up to 1 cm in diameter.

Locally, rare occurrences of float exhibit a highly fragmental texture with subangular to rounded, elongate, white to pale green fragments up to 2cm in length. They consist of very-fine grained (≤0.1mm) quartz, plagioclase and epidote, with minor biotite, sericite, magnetite and hematite in a slightly coarser (≤0.5mm) biotite rich matrix. Abundant quartz overgrowths within these fragments suggest that they may represent relict lithic fragments. Poikiloblastic hornblende and tourmaline porphyroblasts are common. Microcrystalline fragments composed of sericite, epidote and quartz may represent relict pumice. Although slight compaction of the fragments seems apparent, they do not appear to be the result of tectonic transposition.

Phyllites occur in a few outcrops along the ridge to the east of Spring Mountain, along the south side of Daily Creek and at the head of Hollinger Canyon. Northeast of Spring Mountain these rocks are found closely associated with calc-silicate rocks. They are green to greenish-gray in color, very-fine grained (≤0.2mm), well-foliated and may exhibit a phyllitic luster. These rocks consist primarily

of chlorite, actinolite-tremolite and epidote, with lesser amounts of quartz biotite and magnetite.

Pelitic-schists and gneisses of this study area are thought to represent mafic volcaniclastic rocks, or metagraywacke. Their relationship with fine-grained amphibolites suggest that some of these sediments may represent slightly more distal and reworked basaltic lavas. The phyllites are interpreted as mafic metashales and probably represent a low-energy environment (possibly marine) where fine-grained sedimentary material was deposited.

Ferruginous quartzites rarely occur in outcrop, but are commonly found as discontinuous horizons of dark purplish-black float up to several meters thick and generally trending parallel to regional foliations. These horizons appear to be lenticular bodies interlayered with amphibolites, metasediments and felsic volcanic and volcaniclastic rocks. Locally small isolated outcrops exhibit sharp contacts which are concordant to fabrics within the surrounding rocks. In large outcrops along Hollinger Canyon, thin ferruginous quartzite lenses ($\leq$3 cm thick) are intimately interlayered with felsic volcanic and volcaniclastic rocks (Fig. 17). The lenticular and fragmental nature of these horizons suggests that they are tectonically transposed.

Figure 17. Transposition-layering in rhyodacites (pink) and ferruginous quartzite (dark-gray).

These lenses are generally massive and composed of very fine-grained disseminated quartz (0.1-0.4mm) and magnetite (≤0.1mm) grains with trace amounts of feldspar, apatite, chlorite, and muscovite. Quartz grains are typically anhedral, but may exhibit polygonal grain boundaries. Rare relict detrital quartz grains were observed in one thin section. Banding on a millimeter scale within these horizons is common and is produced by magnetite-rich layers alternating with more felsic layers. In thin section, abundant disseminated magnetite grains are commonly observed extending into the surrounding rocks. Hematite may also occur along with the quartz and magnetite. One small occurrence of specular hematite is present in a prospect pit east of Spring Mountain. Possible cross-laminations are defined by magnetite, hematite, epidote, and chlorite-rich laminations (Fig. 18). The small fold seen in the lowermost lamination may represent soft sediment deformation, although transposition may have produced both features.

Although their discontinuity may largely be the result of tectonic transposition, these ferruginous quartzites are referred to as "ironstone" rather than "iron formation", since they do not form a mappable unit (Kimberley, 1978). Ironstone is used to describe a chemical sedimentary rock containing greater than 15% iron, whereas iron formation refers to a mappable rock unit composed primarily of ironstone.

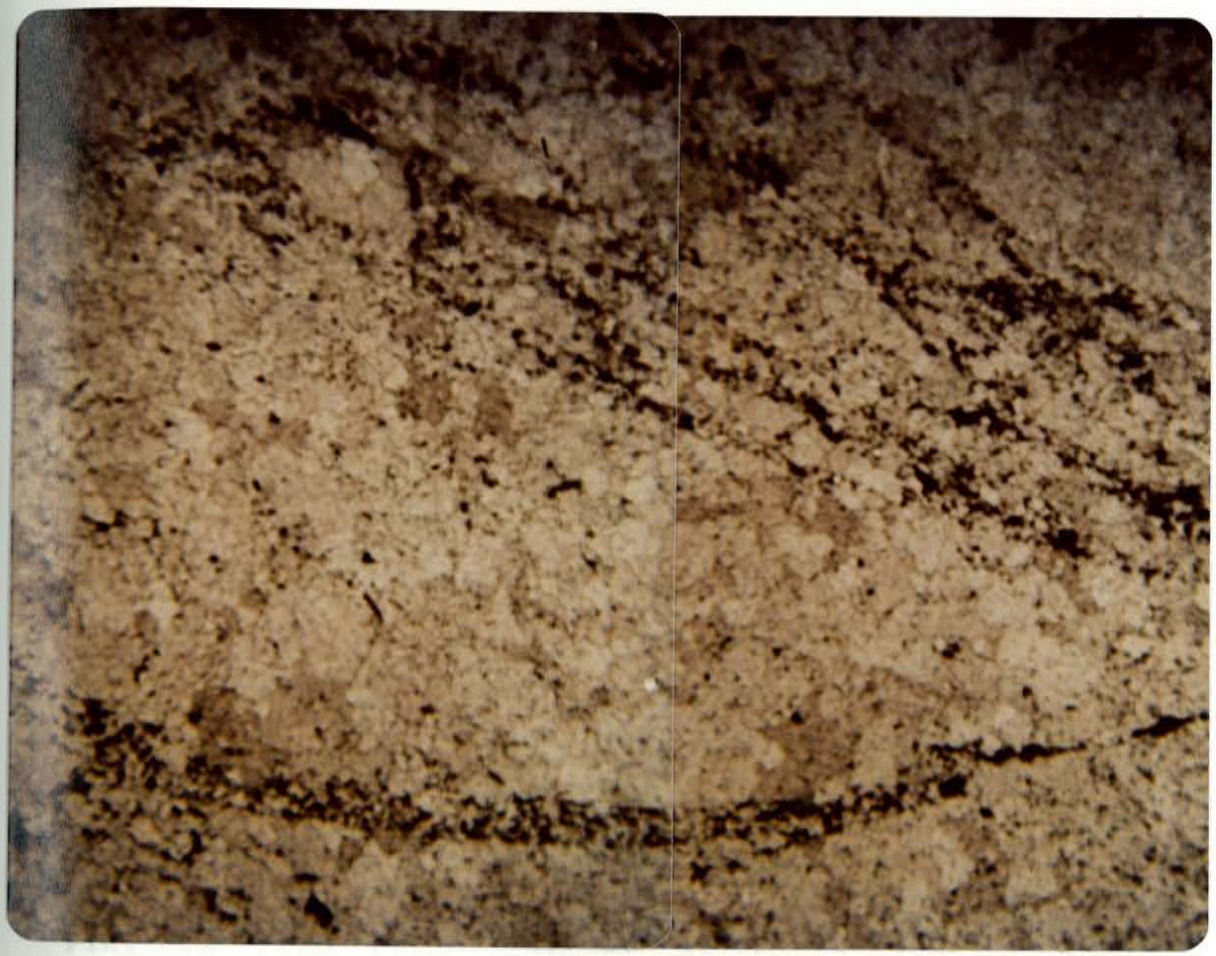

1 mm

Figure 18. Photomicrograph of cross-laminations in ferruginous quartzite, 1X, plane-light.

This definition implies deposition by chemical precipitation. The quartz present in these rocks is primarily interpreted as recrystallized chert. Based on limited observations, it is also believed that some of these rocks may in part be of clastic origin, possibly reworked ironstones or iron formation, as is suggested by relict detrital quartz grains and possible cross-laminations. Such features may represent local influx of terrigenous detritus during chemical sedimentation This, together with the lack of extensive shallow-water domains, and the interruption of chemical sedimentation due to eruption of volcanic material, is thought to be the cause for the thin and localized extent of iron formations within volcanically active terranes. Kimberley further classifies iron formations on the basis of paleoenvironmental interpretations of the ironstones and their rock associations. The close association with submarine volcanic and volcaniclastic rocks suggests that these ironstones resemble Kimberley's Shallow-Volcanic Platform Iron Formation, or according to Gross (1965) resemble Algoma-type deposits.

Calc-silicates form small, discontinuous outcrops along the ridge east of Spring Mountain. These rocks are grayish-green to white in color, thinly laminated and generally are vertically to steeply dipping. Selective weathering along less resistant layers gives the rock a distinctive outcrop appearance. Although contact relations

are obscured in most locations, this unit appears to be closely associated (interlayered ?) with the chlorite - bearing phyllites and less commonly with fine-grained amphibolite (Fig. 19). This assemblage is typically enclosed by the felsic granofels and gneiss unit. The total thickness of this unit rarely exceeds 10 meters, although isoclinal folds found within these rocks (see Fig. 20) suggests that this unit may have undergone tectonic thickening, and therefore may bear no relationship to the original stratigraphic thickness. In this sample the white folded horizon consists almost totally of carbonate. Other samples show lesser amounts of calcite together with variable amounts of quartz, feldspar, diopside, biotite, hornblende, actinolite and epidote, with trace amounts of magnetite, sphene and sericite. Quartz and feldspar grains are generally granoblastic and less than 0.2mm in dimension Biotite occurs as small laths, and hornblende is commonly poikiloblastic with abundant quartz calcite, epidote and biotite inclusions. Calcite megacrysts range up to 2mm in size and may contain inclusions of quartz diopside, biotite and epidote.

This unit is interpreted as impure meta-limestones and marbles. Its close association with mafic phyllites and fine-grained volcaniclastics suggests that quiet deposition of clastic sediments alternated with intervals of chemical precipitation.

Figure 19. Calc-silicate interlayered with aphanitic- to fine-grained para-amphibolite.

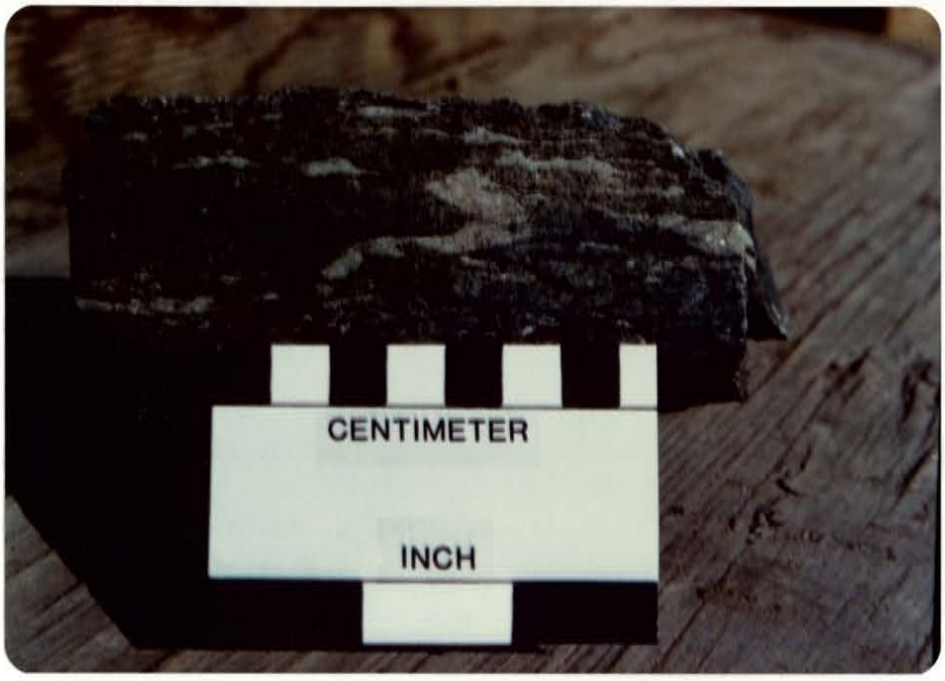

Figure 20. Small-scale isolated fold-nose in calc-silicate.

In general, the volcanic and volcaniclastic rocks are the most likely source for the majority of the sediments found in this area. They are believed to have been deposited very near their source. The abundance of feldspar and lithic fragments in the pelitic-schists and mafic gneisses indicates rapid erosion, transportation, deposition and burial, thus preventing complete chemical weathering. The phyllitic and chemical sediments are characteristic of a low-energy environment, and are believed to represent part of a sedimentary sequence deposited during a pause in volcanic activity, since it is commonly assumed that volcanism and chemical precipitation are antipathetic (Dimroth, 1976).

INTRUSIVE ROCKS

In addition to the intrusive amphibolites previously mentioned, several other varieties of Precambrian igneous plutons and dikes are exposed within the study area (see plate 1). They include tonalite, granite, syenite and pegmatite. These subdivisions are based primarily on mineralogical and textural differences observed in the field but are also in agreement with geochemical classifications (see geochemistry section). Figure 21 also depicts such rock types based on a modal mineral analysis classification system after Streckeisen (1973). Except for the foliated-granite, granitic intrusives are massive and

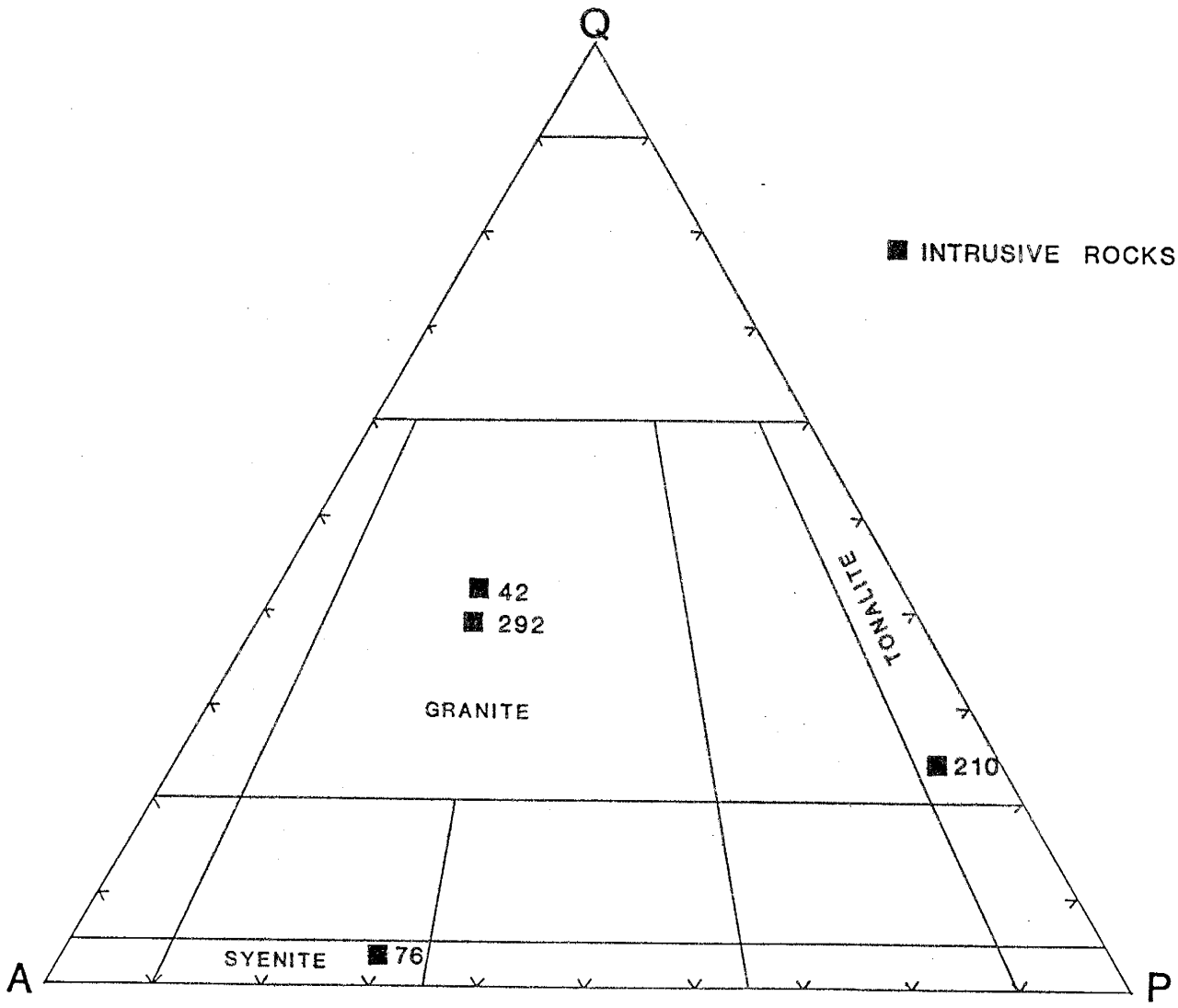

Figure 21. A-Q-P modal analysis classification of granitic intrusive rocks (after Streckeisen, 1973).

generally undeformed. Cross-cutting relationships and xenoliths of country rock within the intrusives suggest that these rocks are younger than both the supracrustal rocks and the intrusive amphibolites.

Tonalite

Tonalite is exposed in outcrop along the southeastern margin of the field area, where it is intrusive into the amphibolites. In this region it is, in turn, intruded by a younger granite and pegmatite dikes. Along the ridge south of Spring Mountain, tonalite occurs only in float, commonly with xenoliths of amphibolite (Fig. 22). Flow-like structures within the tonalite are well developed around such inclusions. This unit comprises approximately 6% of the Precambrian rocks in this region.

The main body of tonalite is dark gray and white, homogeneous, medium-grained (1-5mm) and normally is non-foliated, although along the margins of the pluton the tonalite exhibits a slight foliation, interpreted as flow-structures. Weathered surfaces are rust to medium brown, typically with ovoid quartz and feldspar lenses, up to 0.8 cm in length, standing in relief. Along contacts these lenses are oriented elongate to the developed flow-foliations.

Figure 22. Tonalite with amphibolite xenoliths.

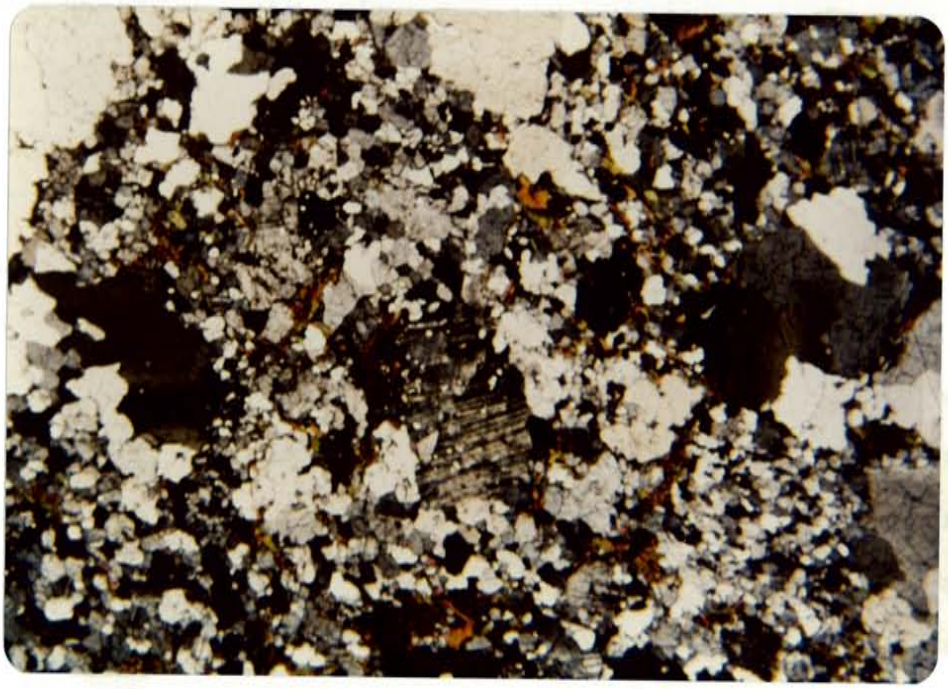

Figure 23. Photomicrograph of cataclastic texture in tonalite.

Mineralogically, the tonalite is composed of plagioclase (30-50%) quartz (15-25%) green hornblende (10-20%) biotite (10-20%), with minor amounts of microcline, magnetite, sphene, zircon, apatite, epidote-zoisite, and chlorite. One sample also contains minor blue-green tourmaline. Plagioclase is andesine (An32-45) in composition and rarely exhibits compositional zoning. Hornblende and biotite are slightly altered to chlorite.

The overall microscopic texture is cataclastic with xenoblastic grains of feldspar and quartz commonly surrounded by a crushed matrix of quartz, feldspar, and biotite (Fig. 23). Most grains show strain fractures, and bent twin lamallae are observed in plagioclase. Quartz grains have sutured boundaries and typically exhibit undulatory extinction. Twinning in plagioclase is generally according to the albite law but is also observed in combination with pericline and carlsbad twinning. Untwinned plagioclase also occurs in thin section and commonly is poikiloblastic with quartz, biotite, apatite, and zircon inclusions. Rarely, plagioclase shows myrmekitic texture. Hornblende and biotite are also poikiloblastic with abundant inclusions, including magnetite, sphene, zircon, and apatite. Bent biotite laths and twinned hornblende grains are also present. Thin sections normally show pervasive sericitic alteration and less commonly saussuritization of plagioclase.

Granites

Two types of granite, a foliated and an unfoliated variety, are differentiated within the study area and make up approximately 4% of the total area of Precambrian rocks. They are very similar to one another both mineralogically and chemically (see geochemistry section). Moench and Robertson (1980) refer to the foliated granite as "quartz-porphyry" and to the unfoliated granite as "pink-biotite granite". Based on outcrops outside of the mapped area, they have interpreted the "quartz-porphyry" as being broadly gradational into the "pink-biotite granite". Such a relationship cannot be substantiated in this region since these two rock units are not found in contact or even near one another.

The foliated-granite is only exposed in one outcrop along the western portion of the map area (see plate 1). Foliations within this unit trend parallel to dominant northeast regional foliations in the surrounding rocks. Intrusive contacts with fine-grained amphibolite are found in float, although the present contact appears to be fault bounded (see structure section). In addition to its well-developed foliation, it is distinguished from the unfoliated-granite by the presence of prominent clear, purplish-gray, elongated quartz lenses up to 1 cm long, and subhedral relict feldspar phenocrysts up to 5 mm long, in an

aphanitic to fine-grained (0.1-0.5mm) matrix (Fig. 24). Such megacrysts commonly comprise 30-50% of the rock (approximately 40% of which are quartz, and 60% are feldspar). In thin section, the quartz lenses are comprised of multi-granular aggregates of quartz biotite clots are rare, and muscovite accounts for roughly 15% of the total mineralogy. Matrix quartz is recrystallized displaying sutured grain boundaries and has undulatory extinction. The porphyritic texture suggests that this foliated-granite may represent a hypabyssal intrusive.

Although more abundant, the only exposures of unfoliated-granite are located in the southeastern portion of the study area within Hollinger Canyon, and along ridges both to the north and south of the canyon. Exposures of float and bedrock form long, narrow, arcuate bands closely associated with the tonalite into which it intrudes (see plate 1). Within Hollinger Canyon and to the north, this granite also intrudes amphibolite in outcrop. Contacts are sharp and both concordant and discordant to foliations within the amphibolite.

The unfoliated-granite is flesh pink with randomly oriented black biotite clots, and weathers to a reddish-brown color (Fig. 25). It is typically fine- to medium-grained (≤3mm), homogeneous, massive, and consists primarily of alkali feldspar (30-40%) quartz (30-35%)

plagioclase (15-20%) and biotite (5-10%). Minor amounts of magnetite, sericite, chlorite, and trace amounts of sphene, epidote, muscovite and calcite are also present. Alkali feldspar is comprised predominantly of microcline plus orthoclase, and plagioclase varies in composition from oligoclase to andesine (An25-32). Secondary alteration products include chlorite after biotite, hematite after magnetite, and sericitization of the feldspars.

The microscopic texture is cataclastic with large (1-2mm) xenoblastic grains of feldspar surrounded by a finer grained crushed matrix of quartz and feldspar. Strain fractures, bent twin lamallae, and sutured grain boundaries are commonly observed. Quartz and feldspar grains show undulatory extinction. Poikiloblastic and exsolution textures in feldspars are also present. Microcline rarely exhibits microperthitic intergrowths. Albite twinning is typical in plagioclase grains, although untwinned plagioclase with myrmekitic intergrowths are also quite common. Plagioclase is more intensely sericitized than alkali feldspar and typically contains abundant inclusions.

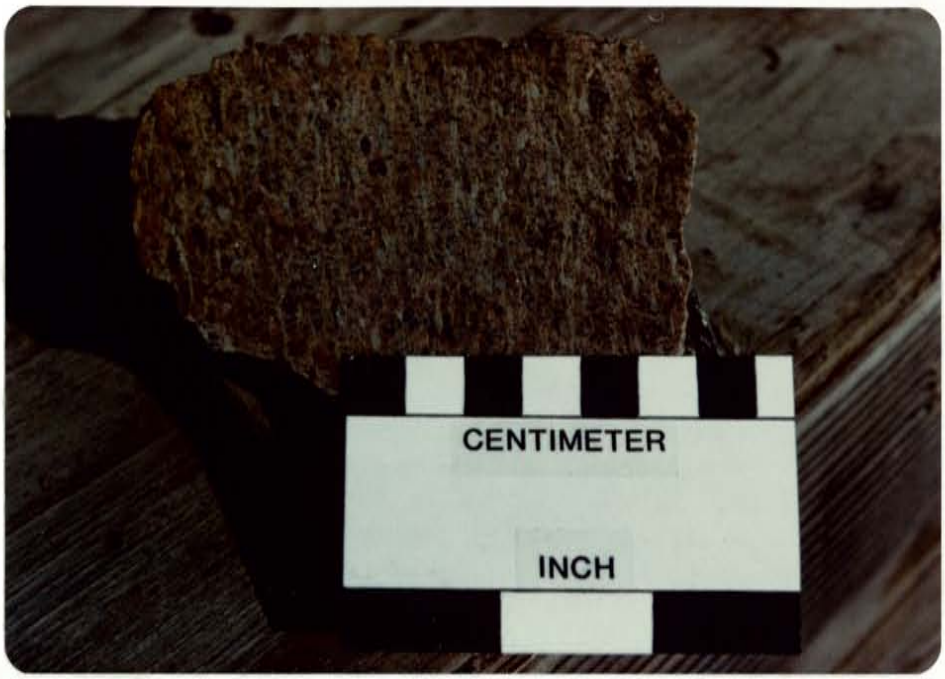

Figure 24. Foliated-granite.

Figure 25. Unfoliated-granite

Syenite

Two north-south trending syenite bodies, comprising approximately 15% of the Precambrian rocks, have been delineated in the north-central region of the field area. These sub-concordant bodies are typically observed intruding amphibolite, although intrusive contacts with the other supracrustal rocks are also locally present. Xenoliths of amphibolite are quite common near the contacts, ranging up to several meters in diameter. Large exposures of amphibolite within the main boundaries of the syenite body are interpreted as roof-pendants (see plate 1). Contacts with the surrounding rocks are sharp and both concordant and discordant to regional foliations.

The syenite is typically massive and medium- to coarse-grained, although locally, along the margins, it becomes much finer grained. Fresh surfaces are pink to pink and black depending on the amount of mafic constituents present (Fig. 26). Weathering commonly produces various shades of buff, pink, brown and gray, and tends to form spheroidal masses. In the field, the fine- to medium-grained syenite closely resembles the granite in both color and texture. Moench and Robertson (1980) mapped a large granite body along with several smaller ones to either side of the main syenite pluton, and postulate that a complete gradation may exist ranging from syenite through

quartz syenite to granite. Although some of the syenite does contain minor amounts of quartz (<10%), in the field, the sparcity of quartz in these rocks was used to classify them as syenites and consequently to distinguish them from the granite. Biotite is typically the major mafic constituent, although hornblende is also observed The coarser-grained syenite commonly exhibits large (up to 1.5 cm) tabular feldspars in synneusis relation.

In thin section, the syenite is comprised of alkali feldspar (45-60%: predominantly microcline, plus orthoclase) plagioclase (20-25%) biotite or blue-green hornblende (10-15%), with minor amounts of magnetite, chlorite, sericite, quartz, epidote, and trace amounts of apatite, sphene, allanite and zircon. Subhedral microcline and orthoclase laths typically exhibit microcline and carlsbad twinning respectively. Plagioclase (An16-30) also occurs as anhedral to subhedral laths with both albite and carlsbad twinning present. Myrmekitic texture and zoning is observed in some plagioclase. Mafic minerals are intergrown in clusters with magnetite, sphene and other accessory minerals, and are surrounded by feldspar laths. Both hornblende and biotite are slightly altered to chlorite.

The overall microscopic texture is cataclastic with feldspars up to several millimeters in length surrounded by a fine-grained crushed matrix. Strain fractures, bent twin

lamallae, and undulatory extinction are common among the feldspars. Alkali feldspars typically exhibit microperthitic intergrowths, and plagioclase, nearly opaque, is preferentially altered to sericite.

Amphibolites near contacts with the syenite are extensively altered, making their identification difficult. Moench and Robertson (1980) defined these altered rocks as "mela-syenite". They are dark green and pink in color, medium grained, and massive to slightly foliated (Fig. 27). Mineralogically, these altered amphibolites are composed of alkali feldspar (25-40%) hornblende (20-25%) biotite (10-15%) plagioclase (10-15%), with minor amounts of quartz, chlorite, sericite, and trace amounts of magnetite, sphene, epidote and apatite. Fractured grains and bent twin lamallae are common. Chemical data also supports potassic metasomatism of these rocks (see geochemistry section).

Figure 26. Coarse-grained syenite.

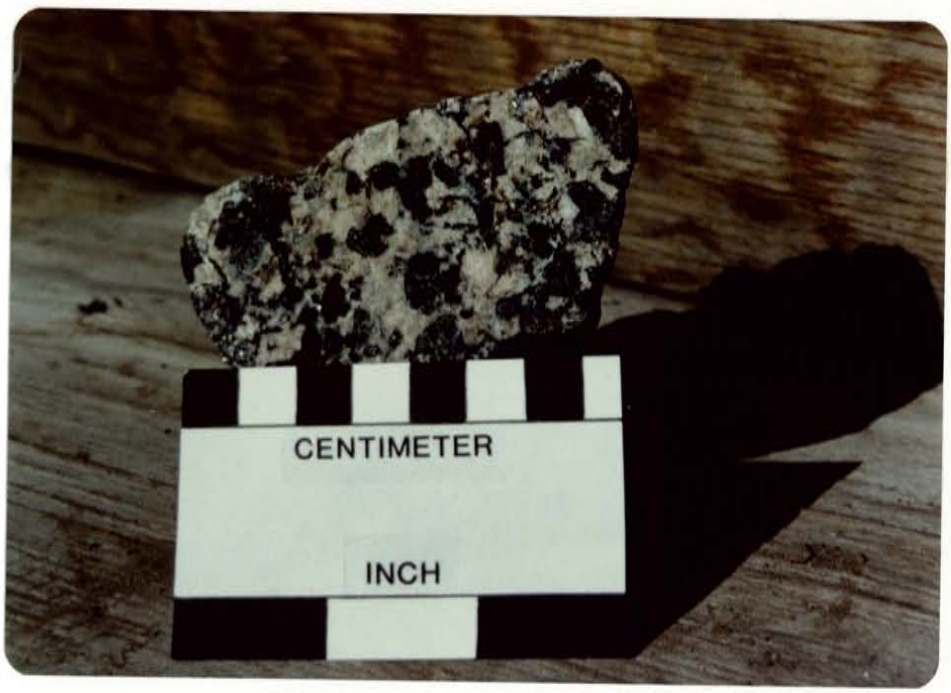

Figure 27. Medium-grained altered amphibolite.

Pegmatites

Outcrops of Precambrian pegmatite are quite abundant in the western and southern portions of the field area but only compose a few percent of the total area of Precambrian rocks. These pegmatites are the source for the mica deposits of the Elk Mountain (Kept Man) Mine located northeast of Elk Mountain and are described in detail by Jahns (1946).

In general, the pegmatites typically form long, narrow dikes and lensed-shaped pods up to twenty meters in width and several hundred meters long. They strike to the north-northeast and vary in dip from vertical to nearly subhorizontal. Pegmatites generally occur within the supracrustal succession rather than in massive granitic rocks, although a few pegmatite bodies are also found within the tonalite and granite units. Contacts with the country rock are sharp and discordant. Concentrations of dark green to black tourmaline occur in the amphibolite and quartz-mica schists adjacent to pegmatite outcrops. The schists are commonly also highly impregnated with fine- to medium-grained muscovite along such contacts.

The pegmatites consist primarily of varying amounts of microcline, quartz albite, and muscovite, with accessory spessartite, fluorite, and columbite (Jahns, 1946). The

accessory minerals were not observed in this study, but instead lepidolite and rose-muscovite, not previously documented in this locality, are commonly found within some pegmatites.

Age Relations Among Intrusive Rocks

The foliated-granite appears to be pre- to syntectonic. The tonalite, unfoliated-granite and syenite are interpreted as being younger, probably late syn- to post-tectonic, since they generally appear to conform to regional foliation trends, but do not exhibit evidence of major deformation. Wyman (1980) documents a foliated granite intruded by a younger non-foliated granite to the southwest of Elk Mountain, but it is unclear whether these units are the same as those found in this study area. A well-foliated tonalite-trondhjemite body is also reported from the same region, but petrographic and geochemical analyses suggest that this unit is not the same as the tonalite found in this study. The tonalite of this study contains much less quartz and plagioclase may be more sodic than the tonalite-trondhjemite described by Wyman. A similar well-foliated tonalite-trondhjemite from the Pecos River area indicates an age of 1.72 b.y. (Bowring, 1982). If indeed these units are of the same age, then explaining the general lack of regional deformation within the tonalite becomes problematic. The presence of a chilled zone within

the syenite indicates that temperatures of the pluton were significantly hotter than the surrounding country rocks. The lack of such a chilled margin within the unfoliated-granite indicates that temperatures of the country rock were closer to that of the intrusion. This relationship suggests that the unfoliated-granite was intruded prior to the emplacement of the syenite, probably shortly after maximum metamorphic temperatures were attained. Cross-cutting relationships between these two units are not observed within the study area. The lack of cross-cutting relationships between pegmatites and the syenite suggest that the syenite may be the latest intrusive event in this region, although such an interpretation is largely influenced by poor outcrop exposures.

STRUCTURE AND METAMORPHISM

Structure

Interpretations of structural relationships in the study area are complicated not only by poor exposures, but by the limited preservation of structural fabrics and stratigraphic indicators within the rocks. Distinctive marker horizons are rare and individual mappable units are lenticular and discontinuous. The supracrustal rocks are complexly interlayered sequences characterized both by sharp contacts and by subtle lithologic gradations. Original sedimentary features indicating stratigraphic younging directions are also rare. Pillowed basalts are the best facing indicators with tops predominantly to the northwest (see plate 1). Despite two periods of tight to isoclinal folding, Precambrian rocks in the area are only rarely well-foliated. The prominent fabrics are northeast trending axial plane cleavages and transposition layering.

FOLDING AND TECTONIC TRANSPOSITION

Rare small-scale isoclinal fold closures may be observed in each of the units comprising the supracrustal succession, although the best exposures are typically found only in float. Figure 28 shows such an isoclinal fold within the felsic gneiss. In addition, rare mesoscopic

tight to isoclinal folds are observed in metasedimentary rocks from the northeastern portion of the study area. Figure 29 is a tight fold refolding discontinuous lenticular fragments of felsic granofels, in addition to earlier isoclinal folds, suggesting at least two periods of folding. Wavelengths of these later folds range up to several centimeters, with folding typically disharmonic possibly due to ductility and thickness differences among the individual layers.

Map units along Hollinger Canyon define a broad map-scale synform trending northeasterly. Inconsistent facing directions of pillow basalts in this region (see plate 1) suggest that this fold is probably more complex than is shown on the map. Detailed mapping of individual lithologies may reveal that this fold is actually comprised of multiple tight to isoclinal folds. Another possibility is that the present fold is refolding an earlier fold, although detailed structural analyses are necessary to verify the presence of such additional folds.

Tectonic transposition results from the rotation of a pre-existing planar surface into parallelism with the axial plane of tight to isoclinal folds.

Figure 28. Small-scale isoclinal fold in felsic gneiss.

Figure 29. Small-scale tight fold in transposed felsic granofels (pink) and pelitic-schist (dark gray).

Continued strain parallel to axial surfaces may completely obscure the fold closures, producing what may resemble a normal stratigraphic sequence and is referred to as transposition layering (Turner and Weiss, 1963; Hobbs et. al., 1976).

Discontinuous, lenticular map units, isolated fold hinges and foliations parallel to compositional layering within the supracrustal rocks suggests that transposition has rotated original bedding parallel to present foliations. Extensive map-scale transposition is suggested by the discontinuous and lenticular nature of the mappable units (see plate 1). The regional northeast trends of these units correlate with an F2 folding event delineated by Codding (in press) to the north of the study area. This map-scale transposition may be related to such an F2 event. In hand-specimen, such transposed lenses may also be seen refolded (see Fig. 29), suggesting that transposition also occurred in a previous (F1) folding event. Preservation of the large-scale fold within Hollinger Canyon suggests that the F2 deformation and its associated map-scale transposition may have been less intense in the southeastern portion of the field area. Map units in this area may thus represent map-scale transposition during F1. To the north and west of this region, large map-scale folds are not recognized.

FOLIATIONS AND LINEATIONS

Foliations are best developed in amphibolites, metasedimentary rocks and some felsic volcanics of the supracrustal succession, and in the foliated granite that intrudes this succession in the northwestern region of the study area. Outcrops typically show one foliation generally trending north-northeast, although in the southeast part of the map area, regional trends are northwest to west-north-west. Regional foliations are typically vertical to steeply dipping. Thin sections show a prominent closely-spaced crenulation cleavage that only rarely crosscuts an earlier foliation at low angles. More commonly only one foliation was recognized. It represents an axial plane cleavage which parallels compositional layering within the felsic volcanic, volcaniclastics and gneisses. An S-pole diagram (Fig. 30) of 27 measurements from the southeast portion of the mapped area depicts folds from this region as reclined, with an axial plane striking N54^{o}W and dipping 70^{o}SW, and a fold axis trending 43^{o}, S35^{o}W. Figure 31 is an S-pole diagram of 135 measured foliations from throughout the rest of the map area and suggests that these foliations are the result of tight to isoclinal folding with a near-vertical axial surface. This style of folding in addition to the northeast trend is similar to the F2 folding event described by Codding (in press). The northwest

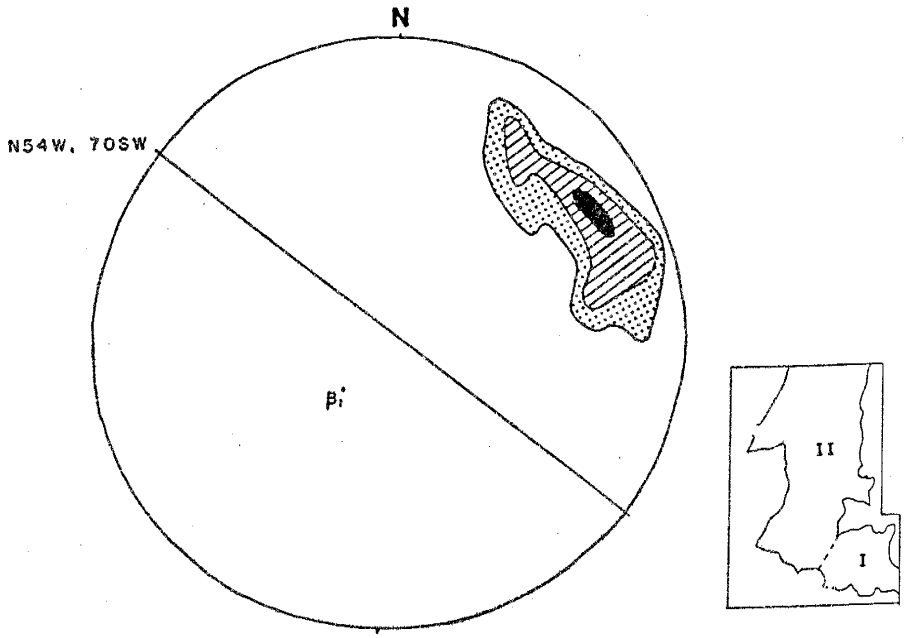

Figure 30. Equal-area stereographic projection of poles to foliation from Area I 6-12-18% contours per 1% area (n=27).

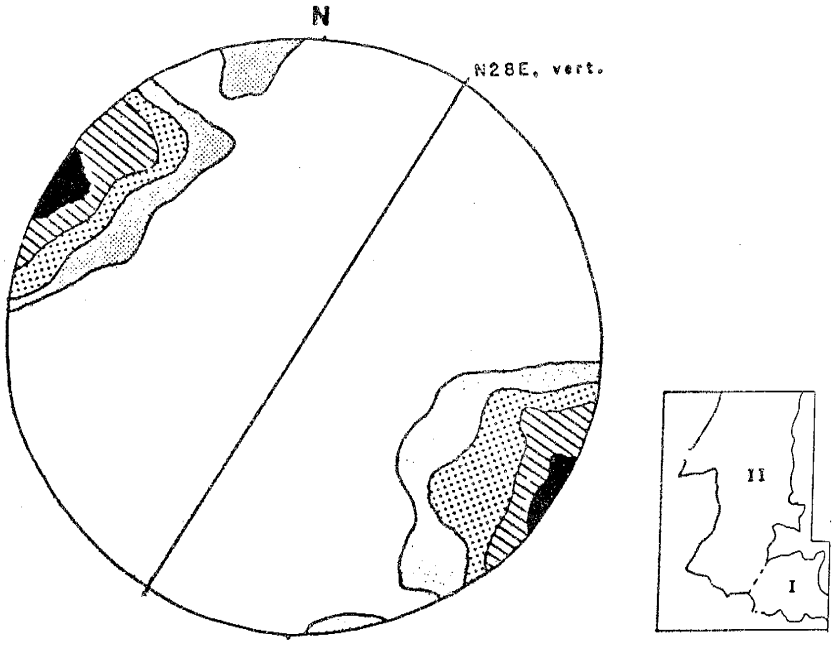

Figure 31. Equal-area stereographic projection of poles to foliation from Area II 3-6-9-18% contours per 1% area (n=135).

trending reclined folds depicted from the southeastern part of the study area may reflect earlier (F1) folding patterns which have not been completely obliterated by later F2 deformation.

Local internal foliations within the tonalite are generally parallel to intrusive contacts and are found only along the margins of the tonalite body. Since the major part of the tonalite body is undeformed, such foliations are thought to reflect primary flow structure developed within the tonalite during its molten stage.

A few mineral lineations consisting predominantly of aligned amphibole crystals within well-foliated amphibolites were measured. To a lesser extent lineations between intersecting foliations were also observed, although additional data are needed before detailed structural interpretations can be made.

FAULTS AND SHEAR ZONES

Several high-angle faults have been delineated on the basis of brecciation, shearing, alteration and the steeply dipping to near vertical orientation of Paleozoic strata. Due to lack of outcrop, dips of the fault planes could not be determined. Therefore these faults may represent normal faulting, high-angle reverse faulting or both. Although each of the faults offsets both Precambrian and Paleozoic

rocks, mapping of faulting within Paleozoic rocks was not attempted. Trends across Paleozoic horizons are therefore only inferred from the general trends of the fault zones as mapped along Precambrian-Paleozoic contacts. Detailed mapping by Baltz (1972) within the Paleozoics along the southeastern boundary shows additional and more complex fault traces.

Along the crest of Spring Mountain, Precambrian rocks appear to be in fault contact with vertical to steeply west-dipping Paleozoic units. Off the main ridge to the southwest, this fault contact becomes completely covered by Quaternary colluvium and only meager float reveals its presence. Although no major evidence of brecciation within Precambrian rocks was found, minor shearing and alteration within amphibolite float, slickenslide striations in Paleozoic float to the north and south of the Precambrian terrane, and the occurrence of springs along this zone suggest that a fault boundary is likely. The linear nature of this northeast trending fault trace, in addition to nearly 125 meters of topographic relief along its trace, suggests a near-vertical dip.

The Precambrian-Paleozoic contact along the southeastern margin of the study area is also fault-bounded. Abundant brecciation, alteration and shearing are observed in both Paleozoic and Precambrian float between Hollinger

Canyon and the ridge just north of Beaver Creek. To the south of Hollinger Canyon nearly vertical-dipping Paleozoic units along with topographic features suggest that this north-northwesterly trending fault zone extends beyond the mapped region to the southeast. The slightly sinuous fault trace across this terrane, with topographic relief up to 400 meters, suggests a steeply-dipping fault plane. Steeply east-dipping Paleozoic beds suggest that segments of the Precambrian-Paleozoic contact along the northeastern boundary of the map area may also be fault bounded. Additional evidence for faulting is meager in this region and therefore the existence of these northeast trending faults is somewhat conjectural. An additional northeast trending fault offsets Precambrian and Paleozoic rocks along the southern boundary of the study area. This fault probably extends into the Precambrian terrane to the northeast, although offset among individual Precambrian map-units is not discernible. Faults observed solely within Precambrian rocks are herein defined as shear zones (see plate 1). These shear zones may range up to 30 meters across and are characterized by intense brecciation, shearing and alteration of the rocks. Some shear zones coincide with post-Paleozoic fault trends and represent an extension of the fault trace into Precambrian rocks, others may be older in age.

JOINTS

Several occurrences of well-defined, parallel joint-sets are recognized throughout the field area. These joints generally trend to the northwest and are steeply dipping or vertical. The spacing between joints ranges from 10 to 20 centimeters.

DISCUSSION

It is clear that the deformational history of this study area is quite complex. Limited outcrop exposures, poor preservation of structural fabrics, and the incomplete knowledge of the stratigraphic sequence within the supracrustal rocks greatly hinders structural analyses in this region, and therefore structural interpretations from this study are only preliminary.

Nonetheless, the limited structural data obtained in this study do provide evidence for at least two periods of folding within the supracrustal rocks of this region. In addition, tectonic transposition is evident on all scales, producing a mixture of lithologies which in small domains simulates bedding. Despite such intense transposition among some of the supracrustal units, there are other units that do preserve original depositional surfaces such as the pillow basalts which appear much less deformed. The

orientation of original bedding may be preserved as enveloping surfaces to transposed lenses of the more competent lithologic units. A possible set of such enveloping surfaces for the combined felsic volcanic, volcaniclastic and metasedimentary units of the study area is shown in Figure 32. However, depending upon the number of folding events in this area, these surfaces may only represent previous folding surfaces. For a better understanding of the structural history, additional detailed analyses of smaller regions with good exposure are necessary. One such region is in the southeastern part of the present study area, along Hollinger Canyon.

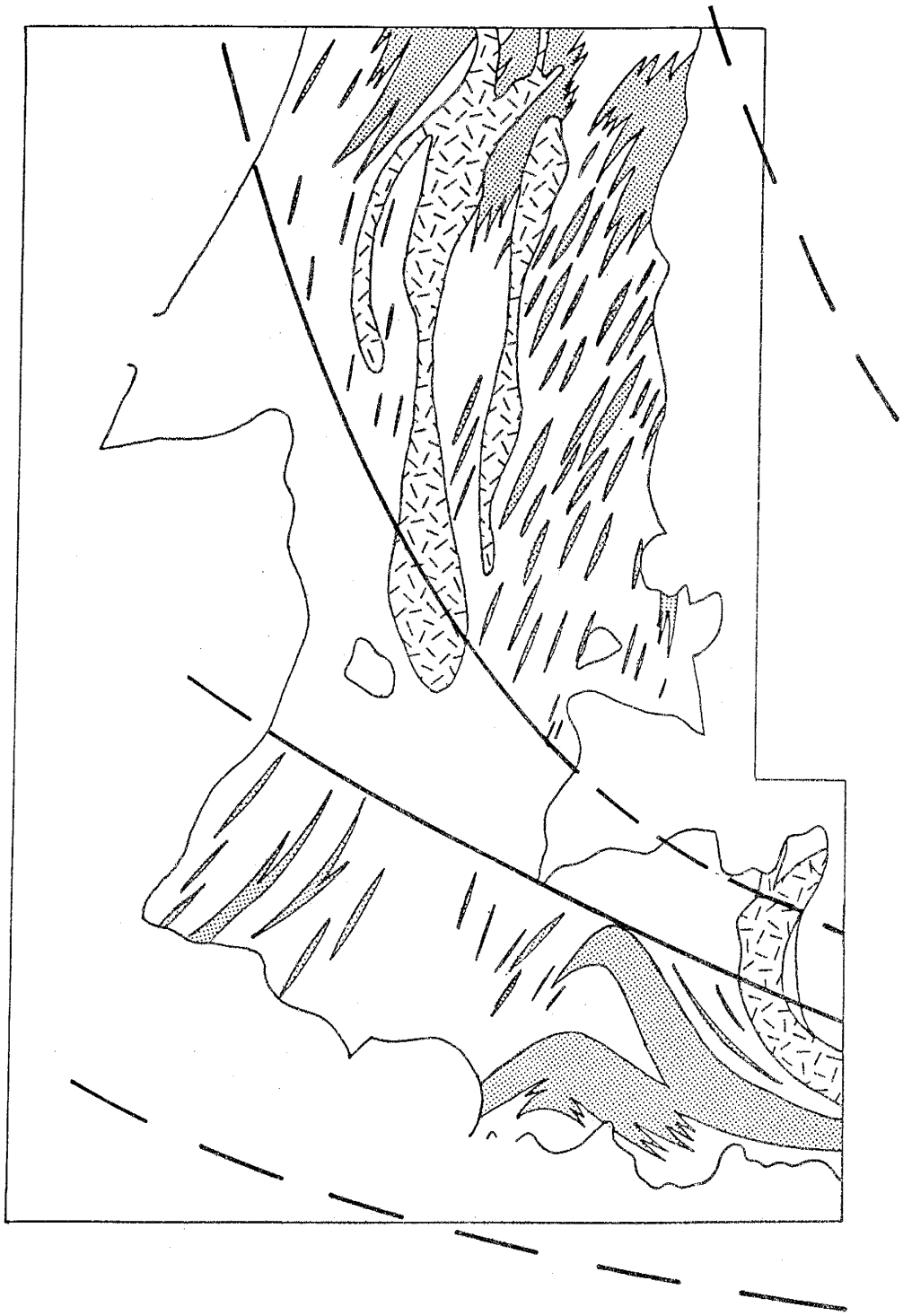

Figure 32. Generalized geologic map with enveloping surfaces defined by discontinous horizons of felsic volcanic, volcaniclastic, and metasedimentary units (stipled).

Metamorphism

During regional metamorphism Proterozoic rocks of the Elk Mountain-Spring Mountain area were subjected to pressure and temperature conditions of medium-grade metamorphism (Winkler, 1979) or lower amphibolite facies of the medium-pressure type as described by Miyashiro (1973). Evidence of both contact- and slight retrograde-metamorphism is observed throughout the study area, locally obliterating original metamorphic assemblages. Changing metamorphic conditions are best reflected in the mineral assemblages of amphibolites and metasedimentary rocks, since the felsic volcanic and plutonic rocks do not lend themselves to the formation of metamorphic index minerals.

Typical mineral assemblages of the amphibolites include: hornblende + plagioclase + quartz ± biotite ± chlorite ± epidote; hornblende + actinolite-tremolite + plagioclase + quartz ± chlorite ± epidote; and biotite + quartz + almandine. Hornblende is typically green to bluish-green and only rarely light brown in color. Miyashiro (1973) places the boundary between greenschist and epidote-amphibolite facies at the temperature where the dominant calcic-amphibole changes from actinolite-tremolite to hornblende. Since hornblende and actinolite-tremolite alternate as the dominant amphibole, it is believed that at least temperatures characteristic of epidote-amphibolite

facies metamorphism were attained. Plagioclase compositions are predominantly andesine (An 30-40) in composition, although a few occurrences of labradorite also occur. Miyashiro (1973) and Winkler (1979) both suggest that, in general, the anorthite content increases with metamorphic grade, although they indicate that exceptions do exist. Condie and Budding (1979) report the same high anorthite content in greenschist facies Precambrian rocks of south and central New Mexico, and attribute it to the incomplete recrystallization of mafic rocks formed at initially high temperatures with subsequent metamorphism to greenschist facies. Therefore, additional criteria must be used in conjunction with the plagioclase compositions to accurately determine metamorphic grade. Almandine rarely occurs within the amphibolites of this area. Since almandine is stable under a wide range of rock pressures, and its formation is dependent on additional variables such as the oxidation state and $Fe^{+2}/(Mg + Fe^{+2})$ ratios, its presence merely establishes a lower limit for temperature and pressure ($500^{o}C$ at 4 kb; Miyashiro, 1973).

ACF values for the amphibolites are plotted in Figure 33. Most of the samples analyzed lie on or near the hornblende-anorthite join, indicating that mineral assemblages are transitional between greenschist and amphibolite facies. Such assemblages are in agreement with those observed in thin section (see Appendix B).

The best indicators of metamorphic temperatures and pressures within metasedimentary rocks are found in the pelitic-schists, gneisses, and phyllites. Mineral assemblages characteristic of medium-grade metamorphism within these rocks include: quartz + biotite ± plagioclase ± muscovite; quartz + biotite ± hornblende; and quartz + biotite + garnet ± staurolite.

The first appearance of staurolite is good evidence that at least the low to middle temperature range of medium-grade metamorphism was attained (Winkler, 1979). Equilibrium conditions for the common staurolite forming reaction:

chlorite + muscovite = staurolite + biotite + quartz + H2O

have been established at 565°C ± 15°C at 7 kb and 540°C ± 15°C at 4 kb (Hoschek, 1969). Ganguly (1969) has shown that the formation of staurolite is restricted to 500-575°C at 4-8 kb in reactions involving the breakdown of chloritoid. He also shows that stability relations of staurolite may in some cases be governed by oxidation reactions involving neither chlorite or chloritoid, and therefore proposes that the formation of staurolite at the expense of chloritoid or chlorite, rather than merely the first appearance of staurolite, should be used to define the isograd "staurolite-in". The band of reaction-isograds "staurolite-in" is shown in Figure 34 and defines the

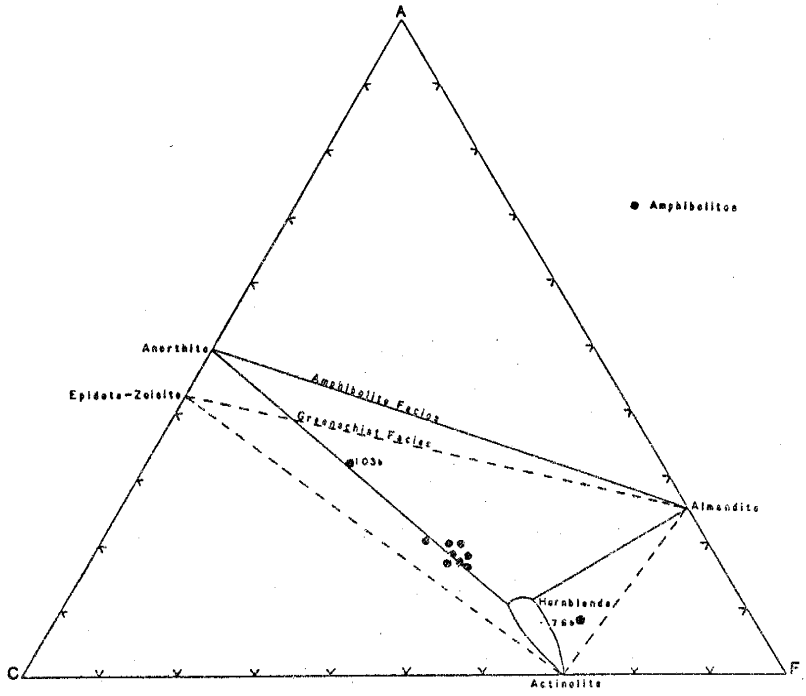

Figure 33. A-C-F diagram for amphibolites.

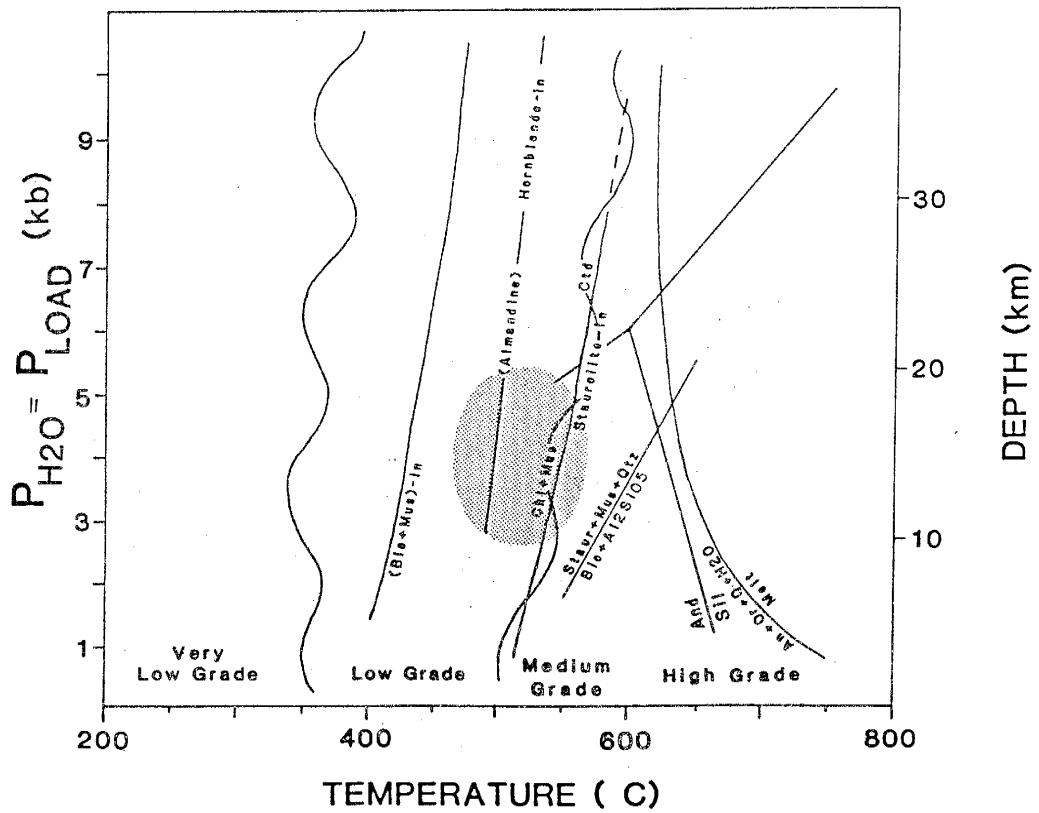

Figure 34. Pressure-Temperature diagram of metamorphic conditions (after Winkler, 1979)
shaded area - this study

beginning of Winkler's medium-grade division of metamorphism. This corresponds to the low-temperature range of the medium-pressure type "amphibolite facies" of Miyashiro (1973), and is in agreement with garnet-biotite geothermometry studies on rocks from this area which suggest temperatures of 500-520^{o}C at 4 kb (Grambling and Codding, per. commun., 1982).

Evidence of slight retrograde metamorphism is generally common to both the supracrustal and intrusive rocks of this study area. Retrograde mineral reactions which have been identified include chloritization of biotite and amphibole, sericitization of feldspars, and minor saussuritization of plagioclase.

The occurrence of weak cataclastic metamorphism, as defined by Winkler (1979), is evident in the field by fault and shear zones present throughout the study area. In thin section such features as strain fractures, bent twin lamallae, undulose extinction, mortar texture, minor exsolution perthite lamallae and pervasive sericitization of feldspars are all indicative of cataclasis within this region.

Although regional contact-metamorphic aureoles could not be identified, locally, the effects of contact metasomatic alteration adjacent to granitic plutons is quite spectacular. Most apparent is the intense, potassic-

metasomatism of amphibolite near the syenite intrusive (see rock descriptions). Approximately 25 percent of such rocks consists of alkali feldspar, typically giving it a distinct green and pink appearance. Chemically, an increase of P_2O_5 and MgO also accompanies the K_2O enrichment. Locally, hydrothermal alteration of the country rock by pegmatite intrusives is indicated by the increasing abundance of muscovite megacrysts, dark green to black tourmaline porphyroblasts, and the conversion of hornblende to biotite, with proximity to the boundary and size of the pegmatite dikes. Contact metamorphism and/or metasomatism has not been recognized in direct association with either the tonalite or granite plutons. This suggests that either the effects of contact metamorphism have been obliterated by later thermal events or, as Winkler (1979) points out, the mineral assemblage of rocks previously subjected to medium- or high-grade metamorphism are stable or at least persistent to contact metamorphic conditions. They therefore commonly do not show signs of contact metamorphic overprinting. The latter case appears most likely for the tonalite and the unfoliated-granite of this study. Randomly oriented porphyroblasts of garnet and staurolite suggest that maximum metamorphic conditions occurred after the last period of deformation (F2). Thus, temperatures of the supracrustal succession were closer to that of the intrusives such that contact-metamorphic aureoles were not extensively developed.

The foliated-granite appears to be pre-metamorphic since it shows evidence of F2 deformation. Therefore, its contact-metamorphic aureole may have been obliterated. Since this unit is only exposed in a very small portion of the study area, additional studies of the foliated-granite and surrounding country rocks are necessary to verify the lack of such aureoles.

GEOCHEMISTRY

Twenty-one samples were analyzed for major, minor and selected trace elements, using X-ray fluorescence (XRF) and instrumental neutron activation analysis (INAA) techniques described in Appendix D and E, respectively. Chemical analyses of amphibolites, felsic volcanic and volcaniclastics, and intrusive rocks are of primary interest in this study. The analyses supplement petrographic classification of these units and depict geochemical trends among the various volcanic and plutonic rocks. Prior to plotting, the major element analyses were recalculated to 100% on an anhydrous basis. CIPW norms are also presented with the respective analyses.

A major problem in studying the chemistry of Precambrian igneous rocks is identifying the extent to which alteration has affected the original composition of the rocks. Numerous investigations, Hart, et. al. (1974); Humphris and Thompson (1978a, 1978b); Hynes (1980); Mac Geehan and Mac Lean (1980); and Staudigel et. al. (1981) indicate that both major and trace element concentrations may be significantly changed during secondary alteration processes. Alteration within the study area is probably related to a number of processes including halmyrolisis and spilitization of submarine volcanics and sediments;

devitrification of original glassy material; hydrothermal alteration associated with submarine, exhalative, massive-sulfide deposition within the Pecos greenstone belt; contact metasomatic alkali enrichment due to the intrusion of granitic plutons; and regional metamorphism. Therefore, recognition of original rock compositions may be difficult, and interpretations based on such "original" compositions may be tenuous. The mobility of the alkali elements (Na, Ca, and K) in rocks from the study area are depicted on a ternary Ab-An-Or diagram (Fig. 35), after Irvine and Baragar (1971). Samples plotting outside of the "average-rock" field on this diagram typically have higher loss-on-ignition values (0.8 to 2.5%), and may have greater than 1% normative corundum, nepheline or hematite, suggesting major-element alteration of these samples (see Tables 3-5). Several elements including Ti, Zr, Sc, Th, Hf, Ta, Nb, and the REE are thought to be relatively immobile during most secondary alteration processes (Condie, et. al., 1977; Menzies, et. al., 1979; Wood et. al., 1979; and Shervais, 1982) and are considered to be most reliable in characterizing altered volcanic rocks. Several of these "immobile" elements are used in the following diagrams to characterize the rocks from this study.

Figure 36 depicts the bimodal and subalkaline nature of volcanic rocks from the study area in a SiO_2 versus Nb/Y variation diagram after Winchester and Floyd (1977). This

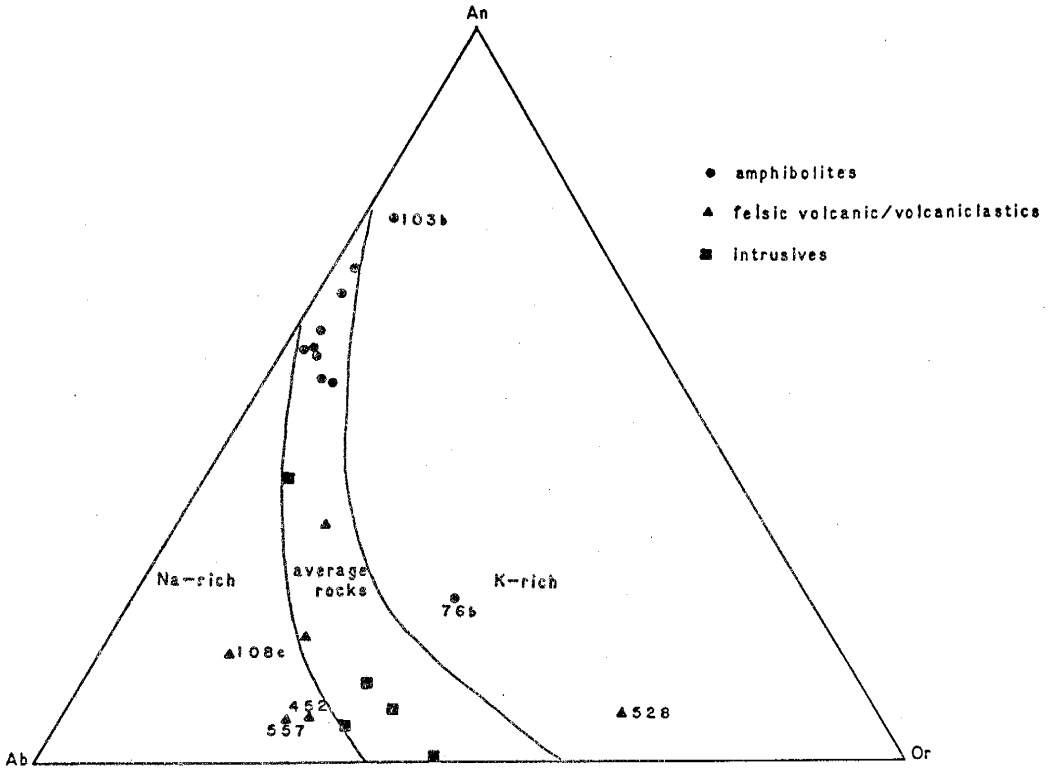

Figure 35. An-Or-Ab diagram (after Irvine and Baragar, 1971).

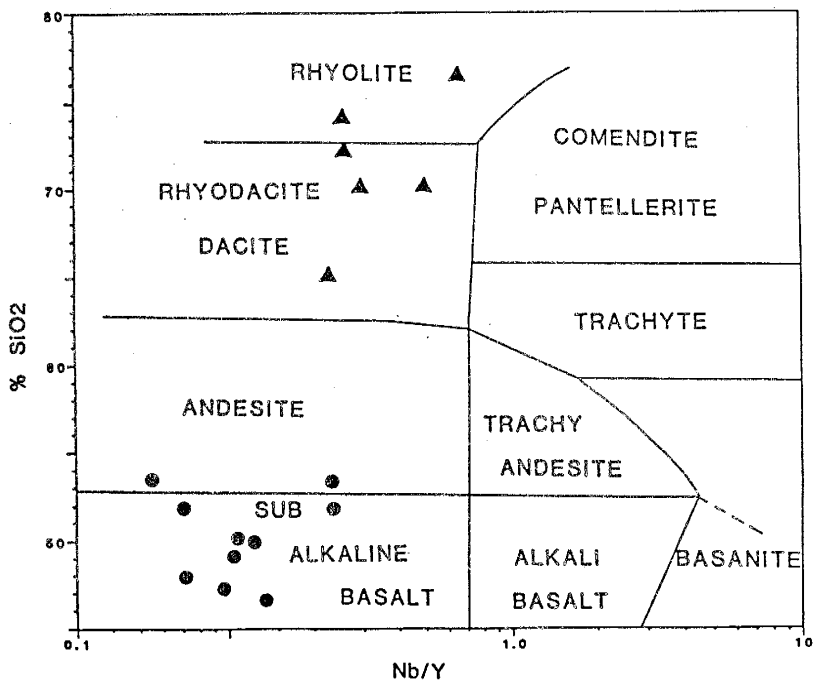

Figure 36. SiO_2 vs Nb/Y diagram (after Winchester and Floyd, 1977).

diagram classifies these rocks as rhyolites, rhyodacites-dacites, and subalkaline basalts. Two amphibolites (151 and 76b) show slight silica enrichment causing them to plot within the andesite field. A compositional gap exists in the 55-65% SiO_2 range.

AMPHIBOLITES

Analyses for ten amphibolite samples exhibiting various textures and field relations are presented in Table 3. Representative samples from the aphanitic- to fine-grained variety include two metabasalts (113 and 228); one mafic intrusive (103c); and one para-amphibolite (532). Six samples from the medium- to coarse-grained variety include two foliated amphibolites, probably of igneous origin (151 and 238); two metadiabase samples (17 and 385); one "altered" amphibolite (76b) collected along the syenite contact; and one porphyritic-amphibolite (103b). In addition, analyses for several average mafic rocks (after Le Maitre, 1976) are included for comparison. Chemical analyses of amphibolites from this study are generally comparable with those of average basalts and gabbros. Slight silica enrichment is observed in a few samples. Potassium metasomatism has significantly affected selected major and trace element abundances in sample 76b. The low TiO_2, plus high Al_2O_3 and CaO values of sample 103b are characteristic of average anorthosites. Petrographic

TABLE 3

Chemical Analysis of Amphibolites

	17	76-b	103-b	103-c	113	151	228	238	385	532	A	B	C
SiO2	49.29	53.57	46.75	46.99	52.03	53.85	48.22	49.82	50.14	51.91	49.20	50.14	50.28
TiO2	0.51	0.94	0.52	1.41	1.25	1.06	1.10	0.89	0.94	0.99	1.84	1.12	0.64
Al2O3	16.65	11.38	24.81	17.31	13.53	13.90	15.50	15.80	15.25	15.01	15.74	15.48	25.86
Fe2O3	2.02	3.49	1.92	2.93	2.77	2.56	2.61	2.40	2.46	2.52	3.79	3.01	0.96
FeO	6.07	5.24	4.78	9.88	10.53	9.76	9.90	8.44	8.59	8.76	7.13	7.62	2.07
MnO	0.18	0.13	0.14	0.26	0.21	0.22	0.20	0.21	0.25	0.19	0.20	0.12	0.05
MgO	8.21	12.20	4.40	6.95	6.36	5.97	7.64	7.77	7.30	6.45	6.73	7.59	2.12
CaO	14.04	7.69	13.63	11.02	10.87	9.99	12.51	11.14	11.76	10.78	9.47	9.58	12.48
Na2O	1.94	2.43	2.54	2.88	2.06	2.25	1.97	3.09	2.59	2.50	2.91	2.39	3.15
K2O	0.23	3.10	0.45	0.22	0.24	0.31	0.25	0.34	0.62	0.69	1.10	0.93	0.65
P2O5	0.06	0.84	0.06	0.15	0.14	0.12	0.09	0.09	0.11	0.19	0.35	0.24	0.09
LOI	0.51	2.54	1.09	0.40	0.60	0.51	0.52	0.72	0.75	0.61	1.49	0.93	1.45
Total	100.51	102.55	101.09	100.40	100.59	100.50	100.60	100.71	100.76	100.60	99.95	99.15	99.80
Rb	4	107	10	2	4	3	11	7	21	12	n/a	n/a	n/a
Cs	18	1	24	0.7	2	2	6	10	6	0.8	n/a	n/a	n/a
Sr	147	536	249	109	160	162	168	175	158	138	n/a	n/a	n/a
Ba	-	1618	126	-	-	-	-	-	212	306	n/a	n/a	n/a
Sc	42	21	36	57	34	40	50	39	38	28	n/a	n/a	n/a
Y	18	25	18	46	26	32	27	29	32	28	n/a	n/a	n/a
Zr	37	218	50	104	62	65	70	65	71	107	n/a	n/a	n/a
Hf	-	5	-	3	3	3	2	2	-	2	n/a	n/a	n/a
Nb	2	6	3	5	2	2	2	4	3	7	n/a	n/a	n/a
Ta	0.4	0.3	-	0.5	0.3	-	0.1	0.2	0.3	0.4	n/a	n/a	n/a
Cr	88	538	225	25	43	55	168	195	106	226	n/a	n/a	n/a
Co	47	50	45	71	50	55	76	49	39	43	n/a	n/a	n/a
U	0.2	3	1.5	0.5	0.4	0.4	-	0.6	0.2	0.4	n/a	n/a	n/a
Th	0.2	13	0.6	1	0.3	0.7	0.1	0.6	0.7	0.9	n/a	n/a	n/a
La	2.3	77.6	4.1	-	2.4	4.5	3.5	3.4	4.7	15.5	n/a	n/a	n/a
Ce	-	175.6	-	11.8	-	-	-	-	-	28.2	n/a	n/a	n/a
Sm	1.4	13.0	-	3.9	2.4	2.6	2.8	2.6	2.7	3.5	n/a	n/a	n/a
Eu	0.4	3.2	0.4	0.7	0.4	0.6	0.6	0.4	0.5	0.9	n/a	n/a	n/a
Tb	0.4	1.4	0.6	1.2	0.6	0.8	1.0	0.8	0.9	0.9	n/a	n/a	n/a
Yb	1.5	-	1.9	4.8	3.1	3.3	-	2.9	2.9	2.2	n/a	n/a	n/a
Lu	-	0.4	-	-	-	-	-	-	-	0.4	n/a	n/a	n/a

TABLE 3 (continued)

C.I.P.W. Mineral Norms (%)

	17	76-b	103-b	103-c	113	151	228	238	385	532	A	B	C
Q	0.0	0.0	0.0	0.0	5.4	7.7	0.0	0.0	0.0	2.1	0.0	0.7	0.0
Or	1.4	18.3	2.7	1.3	1.4	1.8	1.5	2.0	3.7	4.1	6.5	5.5	3.9
Ab	16.4	20.6	16.6	24.4	17.4	19.0	16.7	26.2	21.9	21.2	24.7	20.3	23.2
An	36.0	11.0	55.0	33.7	27.0	26.9	32.7	28.2	28.2	27.7	26.6	28.6	23.2
C	0.0	0.0	0.0	0.0	0.0	0.0	0.0	0.0	0.0	0.0	0.0	0.0	0.0
Di	26.9	17.2	10.0	16.5	21.5	18.1	23.6	21.6	24.1	20.2	14.0	13.7	8.6
Hy	8.4	18.4	0.0	0.1	20.6	20.4	12.5	4.3	9.9	18.9	15.2	22.1	0.0
Ol	6.9	7.2	9.2	16.8	0.0	0.0	7.0	12.4	6.7	0.0	1.5	0.0	2.0
Mt	2.9	3.6	2.8	4.3	4.0	3.7	3.8	3.5	3.6	3.7	5.5	4.4	1.4
Hm	0.0	0.0	0.0	0.0	0.0	0.0	0.0	0.0	0.0	0.0	0.0	0.0	0.0
Il	1.0	1.8	1.0	2.7	2.4	2.0	2.1	1.7	1.8	1.9	3.5	2.1	1.2
Ap	0.2	2.1	0.2	0.4	0.4	0.3	0.2	0.2	0.3	5.0	0.8	0.6	0.2
Ne	0.0	0.0	2.7	0.0	0.0	0.0	0.0	0.0	0.0	0.0	0.0	0.0	0.0

17: medium-grained amphibolite
76-b: medium-grained "altered" amphibolite
103-b: amphibole porphyry
103-c: fine-grained ortho-amphibolite
113: fine-grained amphibolite
151: medium-grained amphibolite
228: fine-grained amphibolite
238: medium-grained amphibolite
385: metadiabase
A: average basalt (Le Maitre, 1976)
B: average gabbro (Le Maitre, 1976)
C: average anorthosite (Le Maitre, 1976)
n/a = not analyzed
- = not determined

descriptions of individual samples are given in Appendix B.

On an AFM diagram (Fig. 37) all but two of the amphibolites plot as tholeiites. 103b plots in the calc-alkaline field together with the "altered" amphibolite (76b). Jensen's (1976) cation plot (Fig. 38) also depicts all but these two amphibolites (103b and 76b) as high-Fe and high-Mg tholeiitic basalts. 103b again plots within the calc-alkaline field, and 76b, due to its high MgO content, falls into the basaltic komatiite field. All but one sample (76b) plot as tholeiites on an SiO_2 versus Cr variation diagram (Miyashiro and Shido, 1975) shown in Figure 39. In this diagram, sample 76b exhibits Cr and/or slight SiO_2 enrichment, thus plotting in the calc-alkaline field.

Rare-earth element patterns for seven of the ten amphibolites sampled define a tight, flat to slightly depleted light-REE envelope with a large negative Eu anomaly (Fig. 40). This REE distribution appears similar to tholeiitic envelopes for Proterozoic mafic volcanics and volcaniclastic rocks described by Condie (1980b) for the Tijeras greenstone, and by Robertson (per. Commun., 1982) for the rest of the Pecos greenstone belt. Samples 532 and 76b are characterized by moderate to extreme light-REE enrichment. 532 is typical of calc-alkaline basalt patterns (Condie, 1981b), but such light-REE enrichment may also be the result of secondary alteration. The strong light-REE

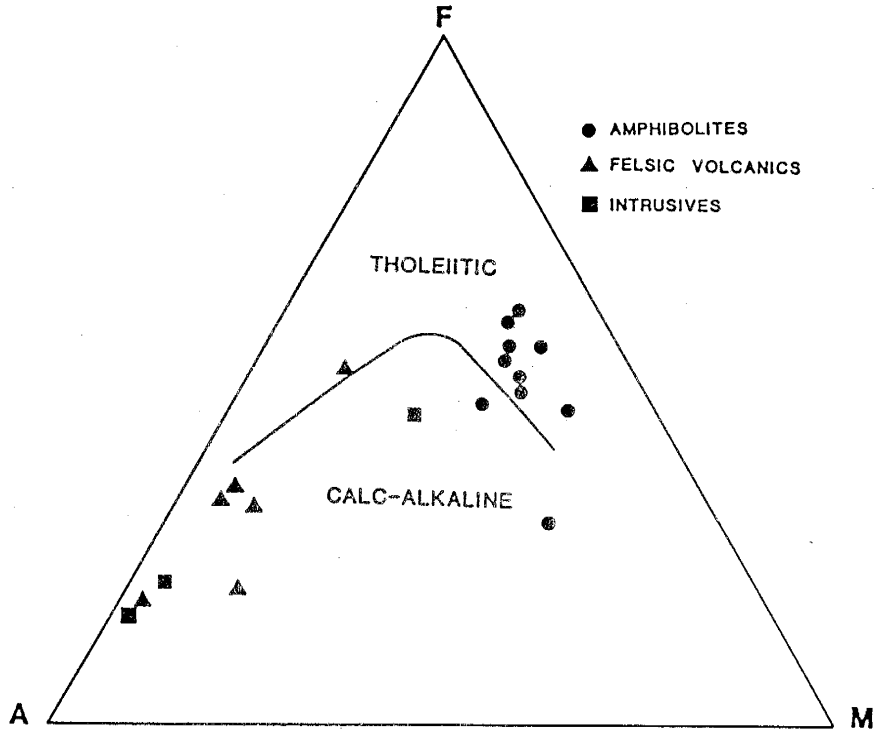

Figure 37. A-F-M diagram
(after Irvine and Baragar, 1971).

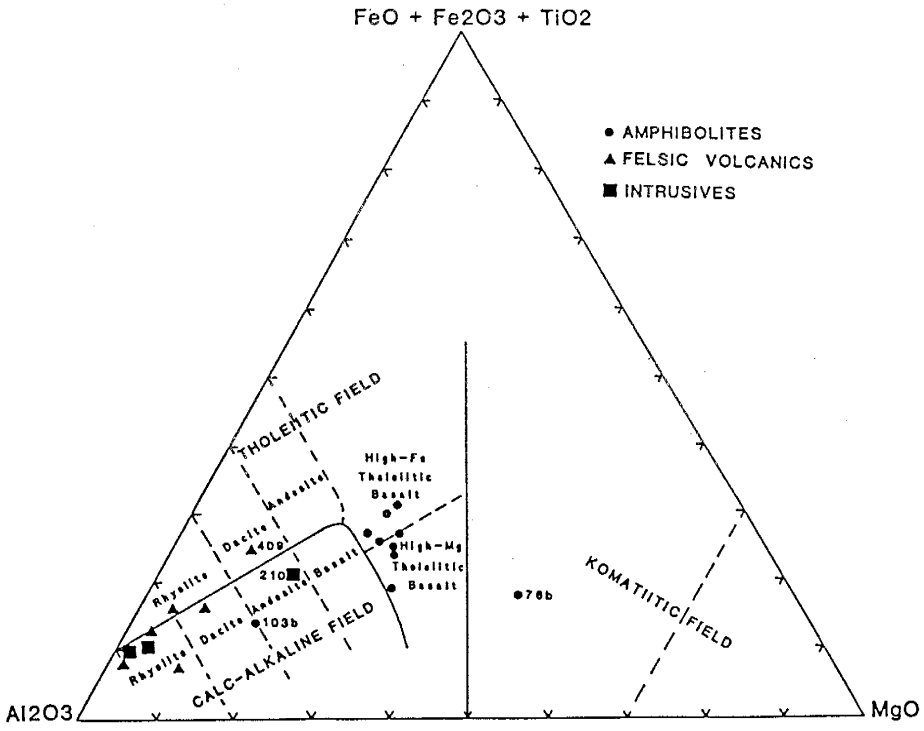

Figure 38. Jensen Cation Plot
(after Jensen, 1976).

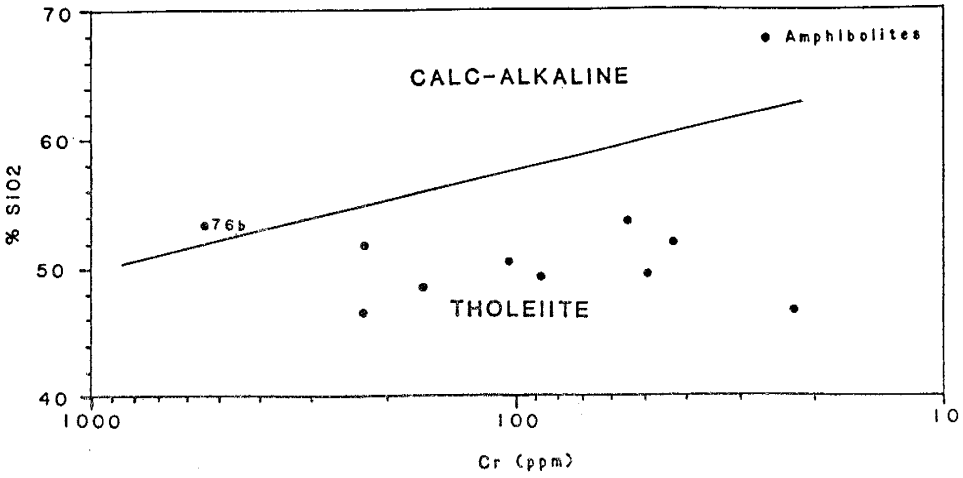

Figure 39. SiO_2 vs Cr diagram (after Miyashiro and Shido, 1975).

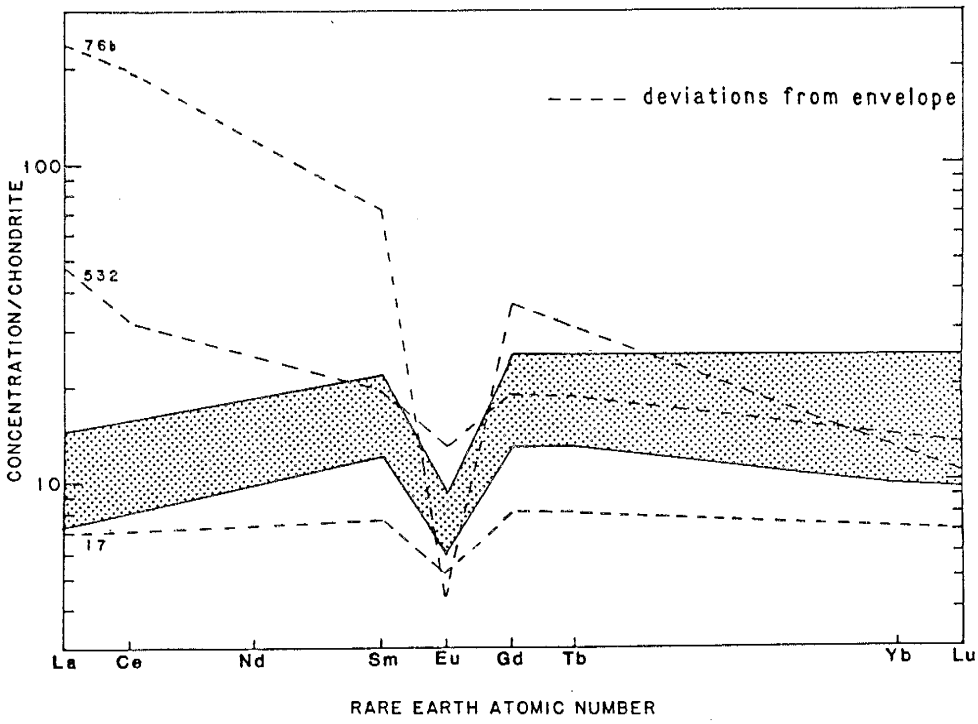

Figure 40. REE envelope for amphibolites (n=7).

enrichment exhibited by sample 76b is believed to be related to the intense potassium metasomatism of this sample. Sample 17 is slightly more depleted in all REE relative to the established envelope, but still exhibits a flat REE pattern typical of tholeiitic basalts. Sample 103b (with major element concentrations characteristic of anorthosites) plots within the tight REE envelope, and does not show the light-REE enriched pattern with strong positive Eu anomaly typical of anorthosites.

In general, most amphibolites from this study consistently plot within the subalkaline and tholeiitic basalt fields using various classification schemes. Samples 76b and 103b generally show the greatest effects of alteration, especially among the major elements. As previously mentioned, alteration of 76b is related to alkali enrichment as a result of close contact with the syenite intrusive. The amphibole porphyry (103b) plots both within calc-alkaline and tholeiitic fields. This variability may be the result of the inhomogeneity caused by the abundance of plagioclase phenocrysts within this rock. A separate analysis of the mafic matrix would be necessary to accurately characterize this rock type.

Possible tectonic settings of amphibolites from this study are suggested by various minor and trace "immobile" element discrimination diagrams. Figures 41 and 42 after

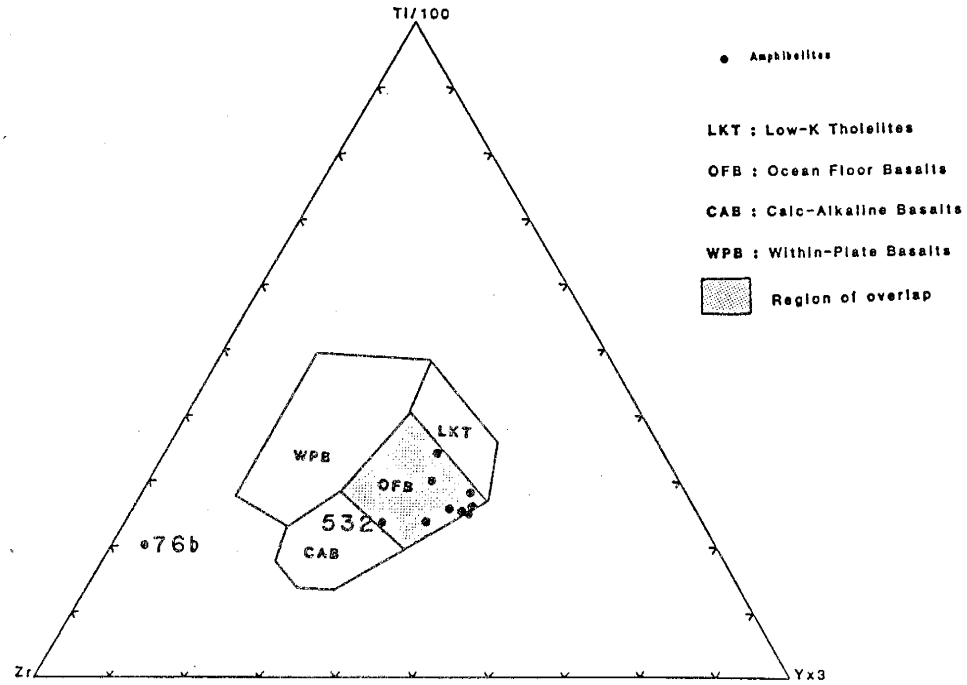

Figure 41. Zr-Ti-Y diagram
(after Pearce and Cann, 1973).

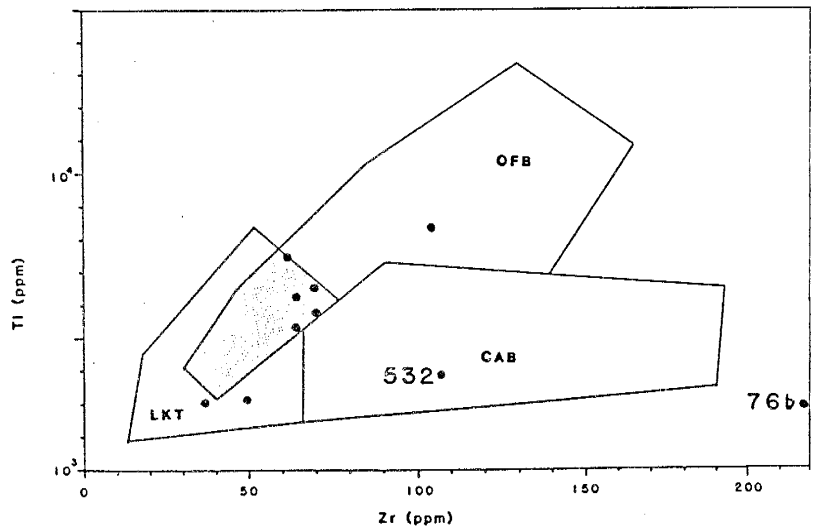

Figure 42. Ti vs Zr diagram
(after Pearce and Cann, 1973).

Pearce and Cann (1973) generally characterize these rocks as low-K tholeiites and as ocean floor basalts using Zr-Ti-Y and Ti versus Zr variation diagrams, respectively. In Figure 41, the ocean floor basalt field also represents a field of overlap for low-K tholeiites and calc-alkaline basalts, and therefore does little more than eliminate within-plate basalts as a possible tectonic setting. In Figure 42, the analyses plot primarily as low-K tholeiites and ocean floor basalts with a large portion again falling within the region of overlap. One exception is sample 532 which shows definite calc-alkaline trends on both of Pearce and Cann's plots. In addition, alteration of sample 76b has significantly affected this sample's Zr content such that it no longer plots within any of the established fields. Figure 43 of Pearce (1975) depicts all of the amphibolites as island-arc (low-K) tholeiites on a Ti versus Cr variation diagram. Wood's (1980) Th-Hf-Ta diagram is presented in Figure 44. The "altered" amphibolite (76b) plus three additional samples lacking detectable quantities of the three necessary components have been omitted from this diagram. The remaining samples do not consistently plot in any particular field. This scatter may be explained by the presence of several percent of cumulus Fe-Ti oxides within some of the amphibolites (see Appendix B). The similar ionic radii of Ta and Ti causes Ta to be more strongly partitioned into Fe-Ti oxides than Th or Hf (Schoek, 1979,

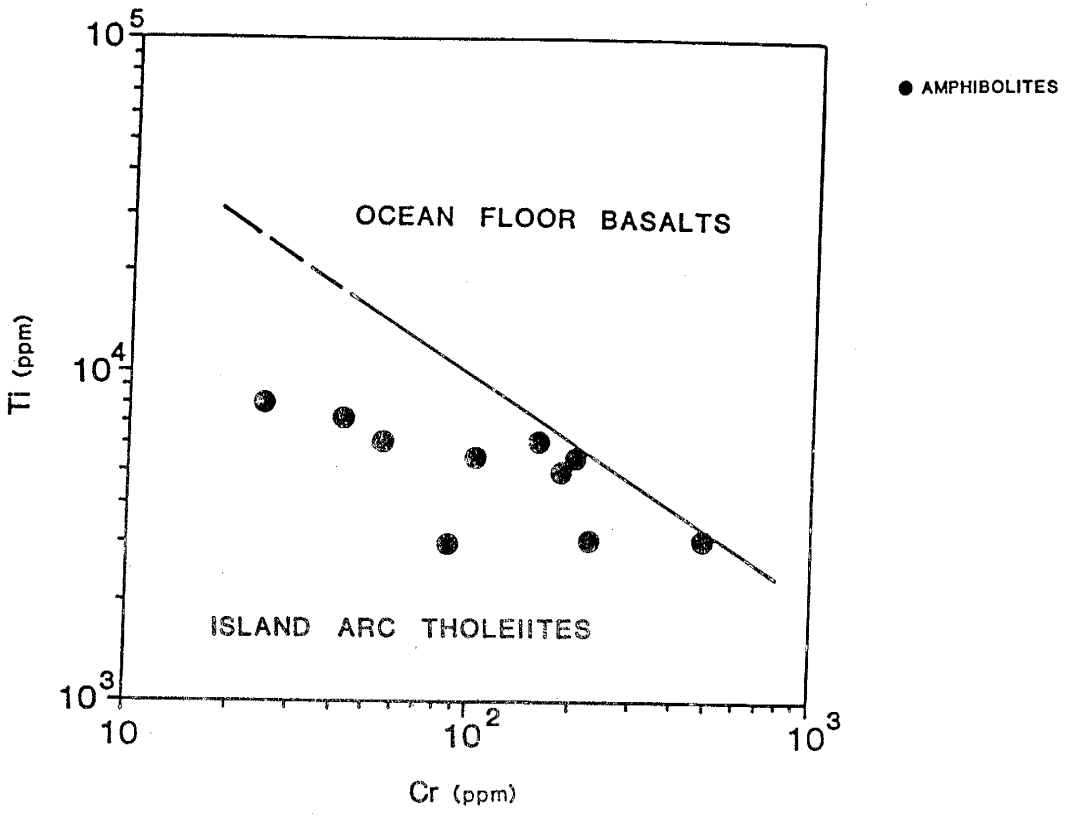

Figure 43. Ti vs Cr diagram (after Pearce, 1975).

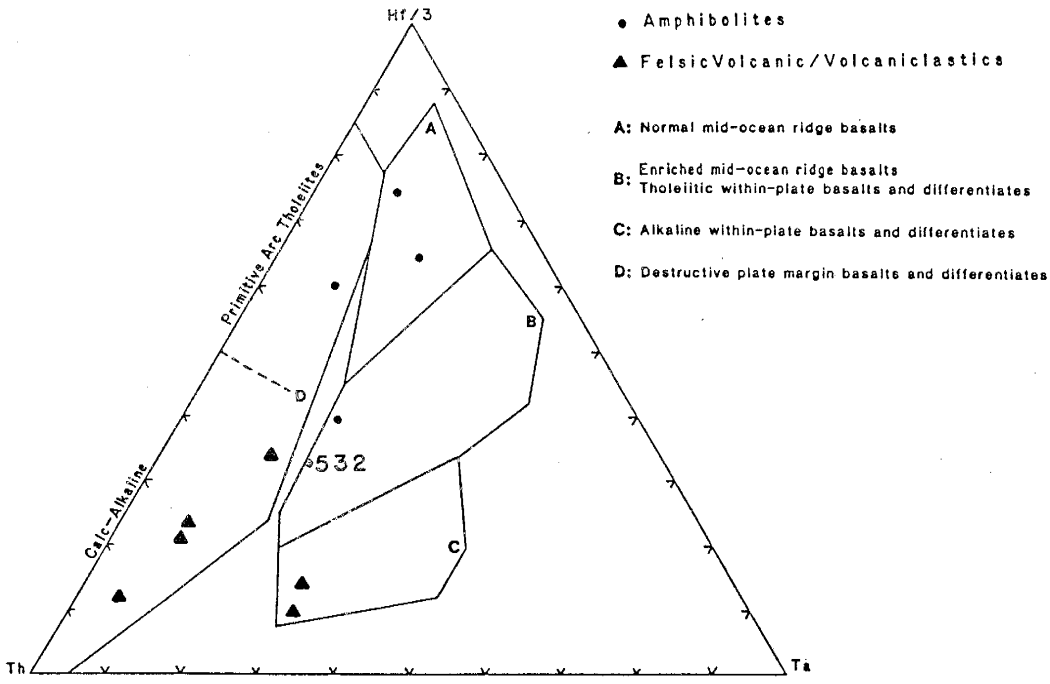

Figure 44. Th-Hf-Ta diagram (after Wood, 1980).

referenced in Wood, 1980). Thus lavas with greater than 2-3% cumulus Fe-Ti oxides may be significantly displaced towards the Ta apex when plotted on this diagram (Wood 1980). Assuming that the observed scatter is due to the variable Fe-Ti oxides in these rocks, it appears that the majority of the amphibolites are characteristic of primitive arc tholeiites from destructive plate margins. Sample 532 again trends towards the calc-alkaline subdivision of this destructive plate margin field.

FELSIC VOLCANIC AND VOLCANICLASTIC ROCKS

Table 4 contains chemical analyses of four felsic volcanic/volcaniclastic rocks (108, 409, 452, and 557); plus a felsic granofels (528), and a felsic gneiss (573) of probable volcaniclastic origin. In addition, average compositions for rhyolite, rhyodacite, and dacite (after Le Maitre, 1976) are presented for comparison.

As is shown in Figure 35, major element analyses exhibit considerable deviation from "average" felsic volcanic rocks. Sample 528 shows the greatest amount of alteration with a significant loss of Na_2O and probably SiO_2, plus enrichment of K_2O. Samples 108, 452, and 557 show slight to moderate Na enrichment. These rocks appear to be mostly calc-alkaline in nature, although for most samples major-element variation diagrams do not consistently

TABLE 4

Chemical Analysis of Felsic Volcanic and Volcaniclastic Rocks

	108	009	452	528	557	573	A	B	C
SiO2	72.61	65.46	76.59	70.30	74.23	70.45	72.82	65.55	65.01
TiO2	0.33	0.73	0.10	0.10	0.23	0.34	0.28	0.60	0.58
Al2O3	13.84	14.63	13.02	15.34	13.98	13.65	13.27	15.04	15.91
Fe2O3	1.86	2.25	1.60	1.62	1.75	1.86	1.48	2.13	2.43
FeO	2.01	5.37	0.19	0.67	1.22	2.09	1.11	2.03	2.30
MnO	0.06	0.12	0.02	0.04	0.04	0.11	0.06	0.09	0.09
MgO	0.64	1.78	0.23	1.69	0.43	1.18	0.39	2.09	1.78
CaO	1.97	4.26	0.81	3.45	0.80	3.47	1.14	3.62	4.32
Na2O	5.04	3.51	4.57	0.47	4.72	4.39	3.55	3.67	3.79
K2O	1.56	1.68	2.84	6.48	2.54	2.33	4.30	3.00	2.17
P2O5	0.08	0.22	0.03	0.03	0.06	0.12	0.07	0.25	0.15
LOI	1.15	0.66	0.78	1.74	0.80	1.74	1.49	1.70	1.25
Total	101.15	100.67	100.78	101.73	100.80	101.73	99.96	99.79	99.78
Rb	22	23	54	184	53	65	n/a	n/a	n/a
Cs	2	2	2	9	2	3	n/a	n/a	n/a
Sr	237	324	113	103	101	203	n/a	n/a	n/a
Ba	915	406	850	720	680	622	n/a	n/a	n/a
Sc	7	18	3	2	3	6	n/a	n/a	n/a
Y	47	27	24	63	38	39	n/a	n/a	n/a
Zr	216	101	148	207	243	108	n/a	n/a	n/a
Hf	6	2	3	6	8	3	n/a	n/a	n/a
Nb	12	6	16	19	10	20	n/a	n/a	n/a
Ta	0.8	0.3	3	1	1	2	n/a	n/a	n/a
Cr	-	8	-	3	-	32	n/a	n/a	n/a
Co	9	16	2	2	3	9	n/a	n/a	n/a
U	3	0.9	2	1	3	2	n/a	n/a	n/a
Th	6	1	6	14	8	4	n/a	n/a	n/a
La	34.6	16.4	39.3	55.9	40.6	27.8	n/a	n/a	n/a
Ce	63.4	34.6	89.2	-	80.0	53.7	n/a	n/a	n/a
Sm	6.0	4.5	3.8	10.1	5.4	4.9	n/a	n/a	n/a
Eu	1.5	0.9	0.9	0.9	1.4	1.3	n/a	n/a	n/a
Tb	1.1	1.0	1.0	1.6	1.2	1.1	n/a	n/a	n/a
Yb	2.7	3.6	3.0	4.2	3.3	-	n/a	n/a	n/a
Lu	-	-	-	0.6	0.5	0.3	n/a	n/a	n/a

TABLE 4 (continued)

C.I.P.W. Mineral Norms (%)

	108	409	452	528	557	573	A	B	C
Q	31.6	24.4	37.2	33.2	34.7	27.5	32.9	22.7	22.7
Or	9.2	9.9	16.8	38.3	15.0	13.8	25.4	17.7	12.8
Ab	42.7	29.7	38.7	40.0	39.9	37.2	30.1	31.1	32.1
An	9.3	19.2	3.8	16.9	3.6	10.7	4.8	15.0	20.0
C	0.5	0.0	1.0	1.4	2.2	0.0	1.0	0.3	0.0
Di	0.0	0.4	0.0	0.0	0.0	4.7	0.0	0.0	0.1
Hy	3.3	11.2	0.6	3.7	1.6	2.6	1.3	6.2	5.7
Ol	0.0	0.0	0.0	0.0	0.0	0.0	0.0	0.0	0.0
Mt	2.7	3.3	0.4	2.0	2.5	2.7	2.1	3.1	3.5
Hm	0.0	0.0	1.3	0.2	0.0	0.0	0.0	0.0	0.0
Il	0.6	1.4	0.2	0.2	0.4	0.7	0.5	1.1	1.1
Ap	0.2	0.6	0.1	0.1	0.2	0.3	0.2	0.6	0.3
Ne	0.0	0.0	0.0	0.0	0.0	0.0	0.0	0.0	0.0

108: felsic volcanic/volcaniclastic
409: felsic volcanic/volcaniclastic
452: felsic volcanic
528: felsic granofels
557: felsic volcanic/volcaniclastic
573: felsic gneiss
A: average rhyolite (Le Maitre, 1976)
B: average rhyodacite (Le Maitre, 1976)
C: average dacite (Le Maitre, 1976)
n/a = not analyzed
- = not determined

differentiate between the two rock series (see Figs. 37 and 38). Sample 409 is an exception and in both cases plots within tholeiitic fields.

Jensen's (1976) cation diagram (Fig. 37) shows the chemical composition of these rocks ranging from rhyolite to dacite. Winchester and Floyd's (1977) SiO_2 versus Nb/Y variation diagram (Fig. 36) also depicts such characteristics. Chemical similarities between the felsic granofels, gneiss and volcanic/volcaniclastic rocks indicate that the granofels and gneiss are similar in composition to the felsic volcanic rocks from which they may have been derived.

Five of the six samples define a tight, moderately fractionated, light-REE enriched envelope with a small to moderate negative Eu anomaly (Fig. 45). This REE pattern with its negative Eu anomaly and slight depletion in heavy-REE (down to 10X chondrite) is characteristic of FII-type Archean felsic volcanics, and is similar to most modern calc-alkaline felsic volcanics (Condie, 1981b). Sample 528 (felsic granofels) shows an overall enrichment in REE relative to this envelope, in addition to a slightly larger negative Eu anomaly. Although deviation from this established envelope may reflect primary differences in the composition of the source rocks, such enrichment may also be the result of weathering during the reworking and/or

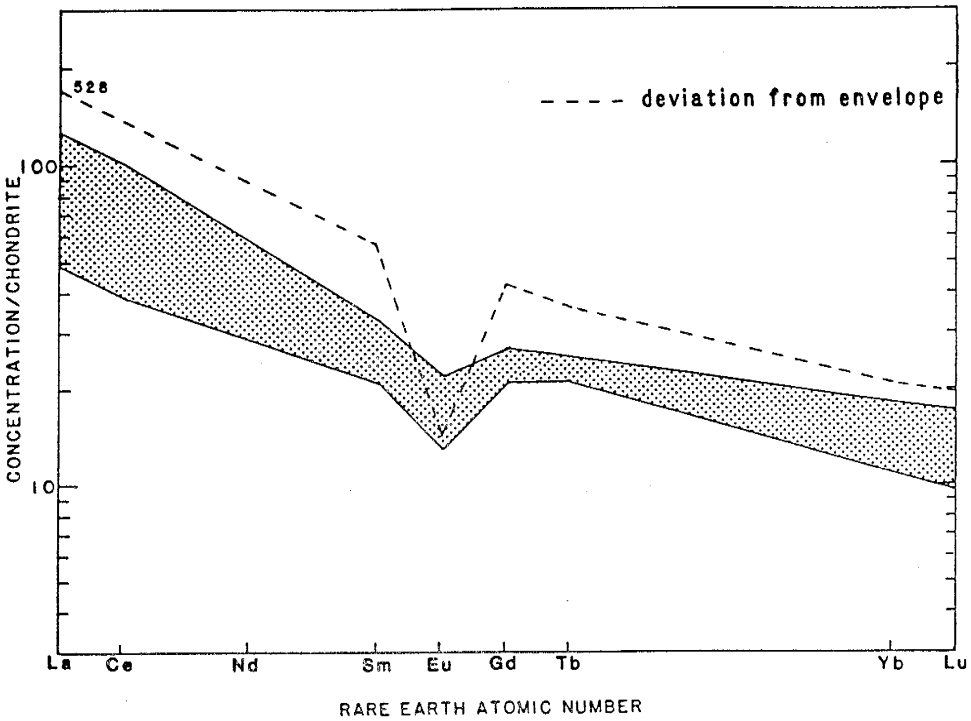

Figure 45. REE envelope for felsic volcanic and volcaniclastic rocks (n=5).

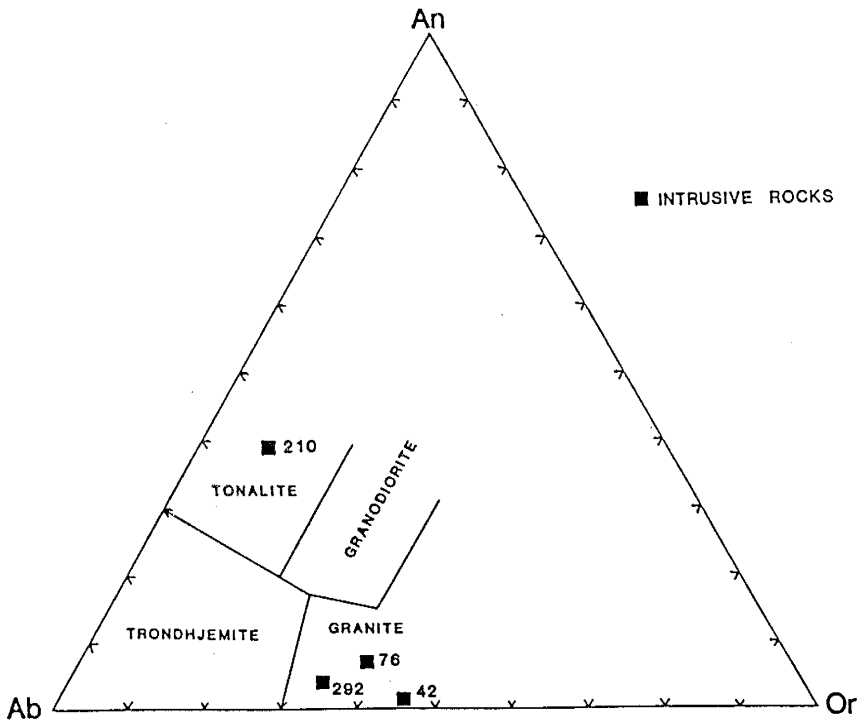

Figure 46. Ab-An-Or normative classification diagram for granitic igneous rocks (after Barker, 1979).

sedimentation of this particular sample. Phyllosilicate minerals are believed to adsorb the REE in addition to yttrium during weathering processes, and thus concentrate these minerals relative to quartz in sandstones (Roaldset, 1975). The greater mica content of this sample as seen in thin section (see Appendix B) is compatible with this REE enrichment and may also account for the increased yttrium concentration observed in this sample.

Possible paleotectonic environments for the felsic volcanic and volcaniclastic rocks are suggested by Wood's (1980) Th-Hf-Ta discrimination diagram (see Fig. 44). Four of the six samples are characteristic of calc-alkaline volcanics from destructive plate margins. The remaining two samples plot within the alkaline field. This displacement towards the Ta apex may again be due to Ta enrichment associated with the presence of several percent Fe-Ti oxides, although thin sections generally show only <1 percent magnetite for these samples.

INTRUSIVE ROCKS

Chemical analyses of the intrusive rocks from the study area are given in Table 5. For comparison, average compositions of similar rock types (from Le Maitre, 1976 and Condie, 1981b) are also presented. Estimated modal mineral abundances were used for the petrographic classification,

TABLE 5

Chemical Analysis of Intrusive Rocks

	42	76	210	292	A	B	C	D	E	F	G
SiO2	78.21	60.89	57.77	76.36	71.30	72.10	58.58	61.90	61.52	69.70	57.48
TiO2	0.11	0.49	0.80	0.18	0.31	0.37	0.84	0.58	0.73	0.35	0.95
Al2O3	11.91	17.45	16.93	12.80	14.32	13.90	16.64	16.90	16.48	15.67	16.67
Fe2O3	1.62	2.01	2.32	1.69	1.21	0.86	3.04	2.32	1.83	0.80	2.50
FeO	0.11	2.74	5.11	0.58	1.64	1.67	3.13	2.62	3.82	2.02	4.92
MnO	0.01	0.06	0.13	0.02	0.05	0.06	0.13	0.11	0.08	0.07	0.12
MgO	0.19	2.03	3.76	0.40	0.71	0.52	1.87	0.96	2.80	1.04	3.71
CaO	0.11	2.84	7.97	1.04	1.84	1.33	3.53	2.54	5.42	2.52	6.58
Na2O	3.44	5.64	3.97	4.25	3.68	3.08	5.24	5.46	3.63	4.70	3.54
K2O	4.22	5.50	1.02	3.27	4.07	5.46	4.95	5.91	2.07	2.12	1.76
P2O5	0.08	0.34	0.21	0.40	0.12	0.18	0.29	0.19	0.25	0.14	0.29
LOI	0.67	0.64	0.75	0.56	0.82	0.53	1.50	0.53	1.38	0.68	1.46
Total	100.68	100.63	100.74	100.55	100.07	100.06	99.74	100.02	100.01	99.81	99.98
Rb	171	85	60	57	n/a	250	n/a	110	n/a	72	n/a
Cs	23	3	19	0.8	n/a	n/a	n/a	n/a	n/a	n/a	n/a
Sr	28	1805	399	91	n/a	100	n/a	200	n/a	530	n/a
Ba	925	3250	397	875	n/a	500	n/a	1600	n/a	575	n/a
Sc	5	7	17	5	n/a	n/a	n/a	2	n/a	n/a	n/a
Y	78	19	20	37	n/a	n/a	n/a	n/a	n/a	n/a	n/a
Zr	147	477	117	194	n/a	200	n/a	500	n/a	-	n/a
Hf	5	14	3	6	n/a	n/a	n/a	n/a	n/a	n/a	n/a
Nb	13	6	8	19	n/a	n/a	n/a	n/a	n/a	n/a	n/a
Ta	2	0.2	0.4	1	n/a	n/a	n/a	n/a	n/a	n/a	n/a
Cr	-	24	50	1.2	n/a	2	n/a	2	n/a	30	n/a
Co	0.6	13	25	49	n/a	2	n/a	1	n/a	-	n/a
U	1	3	1	1	n/a	n/a	n/a	n/a	n/a	n/a	n/a
Th	11	10	4	6	n/a	n/a	n/a	n/a	n/a	5	n/a
La	-	67.1	20.3	26.5	n/a	45	n/a	85	n/a	35	n/a
Ce	64.1	116.1	46.3	61.8	n/a	90	n/a	200	n/a	84	n/a
Sm	-	8.7	3.8	3.9	n/a	10	n/a	18	n/a	7	n/a
Eu	0.5	3.2	1.0	0.5	n/a	0.7	n/a	1	n/a	0.8	n/a
Tb	1.7	0.8	0.9	0.8	n/a	n/a	n/a	n/a	n/a	n/a	n/a
Yb	6.3	-	-	3.4	n/a	4	n/a	6	n/a	4	n/a
Lu	1.0	0.3	0.3	0.6	n/a	0.7	n/a	1	n/a	0.8	n/a

TABLE 5 (continued)

C.I.P.W. Mineral Norms (%)

	42	76	210	292	A	B	C	D	E	F	G
Q	41.8	0.0	8.5	36.4	29.1	n/a	0.83	n/a	16.6	n/a	10.3
Or	24.9	32.5	6.0	19.3	24.5	n/a	29.3	n/a	12.2	n/a	10.4
Ab	29.1	47.7	33.6	36.0	31.1	n/a	44.3	n/a	30.7	n/a	30.0
An	0.1	6.1	25.4	2.6	8.0	n/a	7.2	n/a	22.6	n/a	24.4
C	1.7	0.0	0.0	1.3	0.9	n/a	0.0	n/a	0.0	n/a	0.0
Di	0.0	4.7	10.5	0.0	0.0	n/a	5.4	n/a	1.5	n/a	4.7
Hy	0.5	1.5	10.6	1.0	3.4	n/a	4.2	n/a	9.7	n/a	12.6
Ol	0.0	2.9	0.0	0.0	0.0	n/a	0.0	n/a	0.0	n/a	0.0
Mt	0.1	2.9	3.4	1.4	1.8	n/a	4.4	n/a	2.7	n/a	3.6
Hm	1.6	0.0	0.0	0.7	0.0	n/a	0.0	n/a	0.0	n/a	0.0
Il	0.2	0.9	1.5	0.3	0.6	n/a	1.6	n/a	1.4	n/a	1.8
Ap	0.2	0.9	0.5	1.0	0.3	n/a	0.7	n/a	0.6	n/a	0.7
Ne	0.0	0.0	0.0	0.0	0.0	n/a	0.0	n/a	0.0	n/a	0.0

42: foliated-granite (this study)

76: syenite (this study)

210: tonalite (this study)

292: unfoliated-granite (this study)

A: average granite (Le Maitre, 1976)

B: average Post-Archean granite (Condie, 1981b)

C: average syenite (Le Maitre, 1976)

D: average Post-Archean syenite (Condie, 1981b)

E: average tonalite (Le Maitre, 1976)

F: average Post-Archean high-Al_2O_3 tonalite-trondhjemite (Condie, 1981b)

G: average diorite (Le Maitre, 1976)

n/a = not analyzed

\- = not determined

based on the system recommended by the IUGS (see Fig. 21, after Streckeisen, 1973). In addition, CIPW norms are plotted on an An-Or-Ab ternary diagram (see Fig. 46, after Barker, 1979). This diagram does not differentiate syenite from granite, but otherwise is in agreement with the petrographic classification. Figures 37 and 38 depict the sub-alkaline intrusives (tonalite and granites) predominantly as calc-alkaline rocks, although the granites, especially the foliated granite, are not clearly differentiated between the calc-alkaline and tholeiitic series on these variation diagrams.

Major element abundances of the tonalite (210) appear similar to an "average" diorite, although the high Al_2O_3 and low SiO_2, Rb, and Th values are also characteristic of Barker's (1979) high-Al_2O_3 variety of tonalite. Trace elements values are also consistent with those reported for average post-Archean high-Al_2O_3 tonalites. The REE plot for this tonalite shows an enriched light-REE, slightly depleted heavy-REE pattern with a negative Eu anomaly (Fig. 47). With the exception of slightly higher heavy-REE concentrations, this pattern lies within the established envelope for post-Archean high-Al_2O_3 tonalite-trondhjemites. This pattern is also very similar to the REE envelope for the felsic volcanic and volcaniclastic rocks, suggesting the tonalite and felsic volcanics may have been derived from a similar magma source. Tonalites of similar composition have

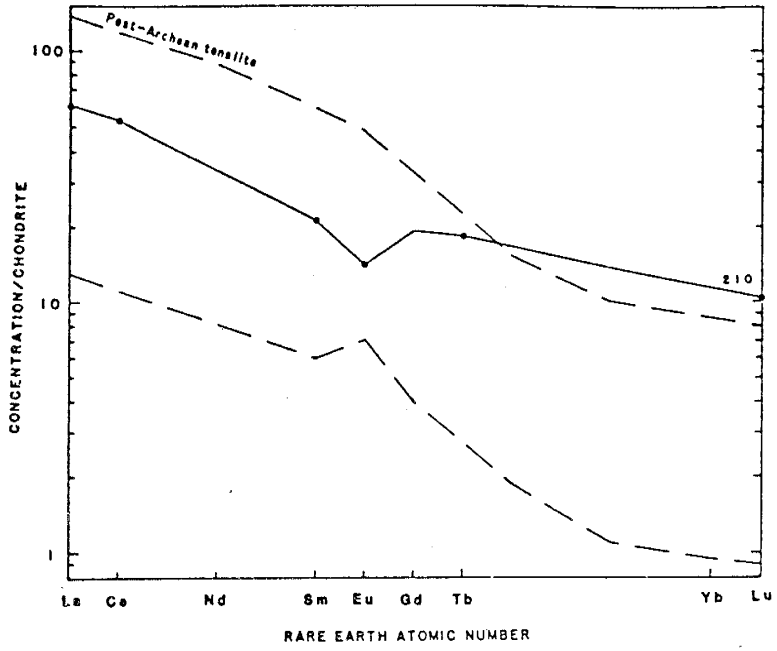

Figure 47. REE pattern for tonalite (this study), plus Post-Archean High Al_2O_3 tonalite-trondhjemite envelope after Condie (1981b).

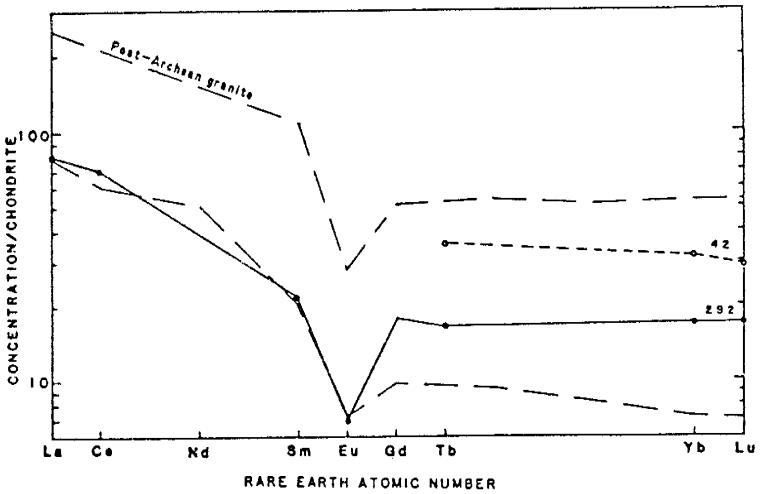

Figure 48. REE pattern for granites (this study), plus Post-Archean granite envelope after Condie (1981b).

been identified in the Taos Range of northern New Mexico, although such plutons are well-foliated and appear to be syntectonic (Mc Crink, 1982). Some of these tonalites have been interpreted as diorites and are thought to be chemically similar to young calc-alkaline andesites from mature arc systems (Condie, per. commun., 1983).

The two granites (42 and 292) have higher SiO_2 and Fe_2O_3 contents than their "average" equivalents, with the rest of the major oxides typically lower than average values for granites. Trace elements are variable and not consistent with average values for post-Archean granites. In Figure 48, REE plots show flat heavy-REE patterns for both samples. Sample 292 has a large negative Eu anomaly and enriched light-REE, characteristic of average post-Archean granites. Light-REE values for sample 42 do not define a consistent pattern and have therefore not been included.

The syenite sample (76) exhibits lower TiO_2, Fe_2O_3 and MnO values, and is higher in Al_2O_3, MgO and P_2O_5 than "average" syenites. Trace elements are generally greater or consistent with average values reported for post-Archean syenites. The REE pattern for the syenite (Fig. 49) is strongly fractionated with enriched light-REE, depleted heavy-REE and a positive Eu anomaly. This highly fractionated pattern is characteristic of average

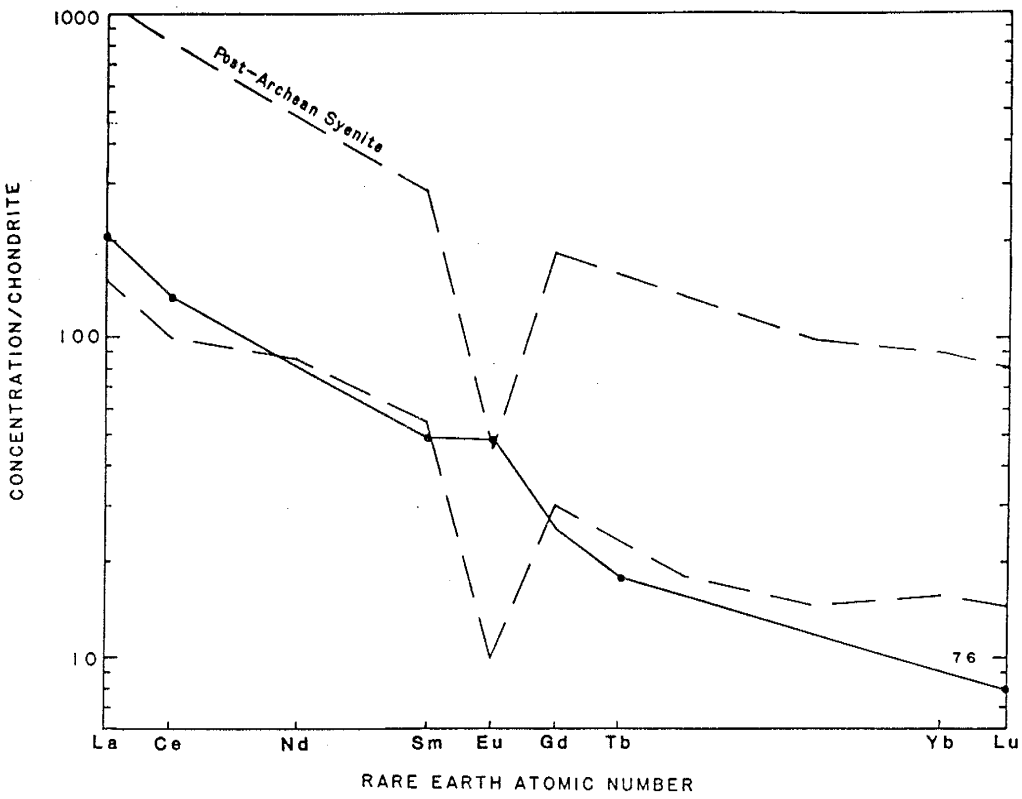

Figure 49. REE pattern for syenite (this study), plus Post-Archean syenite envelope after Condie (1981b).

post-Archean syenites, but the strong negative Eu anomaly typical of such rocks is not present.

DISCUSSION

Geochemical analyses indicate that, in general, metavolcanic rocks from this study area represent a bimodal suite of subalkaline basaltic and felsic volcanics. The basalts are generally characterized as low-K tholeiites, with the exception of one sample (532) that consistently plots as calc-alkaline. Felsic rocks appear both tholeiitic and calc-alkaline, and range in composition from rhyolites to dacites. Various geochemical discrimination diagrams suggest formation of these rocks at a convergent plate boundary and/or island-arc environment. Plutonic rocks from this region include subalkaline granites and tonalite plus an alkaline syenite. The tonalite consistently appears to be calc-alkaline, whereas the granites, in particular the foliated-granite may be tholeiitic or calc-alkaline. The presence of intermediate calc-alkaline rocks in the Pecos greenstone belt would have significant implications on the tectonic processes active in this region during the early Proterozoic. Additional chemical analyses of the subvolcanic and plutonic intrusives throughout the rest of the greenstone terrane are necessary before valid regional interpretations can be made.

The use of geochemical classifications is not without its difficulties. Classification and tectonic discrimination diagrams are typically developed from unaltered Phanerozoic rocks, and therefore may not consistently characterize the nature of Precambrian rocks. As was previously mentioned, secondary alteration of various elements incorporated in such diagrams may cause significant changes in a rock's composition and thus change the original trends of the equivalent unaltered rock. The above interpretations of protoliths and tectonic settings are based on the consistency of samples plotting within similar regions on different variation diagrams, and are believed to be representative of the original rocks. Petrologic structures and textures, both in the field and in thin section are consistent with interpretations of such igneous protoliths.

MINERALIZATION

Late-stage Precambrian pegmatites, abundant throughout the southern and western portions of the map area, constitute the predominant type of mineralization found within this region. Small-scale mining operations at the Elk Mountain (Kept Man) deposit recovered several hundred tons of prepared and scrap mica during the early 1940's (Jahns, 1946). The potential for other associated commodities, such as lithium, beryllium, uranium, bismuth, niobium and rare-earth minerals also appears to be low (Lane, 1980), and under present economic conditions cannot be considered an important resource of these elements.

In addition, hydrothermal quartz veins with rare lead and silver mineralization are found throughout the supracrustal succession. The veins typically pinch and swell and are discontinuous along strike. They are both concordant and discordant to foliations within the host rock and range in thickness from several centimeters up to approximately two meters. Prospect pits are commonly associated with the larger and more extensively mineralized veins. The veins consist of quartz plus abundant epidote, and only rarely contain pyrite and galena. Fire assaying of one such sample from a prospect pit located in the northeast corner of the map-area (T19N, R14E, S30) reports 0.02 oz/ton

of silver and undetectable gold (North, per. commun., 1982).

Intense wall-rock alteration is commonly associated with the pegmatites and to a lesser extent with hydrothermal quartz veins. Propylitic alteration, characterized by abundant epidote and chlorite and minor amounts of pyrite and calcite is accompanied by tourmalinization, potassic alteration with associated muscovite, and silicification.

Ironstone is the only form of mineralization present within the study area that is typically associated with volcanogenic massive-sulfide deposits (see pages 43-46 for descriptions). An adit along a shear zone within Hollinger Canyon is located in an outcrop of quartz-magnetite ironstone, and a prospect pit on the east side of Spring Mountain shows specularite mineralization in addition to magnetite.

DISCUSSION

Relation to Rest of Pecos Greenstone Belt

Supracrustal rocks described in this study are, in general, similar to rocks that comprise the rest of the Pecos greenstone belt The bimodal metavolcanic assemblage comprised primarily of metamorphosed tholeiitic subaqueous basalts, plus locally abundant felsic volcanic and volcaniclastic rocks predominates throughout the region. In addition, metasedimentary rocks consisting largely of metamorphosed volcaniclastic graywacke and arkosic sandstone, plus less abundant pelitic-schists, phyllites, calc-silicate rocks and ironstone are locally important.

A critical problem in this region is the nature of the contact between the Elk Mountain - Spring Mountain metavolcanic succession and the mainly metasedimentary section to the northeast as described by Moench and Robertson (1980). They suggest the relationship represents a lateral facies change between the two assemblages. Detailed mapping has revealed that much of this sedimentary section actually consists of both mafic and felsic metavolcanic and volcaniclastic rocks. Additional sedimentary units have been delineated within the southern portion of the volcanic succession along the headwaters of Hollinger Canyon. It appears that Moench and Robertson's

lateral facies change is, in part, valid. Gradational contacts among the sedimentary and volcanic units are common, suggesting original depositional variations among these lithologies. However, due to intense transposition, the present northeast-southwest orientation of these units no longer represents the original stratigraphy.

Intrusive rocks within the study area also appear, for the most part, to be similar to those identified in other areas of the greenstone terrane. Medium- to coarse-grained meta- diabase and gabbros, plus fine-grained mafic dikes and sills that intrude the supracrustal succession are correlative with Moench and Robertson's subvolcanic complex. Included in this complex are well-foliated tonalite-trondhjemite units which are believed to be intimately intermixed with the intrusive amphibolites. The tonalite identified in this study appears to be both chemically and texturally different, and may actually be younger than the tonalite-trondhjemite units described by Moench and Robertson (1980) and by Wyman (1980). The granites and pegmatites from this region are similar to those of the Pecos greenstone batholithic complex, although gradational contacts, as described by Moench and Robertson (1980), between the two granites of this study were not observed. The sill-like syenite bodies delineated in the north-central portion of the field area are believed to be the only occurrence of this rock type found within the Pecos

greenstone belt (Moench and Robertson, 1980). They appear to be distinctly different and probably younger than the granites of this region. Associated bodies of "mela-syenite" as described by Moench and Robertson (1980) are herein interpreted as intensely potassium-metasomatized zones of amphibolite related to the intrusion of the syenite.

Comparison to Proterozoic Rocks of the Southwestern United States

Recent compilation of geochronologic data suggests that Precambrian rocks in the southwestern United States range in age from 1.1 to 1.8 b.y. (Condie, 1981a). Supracrustal successions define three distinct northeast-southwest trending crustal provinces decreasing in age from the Wyoming shear zone, where Proterozoic rocks are in fault contact with Archean rocks (≥2.5 b.y.) southward to west Texas (Condie, 1982; Fig. 50). Precambrian rocks within the southern Sangre de Cristo Mountains define the southern boundary of the 1.72 to 1.80 b.y.-old age province that underlies most of Colorado; southern Utah and Nevada; portions of southern California; and northern Arizona and New Mexico.

Proterozoic rocks in the Pecos region are similar in terms of lithologic assemblages, style of deformation, and degree of metamorphism to successions of similar age identified in northern New Mexico, Colorado, and Arizona. Grambling and Codding (1982) correlate the Ortega and Vadito Groups of the nearby Picuris Range to similar rocks in the Truchas region and suggest that the metasedimentary Ortega succession of quartzite, pelitic-schist, and phyllites are stratigraphically younger than metavolcanic rocks of the Vadito Group. Recent detailed structural and stratigraphic

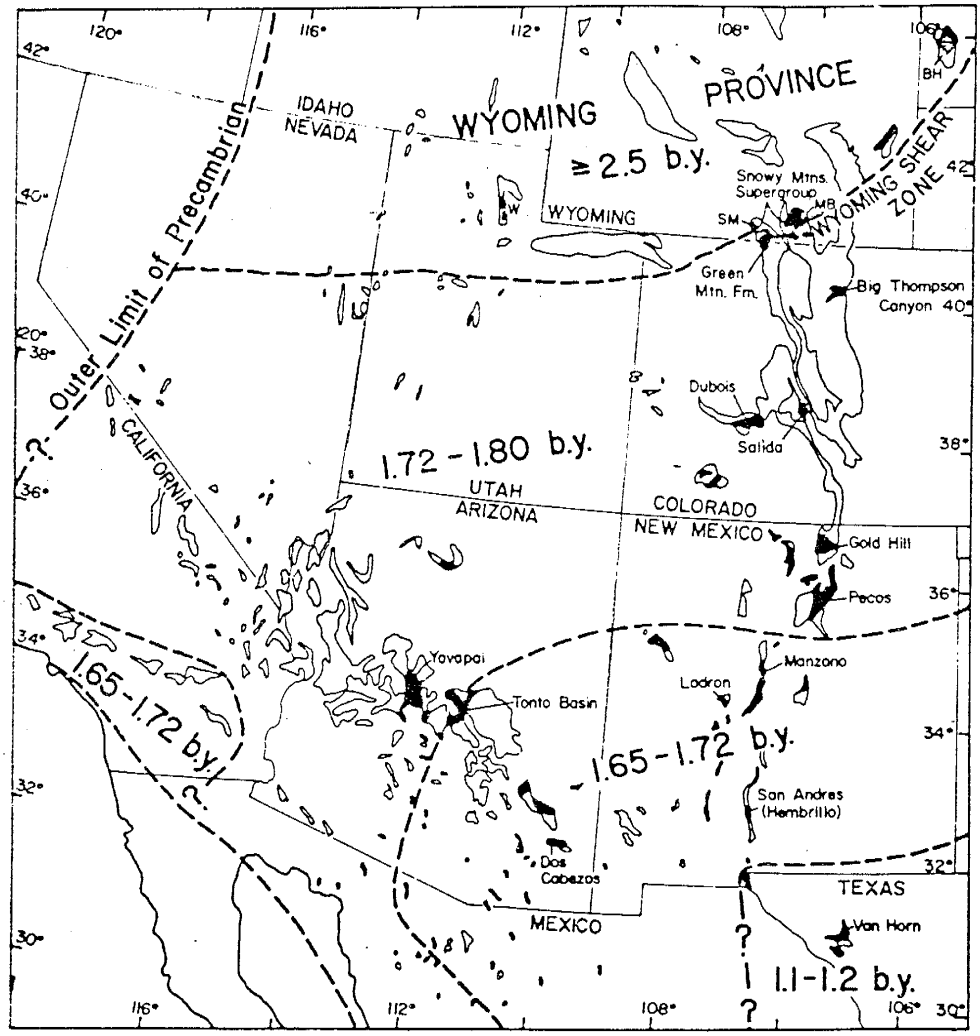

Figure 50. Proterozoic age provinces of the southwestern United States (after Condie, 1982).

analyses by Holcombe and Callender (1982) report similar relationships in the Picuris Range, although in the past, others have interpreted the Vadito Group as being younger (Grambling, 1979; Nielson and Scott, 1979; Robertson and Moench, 1979; Moench and Robertson, 1980). Rocks in both areas have undergone at least two generations of coaxial, tight to isoclinal folding, and a third deformational event as described in the Picuris Range, may have also deformed rocks in the Truchas Peaks region. Both regions have been subjected to amphibolite facies metamorphism. In the Picuris Range, the Embudo Granite of Montgomery (1953), which also intrudes rocks of the Pecos region, has been separated into at least three distinct plutons with ages ranging from 1,547 ± 138 m.y. to 1,441 ± 157 m.y. (Long, 1974).

In the Taos Range of northern New Mexico, bimodal volcanics, volcaniclastics, and sedimentary rocks consisting of quartzites, phyllites, and quartzofeldspathic paragneisses, have been extensively intruded by several pre- to syn-tectonic granitic and tonalitic plutons (Condie, 1980; Reed et. al., 1981; McCrink, 1982). At least two periods of folding, including tectonic transposition, have deformed and metamorphosed these rocks to lower amphibolite facies

Detailed mapping by Kent (1980) and Gibson (1981) in the Tusas Mountains suggests that the Precambrian rocks in this region have been subjected to at least two periods of tight to isoclinal folding, with a widely-spaced crenulation cleavage overprinting previous foliations. Bimodal volcanic and volcaniclastic rocks are reported to be older than interbedded and overlying metasubarkoses, quartzites and minor conglomerates. This succession has been intruded by syntectonic granodiorites, syn- to post-tectonic granites, and by late-stage dikes and pegmatites. All rocks are reported to be metamorphosed to lower greenschist facies.

In the Irving greenstone belt of southwestern Colorado, Barker (1969) documents volcanic rocks of mafic, intermediate and felsic compositions interbedded with graywackes, impure sandstones and quartzites of the Irving Formation, and overlain by a bimodal volcanic sequence (1.67-1.76 b.y. Twilight Gneiss). Following deformation, metamorphism and intrusion of the Tenmile Granite (1.68-1.70 b.y.), a second phase of erosion, deposition of sediments, deformation, and metamorphism to lower amphibolite facies occurred. The post-tectonic Eolus and Trimble granites were subsequently emplaced with age-dates ranging from 1.44 to 1.32 b.y.

The Dubois greenstone terrane of south-central Colorado is composed of bimodal volcanics and volcaniclastics that have been metamorphosed to middle and upper amphibolite facies (Condie and Nuter, 1981). Later syntectonic to post-tectonic granite, granodiorites and tonalite (dated at 1.65-1.70 b.y.) intrude this supracrustal succession. In the nearby Salida belt, Boardman (1976) reports bimodal volcanics and volcaniclastic sediments, plus quartzite and pelitic metasediments that have been metamorphosed to middle amphibolite facies. Intrusion of a quartz monzonite pluton has been dated at 1.65 to 1.70 b.y.

Braddock (1966) recognized two generations of deformation within metasedimentary rocks of the Big Thompson Canyon supracrustal succession of north-central Colorado. Both periods of deformation are associated with separate episodes of metamorphism. Quartz diorite was intruded during the first deformational period, with emplacement of syn- to post-tectonic tonalite, granodiorite and quartz monzonite following the second period of deformation.

The Yavapai Series in the Jerome-Prescott area of central Arizona consists of 1.75 to 1.80 b.y.-old basalts, andesites and rhyolites, along with minor associated sediments (Anderson and Silver, 1976). This assemblage has been intruded by pre-metamorphic granodiorites and the Mingus Mountain Quartz Diorite (dated at 1.74 b.y.). Mafic

volcanics and sediments, including sandstones, shales and impure carbonates, of the Vishnu Complex in the Grand Canyon have undergone at least two major and one minor episode of deformation and metamorphism (Brown et. al., 1979). Syn- to post-tectonic plutons, including the Zoraster Granite (dated at 1.7 b.y.), have intruded this complex.

Thus, Precambrian rocks of the Southwest can be characterized by two distinct assemblages: an older bimodal volcanic assemblage typically overlain by a younger quartzite-shale assemblage (Condie, 1982). With the exception of the Yavapai Series in Arizona and the Irving greenstone belt in Colorado, calc-alkalic volcanics of intermediate composition and graywackes have not been recognized in supracrustal assemblages of the 1.72 to 1.80 b.y.-old age province. Proterozoic rocks of Big Thompson Canyon and of the Vishnu Complex are comprised primarily of sedimentary units, lacking the bimodal volcanic assemblage typical of supracrustal belts of this age province. Pre- to post-tectonic granitic plutons, varying in composition from syenite to trondhjemite, intrude each of the supracrustal belts. Similarities also exist in the style of deformation and grade of metamorphism among the various successions. Detailed petrographic and structural analyses suggest that at least two, possibly three, generations of folding and metamorphism from greenschist to amphibolite facies, are common to each of these Proterozoic terranes.

Tectonic Setting

Although opinions differ as to how crustal interaction processes and/or the style of plate-tectonics have changed throughout geologic time, speculations of possible tectonic settings are still largely based on their comparison to similar rock associations of Phanerozoic-type tectonic environments. Such comparisons are useful, but it must be kept in mind that the processes and products which characterized Precambrian crustal evolution may have differed from present-day plate tectonics.

In general, a bimodal volcanic assemblage, as is developed in the Elk Mountain - Spring Mountain area, is indicative of an extensional environment. Mafic dikes and sills that intrude this supracrustal succession are also compatible with such an extensional environment. The presence of pillowed basalts suggests a subaqueous environment for the emplacement of basalt flows. This may or may not represent the site of eruption, since pillows typically form either when lava erupts directly into water or water-saturated sediments, or when it flows across a shoreline into a body of water. A shallow submarine origin may, however, be inferred by the close association of these basalts with marine sediments (graywacke, shales, ironstone, and limestones). Following deposition, this supracrustal succession was subjected to compressional deformation

accompanied by syn- to post-tectonic plutonism.

In terms of Phanerozoic plate-tectonic models, a shallow submarine extensional environment, as described above, is most compatible with a small back-arc basin. Mature arc-systems typically produce calc-alkaline volcanics including large amounts of andesites and graywackes, which appear to be rare or absent throughout the Proterozoic of the southwestern United States. However, recent studies by Gill and Stork (1979) and Donnelly and Rogers (1980) indicate that some immature island-arc systems are characterized by bimodal volcanic assemblages. Thus, the presence of low-K (island-arc) tholeiitic basalts, and to a minor extent calc-alkaline basalts plus tholeiitic and/or calc-alkaline felsic volcanic and volcaniclastic rocks, and the general absence of andesites within this study suggests deposition within a back-arc basin of an immature island-arc system. The presence of calc-alkaline volcanic rocks suggests evolution from arc-tholeiite series volcanism to calc-alkaline volcanism during the development of such an arc system. Such trends are believed to exist within the mafic rocks throughout other portions of the Pecos greenstone terrane (Robertson, per. commun., 1982).

Proximity of the Pecos greenstone terrane to the quartzite terrane (thought to represent terrigenous sedimentation) to the north favors a marginal back-arc basin

environment adjacent to such an immature island-arc system. Condie (1982) proposes a southward migrating continental-margin arc system to account for the stratigraphic relations typically observed between bimodal volcanic assemblages and quartzite-shale assemblages throughout the southwestern United States. Whether a back-arc basin evolved by rifting of continental crust, or evolved on pre-existing oceanic crust is unclear. Chemical analyses depict the mafic rocks as low-K tholeiites, and their slightly light-REE-depleted patterns are similar to typical mid-ocean ridge and immature arc tholeiites, suggesting partial melting of an ultramafic source. Wyman (1980) describes the occurrence of ultramafic rocks to the southwest of the present study area and suggests that they may represent part of the basal stratigraphy of the Pecos greenstone terrane. In addition, low initial Sr^{87}/Sr^{86} ratios (0.701 - 0.703) of whole-rock isochrons from the Southwestern United States suggest that the crustal basement upon which such a back-arc basin evolved was not older than the volcanics by more than about 200 m.y. (Condie and Budding, 1979).

In either case, subsequent closure of the marginal back-arc basin caused deformation of the supracrustal succession, metamorphism and partial melting to produce granitic magmas that are syn- to post-tectonically intruded. In the Phanerozoic, such orogenic events are also typically

accompanied by calc-alkaline volcanism. Evidence for such volcanism is lacking within the Proterozoic of northern New Mexico and is rare or absent throughout the rest of the Southwest. However, hypabyssal plutons of intermediate composition showing calc-alkaline trends may be present within the Pecos greenstone terrane, and thus may indicate that such magmas never reached the surface. Similar trends are also reported in the Taos Range of northern New Mexico (Mc Crink, 1982).

Repetition of such cycles (opening and closing of marginal back-arc basins) has been proposed for the accretion of more than 1,300 km of sialic crust south of the Wyoming shear zone between 1.8 and 1.1 b.y. ago, and thus account for the lack of Archean crust south of this shear zone (Condie, 1982).

Volcanogenic Massive-Sulfide Potential

Precambrian volcanogenic massive-sulfide deposits typically occur among distinct rock assemblages consisting primarily of submarine basalts; plus felsic volcanics, predominantly rhyolite domes, flows and breccias; iron formation; and immature volcanogenic marine sediments (Franklin, et. al., 1981). Massive-sulfide ores are commonly associated with the rhyolitic rocks, and are thought to precipitate on the ocean floor, at or near discharge sites of hydrothermal fluids.

The two "volcanic centers" delineated by Moench and Robertson (1980) - along Hollinger Canyon, and on Spring Mountain - have been evaluated as low-potential sites for such volcanogenic massive-sulfide deposits. The felsic volcanics from these "centers" and from the rest of the study area appear to be, for the most part, volcaniclastic and/or epiclastic sediments rather than the characteristic flows, domes, or pyroclastic deposits associated with felsic volcanic vents. Although these rocks range in composition from rhyolites to dacites, rhyodacites and dacites appear to be more abundant than rhyolites throughout this region. Thus, detailed mapping has failed to confirm the presence of either "center". Well-defined alteration zones and/or alteration pipes commonly associated with volcanogenic massive sulfide deposits have not been recognized, nor is

there evidence of any significant mineralization in these rocks. The abundance of mafic volcanic and volcaniclastic rocks within the study area also suggests the possible presence of Cyprus and/or Beshi type massive sulfide deposits within this region. Such deposits, if present at depth, may only be discovered using various geochemical and/or geophysical exploration techniques.

The use of tourmaline occurrences as a prospecting guide for massive base-metal sulfide deposits has been proposed by Slack (1980). An abundance of brown dravite typically coexisting with Mg-rich silicates and accessory sulfides is thought to represent hydrothermal alteration related to initial ore formation. Tourmaline is reported as a common gangue mineral at the Pecos Mine (Krieger, 1932; in Moench, et. al., 1980), and also occurs within amphibolites, metasediments and tonalite of this study. Porphyroblasts of tourmaline are typically dark green to black in color and are more commonly associated with Fe-Mg silicates (hornblende, biotite, and epidote), although X-ray diffraction of one such sample from Hollinger Canyon indicates the presence of dravite (North, per. commun., 1982). These tourmaline occurrences are thought to be largely associated with pegmatite mineralization and may therefore only have limited exploration significance.

Thus, results from this study suggest that these areas have little or no potential for volcanogenic base-metal sulfide deposits, although due to poor outcrop exposures the chance that sulfides remain undiscovered does exist.

SUMMARY AND CONCLUSIONS

Summary of the Geologic History in the Elk Mountain-Spring Mountain Area

The geologic history of the study area includes several periods of igneous (both extrusive and intrusive) activity, sedimentation, and metamorphism ranging from early Proterozoic to Tertiary time, as outlined below:

1) Deposition of the complex sequence of supracrustal rocks onto an unknown surface that has been obliterated by subsequent structural, metamorphic, and igneous events. The supracrustal rocks include amphibolites, felsic volcanic and volcaniclastics, and metasedimentary rocks. Although a detailed stratigraphic sequence has not been established for these rocks, multiple phases of igneous and sedimentary activity within this assemblage are likely and include:
   a) Extrusion of subaqueous basalt flows accompanied by deposition of mafic volcaniclastic sediments derived from a mafic source, probably from these mafic igneous rocks, or possibly from older mafic units.
   b) Eruption and deposition of felsic volcanic and volcaniclastic rocks, including emplacement of hypabyssal rhyolite intrusions.
   c) Intermittent deposition of sedimentary rocks, probably eroded, largely in part, from the mafic and

felsic volcanic rocks, plus chemical precipitation of ferruginous cherts and limestones.

2) Intrusion of hypabyssal mafic dikes and sills into the above assemblage of volcanics and sediments. Such intrusions may represent at least in part, feeders for the overlying volcanics.

3) Burial metamorphism (?)

4) Compressional event producing tight to isoclinal folds with axial-plane cleavage and map-scale tectonic transposition.

5) Intrusion of syntectonic foliated-granite.

6) Compressional event producing tight to isoclinal north-northeast trending folds with axial-plane foliation plus variable intensities of map-scale transposition.

7) Regional dynamothermal metamorphism to lower amphibolite facies.

8) Intrusion of anorogenic plutons (tonalite, unfoliated-granite, pegmatite and syenite). General lack of foliation within these units indicates post-deformational emplacement.

9) Uplift and erosion of Precambrian rocks followed by unconformable deposition of Paleozoic and younger rocks.

10) Continued uplift and erosion with emplacement of rhyolite dikes during Tertiary (?) time.

Conclusions

Supracrustal rocks from the Elk Mountain-Spring Mountain area consist of a complex assemblage of meta-volcanic, volcaniclastic and sedimentary rocks. The meta-volcanic and volcaniclastic rocks are bimodal in composition: mafic rocks typically characterized as sub-alkaline, low-K tholeiites; and felsic volcanic rocks as tholeiitic and/or calc-alkaline rhyolites, rhyodacites and dacites. Well preserved pillow-structures indicate that the mafic volcanic rocks were, at least in part, deposited subaqueously. The sedimentary rocks appear to be largely derived from the volcanic rocks, although minor occurrences of ironstone and limestone are also present. The submarine environment, chemistry of the bimodal volcanic suite, and the nature of the associated sedimentary rocks are all compatible with deposition of the supracrustal succession in a marginal back-arc basin adjacent to an immature arc-system.

The stratigraphic relationship among these supracrustal units is still unclear. Two periods of tight to isoclinal folding accompanied by tectonic transposition indicates that the present orientation of lithologic units no longer represents their original stratigraphy. This supracrustal succession has been subjected to at least one regional metamorphic event to lower amphibolite facies, in addition

to several episodes of plutonism.

The volcanogenic massive-sulfide potential appears to be very low within the study area. Except for local occurrences of ironstone, no evidence for associated volcanogenic base-metal sulfide mineralization was observed at the surface. However such deposits may be present at depth.

REFERENCES

Anderson, C.A. and Silver, L.T., 1976, Yavapai Series - A Greenstone Belt: Arizona Geol. Soc. Digest, v.10, p.13-26.

Baltz, E.H., 1972, Geologic map and cross-sections of the Gallinas Creek area, Sangre de Cristo Mountains, San Miguel County, New Mexico: U.S. Geol. Survey Misc. Geol. Invest. Map 1-673.

_____, 1978, Resume of the Rio Grande depression in north-central New Mexico: New Mexico Bureau of Mines and Mineral Resources Circular 163, p.210-228.

Baltz, E.H. and Bachman, G.O., 1956, Notes on the geology of the southeastern Sangre de Cristo Mountains, New Mexico: New Mexico Geol. Soc. Guidebook 7, p.96-108.

Baltz, E.H. and O'Neill, J.M., 1980, Preliminary geologic map of the Sapello River area, Sangre de Cristo Mountains, Mora and San Miguel Counties, New Mexico: U.S. Geol. Survey Open-File Report 80-398.

Barker, F., 1969, Precambrian geology of the Needles Mountains Southwestern Colorado: U.S. Geol. Survey Professional Paper 644-A, 32p.

_____, 1979, Trondhjemite: definition, environment and hypothesis of origin: in F. Barker (ed) Trondhjemites, Dacites and Related Rocks: New York, Elsevier, p.1-12.

Barker, F., Peterman, Z.E., Henderson, W.T. and Hildreth, R.E., 1974, Rubidium-strontium dating of the trondhjemite of Rio Brazos, New Mexico, and of the Kroenke granodiorite, Colorado: U.S. Geol. Survey Journal of Research, v.2, p.705-709.

Barker, F., Arth, J.G., Peterman, Z.E. and Friedman, I., 1976, The 1.7-1.8b.y.-old trondhjemites of southwestern Colorado and northern New Mexico: Geochemistry and depths of genesis: Geol. Soc. Amer. Bull., v.87, p.189-198.

Boardman, S.J., 1976, Geology of the Precambrian metamorphic rocks of the Salida area, Chaffee County, Colorado: The Mountain Geologist, v.13, no.3, p.89-100.

Bowring, S.A., 1982, U-Pb zircon ages from northern and central New Mexico, Abs: Geol. Soc. of America, v.14, no.4, p.304.

Braddock, W.A., 1966, Precambrian geology of the east flank of the Front Range near Fort Collins, Colorado (abs): Geol. Soc. Amer. Special Paper 87, p.277.

Brown, E.H., Babcock, R.S., Clark, M.D. and Livingston, D.E., 1979, Geology of the older Precambrian rocks of the Grand Canyon Part 1: Petrology and structure of the Vishnu Complex: Precambrian Research, v.8, p.219-241.

Budding, A.J., 1972, Geologic map of the Glorieta quadrangle, Santa Fe County, New Mexico: New Mexico Bureau of Mines and Mineral Resources, Geologic Map 24.

Callender, J.F., Robertson, J.M. and Brookins, D.G., 1976, Summary of Precambrian geology and geochronology of northeastern New Mexico: New Mexico Geol. Soc. Guidebook 27, p.129-135.

Codding, D.B., (in press), Precambrian geology of the Rio Mora area, New Mexico; Structural and Stratigraphic Relations: MS Thesis, Univ. of New Mexico.

Clark, K.F. and Read, C.B., 1972, Geology and ore deposits of Eagle Nest area, New Mexico: New Mexico Bureau of Mines Bulletin 94, 149p.

Condie, K.C., 1980a, Precambrian rocks of the Red River-Wheeler Peak area in northern New Mexico: New Mexico Bureau of Mines and Mineral Resources Geologic Map 50.

_____, 1980b, The Tijeras greenstone: Evidence for depleted upper mantle beneath New Mexico during the Proterozoic: Journal of Geology, v.88, p.603-609.

_____, 1981a, Precambrian rocks of the southwestern United States and adjacent areas of Mexico: New Mexico Bureau of Mines and Mineral Resources Resource Map 13.

_____, 1981b, Archean Greenstone Belts: Developments in Precambrian Geology (3): New York, Elsevier, 434p.

_____, 1982, Plate-tectonics model for Proterozoic continental accretion in the southwestern United States: Geology, v.10, p.37-42.

Condie, K.C. and Budding, A.J., 1979, Geology and geochemistry of Precambrian rocks, central and south-central New Mexico: New Mexico Bureau of Mines and Mineral Resources Memoir 35, 58p.

Condie, K.C. and Nuter, J.A., 1981, Geochemistry of the Dubois greenstone succession: an early Proterozoic bimodal volcanic association in west-central Colorado: Precambrian Research, v.15, p.131-155.

Condie, K.C., Viljoen, M.J., Kable, E.J.D., 1977, Effects of alteration of element distributions in Archean tholeiites from the Barberton Greenstone Belt, South Africa: Contrib. Miner. and Petrol., v.64, p.75-89.

Dewit, M.J. and Stern, C., 1978, Pillow-talk: Journal of Volcanology and Geothermal Research, v.4, p.55-80.

Dimroth, E., 1976, Aspects of the sedimentary petrology of cherty iron formation: in K.H. Wolf (ed.), Handbook of Stratabound and Strataform Ore Deposits, II Regional studies and specific deposits, v.7, p.203-254.

Donnelly, T.W. and Rogers, J.J.W., 1980, Igneous series in island-arcs: The northeastern Caribbean compared with world wide island-arc assemblages: Bull. Volcanol., v.43, p.347-382.

Ewart, A., 1979, A review of the mineralogy and chemistry of Tertiary-Recent dacitic, latitic, rhyolitic, and related salic volcanic rocks; in Barker, F., ed., Trondhjemites, Dacites, and Related Rocks: New York, Elsevier, p.13-121.

Ewart, A. and Le Maitre, R.W., 1980, Some regional compositional differences within Tertiary-Recent orogenic magmas: Chemical Geology, v.30, p.257-283.

Floyd, P.A. and Winchester, J.A., 1975, Magma type and tectonic setting discrimination using immobile elements: Earth and Planet. Sci. Let., v.27, p.211-218.

Franklin, J.M., Lydon, J.W. and Sangster, D.F., 1981, Volcanic-associated massive sulfide deposits: in Skinner (ed) Economic Geology Seventy-Fifth Anniversary Volume, p.485-627.

Fullagar, P.D. and Shiver, W.S., 1973, Geochronology and petrochemistry of the Embudo Granite, New Mexico: Geol. Soc. Amer. Bull., v.84, p.2705-2712.

Ganguly, J., 1969, Chloritoid stability and related paragenesis: Theory, experiment, and applications: Amer. Jour. Sci., v.267, p.910-944.

Gibson, T.R., 1981, Precambrian geology of the Burned Mountain-Hopwell Lake area, Rio Arriba County, New Mexico: M.S. thesis, New Mexico Institute of Mining and Technology, 105p.

Gill, J.B. and Stork, A.L., 1979, Miocene Low-K Dacites and Trondhjemites of Figi: in F. Barker (ed) Trondhjemites, Dacites, and Related Rocks: New York, Elsevier, p.629-649.

Gordon, G.E., Randle, K., Goles, G.G., Corliss, J.B., Beeson, M.H. and Oxley, S.S., 1968, Instrumental activation analysis of standard rocks with high resolution gamma-ray detectors: Geochem. Cosmochim. Acta, v.32, p.369-396.

Grambling, J.A., 1979, Precambrian geology of the Truchas Peaks region, north-central New Mexico, and some regional implications: New Mexico Geol. Soc. Guidebook 30, p.135-143.

Grambling, J.A. and Codding, D.B., 1982, Stratigraphic and structural relationships of multiply deformed Precambrian metamorphic rocks in the Rio Mora area, New Mexico: Geol. Soc. Amer. Bull., v.93, p.127-137.

Gresens, R.L., 1975, Geochronology of Precambrian metamorphic rocks, north-central New Mexico: Geol. Soc. Amer. Bull., v.86, p.1444-1448.

Gross, G.A., 1965, Geology of iron deposits of Canada: General geology and evaluation of iron deposits: Econ. Geol. Surv. Canada, Rept. 22, pt. 1, 181p.

Hart, S.R., Erlank, A.J. and Kable, E.J.D., 1974, Sea-floor basalt alteration: Some chemical and Sr isotope effects: Contrib. Mineral. Petrol., v.44, p.219-230.

Haskin, L.A. and Paster, T.P., 1979, Geochemistry and mineralogy of the rare earths: in Gschneider, K.A. and Eyring, L. (ed) Handbook on the Physics and Geochemistry of Rare Earths, Ch.21, 80p.

Hobbs, B.E., Means, W.D. and Williams, P.F., 1976, An Outline of Structural Geology: New York, John Wiley and Sons, 571p.

Holcombe, R.J. and Callender, J.F., 1982, Structural analysis and stratigraphic problems of Precambrian rocks of the Picuris Range, New Mexico: Geol. Soc. Amer. Bull., v.93, p.183-149.

Holmquist, R.J., 1946, Exploration of the Elk Mountain mica deposit, San Miguel County, New Mexico: U.S. Bureau of Mines Report of Investigation 3921, 7p.

Hoschek,G., 1969, The stability of staurolite and chloritoid and their significance in metamorphism of pelitic rocks: Contr. Mineral. Petrol., v.22, p.208-232.

Humphris, S.E. and Thompson, G., 1978a, Hydrothermal alteration of oceanic basalts by seawater: Geochem. Cosmochim. Acta, v.42, p.107-126.

_____, 1978b, Trace element mobility during hydrothermal alteration of oceanic basalts: Geochem. Cosmochim. Acta, v.42, p.127-136.

Hynes, A., 1980, Carbonatization and mobility of Ti, Y, and Zr in Ascot Formation metabasalts, SE Quebec: Contrib. Mineral. Petrol., v.75, p.79-87.

Irvine, T.N. and Baragar, W.R.A., 1971, A guide to the chemical classification of the common volcanic rocks: Can. Jour. Earth Sci., v.8, p.523-548.

Jahns, R.H., 1946, Mica deposits of the Petaca district, New Mexico: New Mexico Bureau of Mines and Mineral Resources Bulletin 25, 294p.

Jenkins, R. and De Vries, J.L., 1975, Practical X-Ray Spectrometry: New York, Springer-Verlag, 190p.

Jensen, L.S., 1976, A new cation plot for classifying subalkaline volcanic rocks: Ontario Division of Mines, Miscellaneous Paper 66, 22p.

Kerr, P.F., 1977, Optical Mineralogy: New York, McGraw Hill, 492p.

Kent, S.C., 1980, Precambrian geology of the Tusas Mountain area, Rio Arriba County, New Mexico: M.S. thesis, New Mexico Institute of Mining and Technology, 151p.

Kimberley, M.M., 1978, Paleoenvironmental classification of iron formations: Economic Geology, v.73, p.215-229.

Lane, M.E., 1980, Mines, prospects, and mineralized areas in the Pecos Widerness and adjacent areas, Santa Fe, San Miguel, Mora, Rio Arriba, and Taos Counties, New Mexico, Chapter C of U.S. Geol. Survey, U.S. Bureau of Mines, and New Mexico Bureau of Mines and Mineral Resources, 1980, Mineral resources of the Pecos Wilderness and adjacent areas, Santa Fe, San Miguel, Mora, Rio Arriba, and Taos Counties, New Mexico: U.S. Geol. Survey Open-File Report 80-382, p.70-103.

Le Maitre, R.W., 1976, The chemical variability of some common igneous rocks: Journal of Petrology, v.17, part 4, p.589-637.

Lipman, P.W., Prostka, H.J. and Christiansen, R.L., 1972, Cenozoic volcanism and plate tectonic evolution of the Western United States: I Early and Middle Cenozoic: Phil. Trans. Roy. Soc. Lond., Series A, v.271, p.217-248.

Long, L.E., 1972, Rb-Sr chronology of Precambrian schist and pegmatite La Madera quadrangle, northern New Mexico: Geol. Soc. of Amer. Bull., v.83, p.3425-3432.

Long, P.E., 1974, Contrasting types of Precambrian granitic rocks in the Dixon-Penasco area, northern New Mexico: New Mexico Geol. Soc. Guidebook 25, p.101-108.

Mac Geehan, P.J. and Mac Lean, W.H., 1980, An Archean sub-seafloor geothermal system, calc-alkali trends, and massive sulfide genesis: Nature, v.286, p.767-771.

McCrink, T.P., 1982, Precambrian geology of the Taos Range, Taos County, New Mexico: M.S. thesis, New Mexico Institute of Mining and Technology, 123p.

Menzies, M., Seyfried, W.Jr. and Blanchard, D., 1979, Experimental evidence of rare-earth element mobility in greenstones: Nature, v.282, p.398-399.

Miller, J.P., Montgomery, A. and Sutherland, P.K., 1963, Geology of part of the southern Sangre de Cristo Mountains, New Mexico: New Mexico Bureau of Mines and Mineral Resources Memoir 11, 106p.

Miyashiro, A., 1973, Metamorphism and Metamorphic Belts: George, Allen and Unwin, London, 492p.

Miyashiro, A., 1974, Volcanic rock series in island arcs and active continental margins: Amer. Jour. Sci., v.274, p.321-355.

Miyashiro, A. and Shido, F., 1975, Tholeiitic and calc-alkaline series in relation to the behaviors of titanium, vanadium, chromium, and nickel: Amer. Jour. of Sci., v.275, p. 265-277.

Moench, R.H. and Erickson, M.S., 1980, Occurrence of tungsten in the Sangre de Cristo Range near Santa Fe, New Mexico: possible stratabound scheelite peripheral to favorable settings for volcanogenic massive-sulfide deposits: U.S. Geol. Survey Open-File Report 80-1162, 21p.

Moench, R.H. and Robertson, J.M., 1980, Geology of the Pecos Wilderness and adjacent areas, Santa Fe, San Miguel, Mora, Rio Arriba, and Taos Counties, New Mexico, Chapter A of U.S. Geol. Survey, U.S. Bureau of MInes, and New Mexico Bureau of Mines Mineral Resources, 1980, Mineral resources of the Pecos Wilderness and adjacent areas, Santa Fe, San Miguel, Mora, Rio Arriba, and Taos Counties, New Mexico: U.S. Geol. Survey Open-File Report 80-382, p.6-41.

Moench, R.H., Robertson, J.M. and Sutley, S.J., 1980, Geological, geochemical, and geophysical evaluation of the mineral resources of the Pecos Wilderness and adjacent areas, Santa Fe, San Miguel, Mora, Rio Arriba, and Taos Counties, New Mexico, Chapter B of U.S. Geol. Survey, U.S. Bureau of Mines, and New Mexico Bureau of Mines and Mineral Resources, 1980, Mineral resources of the Pecos Wilderness and adjacent areas, Santa Fe, San Miguel, Mora, Rio Arriba, and Taos Counties, New Mexico: U.S. Geol. Survey Open-File Report 80-382, P.42-68.

Montgomery, A., 1953, Precambrian geology of the Picuris Range, north-central New Mexico: New Mexico Bureau of Mines and Mineral Resources Bulletin 30, 89p.

Nielson, K.C. and Scott, T.E., 1979, Precambrian deformational history of the Picuris Mountains, New Mexico: New Mexico Geol. Soc. Guidebook 30, p.113-120.

Norrish, K. and Hutton, J.T., 1969, An accurate X-ray spectrographic method for the analysis of a wide range of geological samples: Geochem. Cosmochim. Acta, v.33, p.431-453.

Pearce, J.A., 1975, Basalt geochemistry used to investigate past tectonic environments on Cyprus: Tectonophysics, v.25, p.41-67.

Pearce, J.A. and Cann, J.R., 1973, Tectonic setting of basic volcanic rocks determined using trace element analyses: Earth and Planet. Sci. Let., v.19, p.290-300.

Peccerillo, A. and Taylor, S.R., 1976, Geochemistry of Eocene calc-alkaline volcanic rocks from Kastamonu area, northern Turkey: Contrib. Mineral. Petrol., v.58, p.63-81.

Redmon, D.E., 1961, Reconnaissance of selected pegmatite districts in north-central New Mexico: U.S. Bureau of Mines Information Circular 8013, p.79.

Reed, J.C., Robertson, J.M. and Lipman, P.W., 1980, Preliminary geologic map of the Wheeler Peak-Hondo Canyon area, Taos County, New Mexico: U.S. Geol. Survey Misc. Geol. Invest. Map 81-1077.

Register, M.E. and Brookins, D.G., 1979, Geochronologic and rare-earth study of the Embudo Granite and related rocks: New Mexico Geol. Soc. Guidebook 30, p.155-158.

Riesmeyer, W.D., 1978, Precambrian geology and ore deposits of the Pecos mining district, San Miguel, and Santa Fe Counties, New Mexico: M.S. thesis, University of New Mexico, 215p.

Rittman, A., 1962, Volcanoes and their activity: New York, Wiley and Sons, 305p.

Roaldset, E., 1975, Rare earth element distributions in some Precambrian rocks and their phyllosilicates, Neumedal, Norway: Geochem. Cosmochim. Acta, v.39, p.455-469.

Robertson, J.M. and Moench, R.H., 1979, The Pecos greenstone belt: A proterozoic volcano-sedimentary sequence in the southern Sangre de Cristo Mountains, New Mexico: New Mexico Geol. Soc. Guidebook 30, p.165-173.

Shervais, J.W., 1982, Ti-V plots and the petrogenesis of modern ophiolitic lavas: Earth and Planet. Sci. Let., v.59, p.101-118.

Slack, J.F., 1980, Tourmaline - a prospecting guide for massive base-metal sulfide deposits in the Penobscot Bay area, Maine: Maine Geol. Surv. Spec. Econ. Study, series 8, 25p.

Snyder, G.L. and Fraser, G.D., 1963a, Pillowed lavas, I: Intrusive layered lava pods and pillowed lavas, Unalaska Is., Alaska: U.S. Geol. Survey Prof. Paper 454-B, 23p.

_____, 1963b, Pillowed lavas,II: A review of selected recent literature: U.S. Geol. Survey Prof. Paper 454-C, 7p.

Stacey, J.S., Doe, B.R., Silver, L.T. and Zartman, R.E., 1976, Plumbotectonics II-A, Precambrian massive sulfide deposits: U.S. Geol. Survey Open-File Report 76-476, 26p.

Staudigel, H., Hart, S.R. and Richardson, S.H., 1981, Alteration of the oceanic crust: Processes and timing: Earth and Planet. Sci. Let., v.52, p.311-327.

Streckeisen, A.L., 1973, Plutonic rock classification and nomenclature recommended by the IUGS subcommission on the systematics of igneous rocks: Geotimes, v.18, no.10, p.26-30.

Turner, F.S. and Weiss, L.E., 1963, Structural Analysis of Metamorphic Tectonites: New York, Mc Graw-Hill, 545p.

Tweto, O., 1977, Nomenclature of Precambrian rocks in Colorado: U.S. Geol. Survey Bulletin 1422-D, p.D1-D22.

U.S. Geological Survey, U.S. Bureau of Mines, and New Mexico Bureau of Mines and Mineral Resources, 1980, Mineral resources of the Pecos Wilderness and adjacent areas, Santa Fe, San Miguel, Mora, Rio Arriba, and Taos Counties, New Mexico: U.S. Geol. Survey Open-File Report 80-382, 103p.

Winchester, J.A. and Floyd, P.A., 1977, Geochemical discrimination of different magma series and their differentiation products using immobile elements: Chemical Geology, v.20, p.325-343.

Winkler, H.G.F., 1979, Petrogenesis of Metamorphic Rocks, 5th ed: New York, Springer-Verlag, 348p.

Wood, D.A., 1980, The application of a Th-Hf-Ta diagram to problems of tectonomagmatic classification and to establishing the nature of crustal contamination of basaltic lavas of the British Tertiary volcanic province: Earth and Planet. Sci. Let., v.50, p.11-30.

Wood, D.A., Jordon, J.L. and Treuil, M., 1979, A re-appraisal of the use of trace elements to classify and discriminate between magma series erupted in different tectonic settings: Earth and Planet. Sci. Let., v.45, p.325-336.

Wyman, B.F., 1980, Precambrian geology of the Cow Creek ultramafic complex, San Miguel County, New Mexico: M.S. thesis, New Mexico Institute of Mining and Technology, 125p.

APPENDIXES

APPENDIX A

Sample Location Map

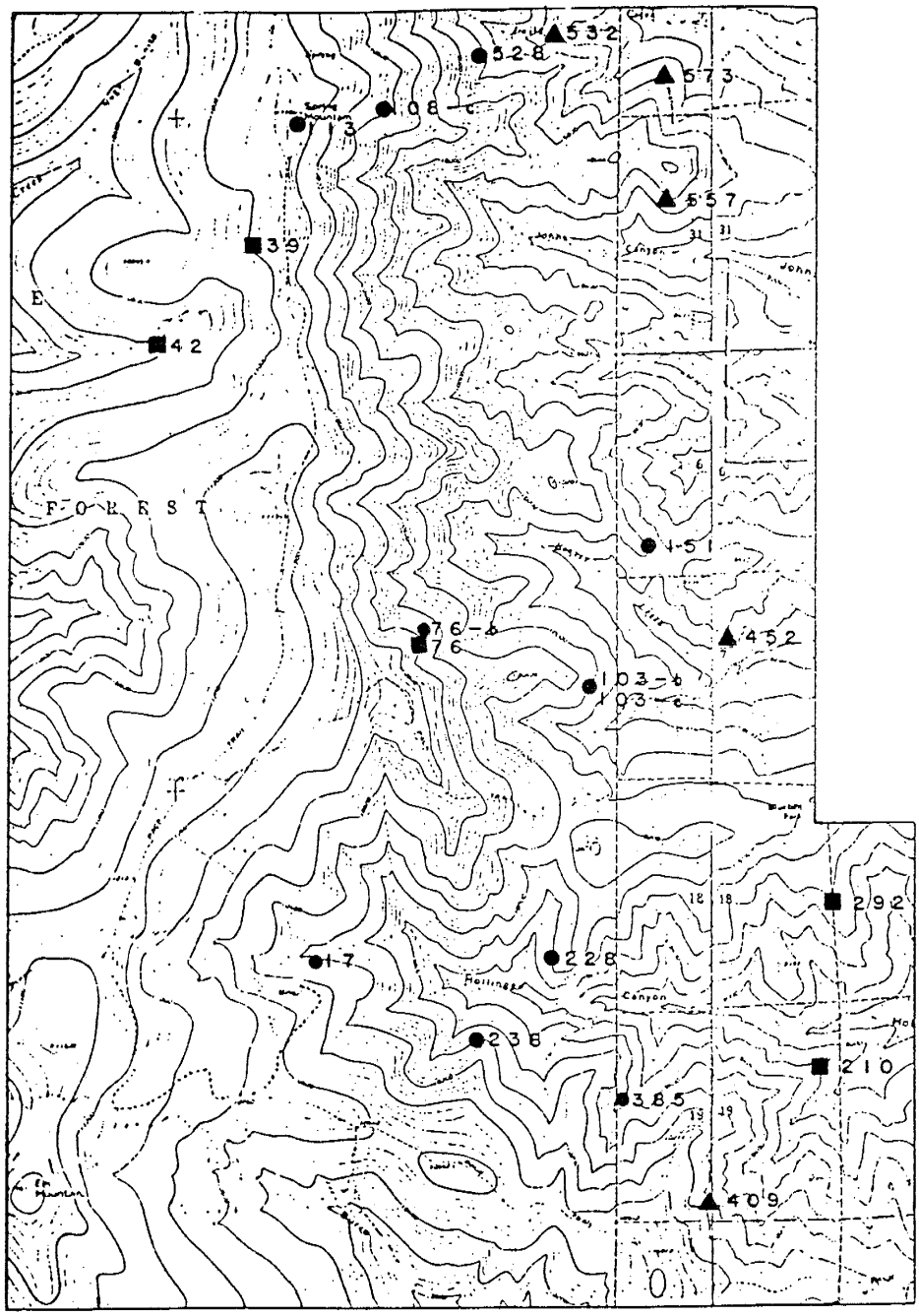

● Amphibolites

▲ Felsic Volcanic/Volcaniclastics

■ Intrusives

APPENDIX B

PETROLOGIC DESCRIPTIONS OF GEOCHEMICAL SAMPLES

SAMPLE TYPE	SAMPLE NO.	MAJOR ELEMENTS	MINOR MINERALS	TEXTURE	COMMENTS
Amphibolite	17	Actinolite (35) Plagioclase (30) Chlorite (25)	Epidote (5) Quartz (3) Sphene, Sericite Magnetite, Hematite	medium-grained decussate relict subophitic	meta-diabase near pegmatite intrusion
Amphibolite	76-b	Hornblende (25) Plagioclase (12) Alkali-Feldspar (25) Chlorite (20)	Biotite (10) Quartz (5) Epidote, Sphene, Apatite	medium-grained decussate	extensive potassic-metasomatism due to syenite intrusion
Amphibole Porphyry	103-b	Hornblende (10) Actinolite (20) Plagioclase (15) Sericite (30) Chlorite (10)	Biotite (7) Quartz (5) Magnetite, Epidote	porphyritic synneusis texture	chloritization of amphibole, intense sericitization of plagioclase
Amphibolite	103-c	Hornblende (25) Actinolite (12) Plagioclase (35)	Chlorite (10) Magnetite (8) Sericite (5) Quartz (5) Ilmenite, Epidote	fine-grained decussate	mafic dike/sill slight chloritization of amphibole
Amphibolite	113	Hornblende (25) Actinolite-Tremolite (20) Plagioclase (15) Chlorite (15)	Quartz (10) Magnetite (5) Biotite, Sericite, Sphene	fine-grained granoblastic	meta-basalt chloritizaton of biotite and amphibole
Amphibolite	151	Hornblende (40) Actinolite (15) Plagioclase (20) Chlorite (12)	Quartz (7) Magnetite (3) Sericite	medium-grained foliated	ortho-amphibolite (?) chloritization of amphibole
Amphibolite	228	Hornblende (20) Actinolite (25) Plagioclase (35)	Quartz (9) Sericite, Epidote Magnetite, Hematite, Sphene	fine-grained slightly foliated	meta-basalt sericitization of plagioclase
Amphibolite	238	Hornblende (15) Actinolite (15) Plagioclase (25) Chlorite (15)	Quartz (3) Sericite (3) Magnetite, Sphene	medium-grained foliated	ortho-amphibolite (?) chloritization of amphibolite
Amphibolite	385	Hornblende (50) Actinolite (10) Plagioclase (25)	Sericite (5) Chlorite (3) Quartz, Sphene, Magnetite Hematite	medium-grained decussate relict subophitic	meta-diabase sericitization of plagioclase
Amphibolite	532	Hornblende (40) Biotite (20) Plagioclase (10) Quartz (15)	Chlorite (8) Sericite, Sphene, Epidote, Magnetite	fine-grained foliated	para-amphibolite chloritization of biotite

SAMPLE TYPE	SAMPLE NO.	MAJOR ELEMENTS	MINOR MINERALS	TEXTURE	COMMENTS
Felsic Volcanic Volcaniclastic	108	Quartz (35) Alkali-Feldspar (35) Plagioclase (10) Muscovite (15)	Biotite, Magnetite, Chlorite Epidote, Sericite	porphyritic slightly foliated	sericitization of feldspar
Felsic Volcanic Volcaniclastic	409	Plagioclase (40) Quartz (27) Biotite (20) Hornblende (10)	Sericite, Magnetite Ilmenite	porphyritic granoblastic	sericitization of plagioclase
Felsic Volcanic Volcaniclastic	452	Quartz (35) Alkali-Feldspar (30) Plagioclase (10) Muscovite (13)	Biotite (6) Chlorite, Sphene Magnetite, Sericite, Epidote	porphyritic granoblastic	slight chloritization of biotite
Felsic Granofels	528	Quartz (30) Alkali-Feldspar (20) Muscovite (22) Plagioclase (10)	Biotite (10) Epidote-Zoisite (5) Calcite, Magnetite	fine-grained granoblastic	compositional layering
Felsic Volcanic Volcaniclastic	557	Plagioclase (40) Quartz (30) Muscovite (13) Biotite (10)	Chlorite (5) Magnetite Calcite, Sericite	porphyritic granoblastic	slight chloritization of biotite
Felsic Gneiss	573	Quartz (30) Alkali-Feldspar (25) Muscovite (15) Biotite (15) Plagioclase (10)	Sericite, Epidote, Calcite Apatite, Magnetite	compositional layering	tectonic fragmentation sericitization of feldspars
Foliated Granite	42	Quartz (32) Alkali-Feldspar (30) Plagioclase (15) Muscovite (15)	Biotite (5) Chlorite, Sericite Epidote, Magnetite	fine-grained foliated	sericitization of feldspars, slight chloritization of biotite
Syenite	76	Alkali-Feldspar (50) Plagioclase (22) Hornblende (17)	Biotite (5) Quartz (3) Magnetite, Chlorite, Sphene Apatite, Zircon	medium-grained decussate cataclastic	sericitization of feldspars, quartz-filled fractures
Tonalite	210	Plagioclase (40) Hornblende (15) Quartz (15) Biotite (13)	Chlorite (7) Sericite (5) Magnetite, Epidote, Sphene	medium-grained non-foliated cataclastic	sericitization of plagioclase
Unfoliated Granite	292	Alkali-Feldspar (35) Quartz (30) Plagioclase (20)	Biotite (0) Chlorite, Magnetite Sphene, Epidote, Calcite	equigranular cataclastic	sericitization of feldspars, slight chloritization of biotite

APPENDIX C

Sample Preparation

Twenty-one samples were selected to represent the various rock types identified within the study area, with special emphasis placed on amphibolites, felsic volcanic and volcaniclastics, and the intrusive rocks. Sample locations and petrologic descriptions are given in Appendix A and B respectively.

The fist-sized rock samples were crushed to approximately 3-5mm using a series of jaw crushers provided by the New Mexico Bureau of Mines and Mineral Resources. After the initial crushing, each sample was hand picked to avoid sampling any secondary weathering products. The least weathered of this residue was used to contaminate the next grinder in sequence, prior to crushing the actual sample. Between samples the crushers were cleaned using wire brushes and/or compressed air. The resulting rock chips were then ground to approximately sand-sized grains in a rotary grinder. The final stage involved pulverizing the samples to 10mμ in a high-speed mortar and pestal, for 5-10 minutes to insure complete grinding and homogenization.

For neutron activation analyses, approximately 0.5 gram of rock powder was placed in small polyurethane vials and sent to Sandia National Labratory's nuclear reactor for irradiation. Sample preparation for X-ray fluorescence was two-fold. Major elements were analyzed using fused-glass discs, prepared by melting a mixture of rock powder (0.5 gram) and Spectroflux (2.7 grams) in a platinum crucible. Once molten, the flux is pressed into thin glass discs and allowed to slowly cool. Pressed-powder pellets, used to analyze for trace elements, were made using microcrystalline cellulose as a binder and backing agent. Four grams of sample powder were combined with one gram of binder to insure sufficient thickness for the X-ray fluorescence determination. Each pellet was then compressed to 20 tons.

APPENDIX D

X-ray Fluorescence Analysis

New Mexico Bureau of Mines and Mineral Resources' Rigaku X-ray Fluorescence Spectrometer was used to analyze the major and minor elements Si, Ti, Al, Fe, Mg, Ca, Na, K, Mn, and P, and the trace elements Rb, Sr, Zr, and Y. K-alpha peaks were measured using a flow proportional counter for the major and minor elements, and a scintillation counter for the trace elements. Additional instrumental parameters are summarized in Table 6.

Specific procedures for X-ray fluorescence analyses are given in Norrish and Hutton (1969), and Jenkins and De Vries (1975). In general, this technique involves the comparison of an element's X-ray intensity from an unknown sample with that of a standard of known concentration using linear calibration curves. U.S.G.S. standards GSP-1, AGV-1, BHVO, BCR-1, PCC-1, G-2, and QLO-1; French standards GH, GA, AN-G, BE-N, and MA-N; South African standards NIM-S, NIM-D, and NIM-N; and Japanese standards JG-1 and JB-1 were used in constructing the calibration curves. In addition, three New Mexico Tech intralab standards (BLCR, HI-31, and LOSP) were also included in these curves. Their analyses are given in Table 7. Computer programs which received raw counting data from the spectrometer were used to calculate concentrations

for the major oxides. Using calculated mass absorption coefficients for each sample at the specific wavelength of each element, correction and concentration calculations for the trace elements were done with the aid of a pocket calculator. Analytical error is ≤10% for the trace elements and ≤1% for the major and minor elements.

TABLE 6

X-Ray Fluorescence Instrumental Parameters

ELEMENT	Kv/Ma	CRYSTAL	COLLIMATOR
Si	45/55	RX4	Fine
Al	45/55	PET	Coarse
Na	45/55	TAP	Fine
Mg	45/55	TAP	Coarse
Fe	45/55	LiF(200)	Fine
Ca	45/55	LiF(200)	Coarse
K	45/55	LiF(200)	Coarse
Ti	45/55	LiF(200)	Coarse
Mn	45/55	LiF(200)	Coarse
P	45/55	LiF(200)	Coarse
Rb	40/60	LiF(200)	Coarse
Sr	40/60	LiF(200)	Coarse
Zr	40/60	LiF(200)	Coarse
Y	40/60	LiF(200)	Coarse

TABLE 7

Revised Results for Intralab Rock Standards
at New Mexico Tech (1982)

	LOSP	BLCR	HI31
SiO2	75.90	53.50	58.80
TiO2	0.20	0.89	0.88
Al2O3	12.30	18.10	16.70
Fe2O3T	1.63	6.86	6.47
MgO	0.07	4.85	4.21
CaO	0.93	8.39	6.50
Na2O	3.49	3.57	3.11
K2O	4.83	1.32	2.88
Total	99.53	98.24	99.56
Sc	4.2	38	20
Co	0.6	30	13
Cr	2.7	130	34
Ni	-	100	-
Rb	179	37	59
Sr	41	234	684
Ba	960	370	772
Zr	256	188	-
Cs	2.0	2.5	0.5
Hf	11	4.3	-
Ta	1.9	0.5	-
Th	20	3.8	-
La	82	12	33
Ce	160	28	67
Nd	70	15	-
Sm	17.8	4.0	7.5
Eu	2.4	1.3	1.8
Tb	3.1	0.8	0.9
Yb	11	3.1	3.3
Lu	1.8	0.5	0.6
U	4.2	1.5	-
Y	70	37	-

APPENDIX E

Instrumental Neutron Activation Analysis

Powdered rock samples, irradiated at Sandia National Laboratory's reactor in Albuquerque, New Mexico, were analyzed for seventeen trace elements on a Nuclear Data 4,096 channel gamma-ray spectrometer, equipped with a high resolution Li-drifted germanium detector. Detailed procedures are described by Gordon et. al. (1968) and the instrumental parameters are summarized in Table 8. Counting times were 5000, 8000, and 12,000 seconds at intervals of 4, 7, and 28 days after irradiation, respectively, depending on the half-life of the analyzed radionuclide.

Unknown sample concentrations were calculated using a computer program that compares the peak area of a given element in the unknown sample with that of a standard. U.S.G.S. rock standard G-2 and intralab standard BLCR (Table 7) were used in this analysis. Errors associated with weight differences between sample and standard, dead time, and radioactive decay occurring between sample and standard counting times are also corrected for in the program. Analytical errors are estimated within 10% for trace elements.

TABLE 8

Neutron Activation Instrumental Parameters

RADIONUCLIDE	Peak ENERGY(KeV)	COOLING TIME(DAYS)	COUNTING TIME(SECS)
Sm-153	103.2	4	5000
Np-239 (U)	277.6	4	5000
La-140	487.0	4	5000
Lu-177	208.8	7	8000
Np-239 (U)	277.6	7	8000
Yb-175	282.6	7	8000
Tb-160	298.6	7	8000
Yb-175	396.1	7	8000
Eu-154	121.8	28	12000
Ce-140	145.5	28	12000
Yb-169	177.2	28	12000
Eu-152	216.0	28	12000
Ta-182	222.1	28	12000
Tb-160	298.6	28	12000
Pa-233 (Th)	311.8	28	12000
Cr-51	320.1	28	12000
Hf-181	482.2	28	12000
Ba-131	496.3	28	12000
Eu-152	779.1	28	12000
Cs-134	795.8	28	12000
Tb-160	879.3	28	12000
Sc-46	889.3	28	12000
Tb-160	1178.1	28	12000
Co-60	1332.5	28	12000
Eu-152	1408.1	28	12000

This thesis accepted on the behalf of the faculty of the Institute by the following committee:

Adviser

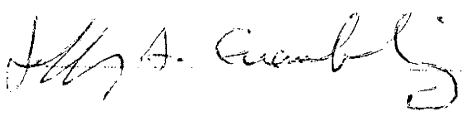

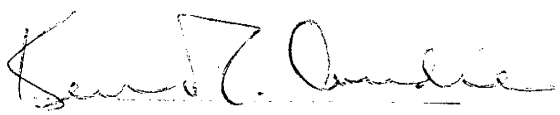

Feb 21, 1983
Date